

Statistical Signal Analysis and Estimation Algorithms for Mud Pulse Telemetry Systems

Von der Fakultät für Elektrotechnik und Informatik der
Gottfried Wilhelm Leibniz Universität Hannover
zur Erlangung des akademischen Grades
Doktor-Ingenieur (Dr.-Ing.)
genehmigte

Dissertation

von M.Sc. Sanam Moghaddamnia
geboren am 25. Juli 1979 in Tabriz-Iran

2012

Referent: Prof. Dr.-Ing. T. Kaiser
Korreferent: Prof. Dr. J. Peissig
Vorsitzender: Prof. Dr.-Ing. H. Blume
Tag der Promotion: 24.04.2012

Kurzfassung

Bohrdaten-Telemetrie spielt eine wichtige Rolle innerhalb der modernen Bohrtechnologie. Darunter werden die Verfahren zusammengefasst, die zur Erfassung von Messinformation, wie z.B. Bohrlochgeometrie, Erdformation und Richtung der Bohrmeißel dienen und deren Übertragung von mehreren Sensoren an der Bohrlochsohle zu der Auswerteeinheit an der Oberfläche ermöglichen. Mud-Pulse Telemetrie ist eine spezielle Variante der drahtlosen Telemetrie, die bei Bohrtechniken zur Unterstützung von Messungen während des Bohrvorgangs entwickelt wurde. Das Übertragungsmedium ist dabei Spülflüssigkeit, welche durch die Spülpumpen entsteht und im Bohrstrang zirkuliert. Mit Hilfe eines Pulserventils im Bereich des Bohrkopfs werden entsprechend der Telemetriedaten Druckpulse erzeugt und für die Verarbeitung zur Oberfläche gesendet. Aufgrund der hohen Zuverlässigkeit und der großen Reichweite ist der Gebrauch der Mud-Pulse Telemetrie weitverbreitet.

Das grundlegende Problem bei den auf Mud-Pulse Telemetrie basierenden Messungen während des Bohrvorgangs ist, dass die Telemetriedruckpulse durch die um ein Vielfaches stärkeren Druckschwankungen des Bohrschlamms, ausgelöst durch den Pumpvorgang, überlagert werden. Dabei liegen die Pumpschwankungen und die Telemetriedaten im gleichen Frequenzbereich. Darüber hinaus wird, besonders für hochratige Datenübertragung im Bereich von 40 bit/sec, eine Kanalverzerrung vorgenommen. Die robuste bzw. zuverlässige Übertragung der Telemetriedaten während des regulären Betriebs stellt eine große Herausforderung dar. Der Grund hierfür ist, dass kein Referenzsignal für die Pumpeninterferenz vorhanden ist. Hinzu kommen die instabilen Pumpendrehzahl und Mehrpumpenbetrieb bei den meisten Bohrungen. Derzeitige Telemetrieverfahren sind kostenineffizient und liefern eine moderate Performanz besonders hinsichtlich des Trackings der Systemparameter. In der vorliegenden Arbeit werden weiterführende Untersuchungen für die adaptive Schätzung des Telemetriesignals durchgeführt, um die Leistungsfähigkeit bzw. die Robustheit der Telemetrieverfahren in realitätsnahen Bohrszenarien zu steigern.

Die Anwendungsmöglichkeit der auf bestimmten Eigenschaften der Interferenz- sowie des Telemetriesignals basierenden semi-blinden Verfahren werden untersucht und hinsichtlich deren Einschränkungen und Trackingansätze diskutiert.

Unterschiedliche Empfängerstrukturen, bei denen die Nutzung der Mehrempfängersysteme sowie einer Trainingssequenz vorliegt, werden vorgestellt. Vielversprechend ist das adaptive Diversitätsverfahren mit Optimal-Kombinierung, wobei die sogenannte Co-Channel Interferenzdiversität zur Interferenzunterdrückung eingesetzt wird. Die Besonderheit dieser Technik liegt in dem einfachen und robusten Trackingverhalten.

Durch Einsatz der Transform-Domain-Median-Filterung wird die Pumpeninterferenz blind entfernt und damit das Tracking automatisch gewährleistet. Diese Methode ist nicht nur von wirtschaftlichem Interesse, sondern ermöglicht sowohl nützliche Kenntnisse über das Übertragungsmedium zu erhalten als auch signifikante Verbesserung der Synchronisationszuverlässigkeit zu erzeugen. Schließlich werden hybride Empfängeransätze eingeführt. Hierbei handelt es sich um eine Kombination der Transform-Domain-Median-Filterung und der adaptiven Diversitätsverfahren. Solche hybride Empfängerstrukturen ermöglichen sowohl eine Verbesserung der Bitfehlerrate auch als ein effizientes und zuverlässiges Tracking der Systemparameter.

Zum Schluss wurden alle Verfahren Hinsicht ihrer Effizienz in realistischen Anwendungen der Mud-Pulse Telemetrie eingehend untersucht. Mit Hilfe der Messdaten von unter-

schiedlichen Bohranlagen wurde die Tauglichkeit der oben genannten Verfahren bewiesen und das optimale Empfängersystem für Mud-Pulse Telemetrie-Anwendungen spezifiziert.

Schlagwörter

Mud-Pulse Telemetrie, Semi-blinde und trainingsbasierende Signalverarbeitung, Charakterisierung von Pumpinterferenz und Kanal, Transform-Domain Interferenzunterdrückung, Mehrkanal Diversitätsverfahren, Hybride Empfänger

Abstract

Telemetry is an important feature of recent drilling technologies. It is a process of gathering information on the wellbore geometry, formation properties and the direction of the drill bit from multiple sensors located at the bottom of the borehole and transmitting them to the surface evaluation units. Mud pulse telemetry is a special type of wireless data telemetry, developed to support Measurement-While-Drilling operations in drilling technologies. The transmission medium is mud, which is generated by pumps and circulated in the drill string. The telemetry information is formed to the telemetry pressure waves by a valve pulser near the drill bit and transmitted to the processing unit at the surface. Due to the high reliability and great reach in mud-filled boreholes, mud pulse telemetry has been widely applied in drilling operations.

In the application of Measurement-While-Drilling based on mud pulse telemetry, the common problem is that the telemetry signal pressure is subject to the much stronger pump interference pressures in the whole operation frequency of mud pulse telemetry. Moreover, the distortions caused by the mud communication channel need to be equalized especially for high data rate telemetry applications. The absence of a reference signal for the pump interference, instable behavior and the need for multiple pumps in the drilling tasks make reliable and robust data telemetry much more challenging during the regular operations. The current technologies suffer from shortcomings in terms of the installation costs and the limited performance especially in terms of system parameters tracking and BER at high data rates. Concerning these issues, further studies on the adaptive telemetry signal estimation are performed to develop reliable and feasible techniques for real-world drilling scenarios.

The application of semi-blind signal processing schemes, where the data recovery is solely based on the special features of both interference and telemetry signals, is proposed and discussed in terms of feasibility constraints and tracking issue.

Different receiver architectures which rely on multichannel receivers and the training sequence facilities in the MPT system are demonstrated. An effective method of interference rejection termed as the optimal adaptive diversity combining is presented, where the co-channel interference diversity is needed to reconstruct the telemetry data. Of great importance is the simple and straightforward tracking capabilities of this scheme.

In order to fulfill the MPT requirements on adaptive interference suppression without requiring any kind of knowledge on system signals, the concept of transform domain median filtering is introduced. The application of transform domain median filtering turned out to be not only of economical interest but also allows providing knowledge on the mud channel behavior and achieves significant improvement in terms of reliable synchronization. In addition, hybrid receiver-structures are proposed, where the combination of transform domain median filtering and adaptive diversity combining schemes are investigated. Such hybrid receiver-systems not only improve the performance in terms of BER but also provide simple and reliable tracking of system parameters.

Finally, a comparison between all proposed techniques is provided to reveal their practicability and efficiency in real MPT applications. With the help of field-test data measurements, the capability of the above-mentioned schemes and the optimal MPT receiver-system have been found and validated.

Key words

Mud pulse telemetry, Semi-blind and training sequence based signal processing, Interference and channel characterization, Transform domain interference suppression, Multi-channel diversity schemes, Hybrid receivers

Contents

List of Abbreviations	VIII
1 Introduction	1
1.1 Drilling technology	1
1.2 MPT system	3
1.3 Motivation and scope	6
1.3.1 State of the art in MPT systems	8
1.3.2 Open issues	9
1.4 Dissertation overview	10
2 Statistical signal analysis	12
2.1 Analysis of telemetry signal	12
2.1.1 Digital modulation scheme	12
2.1.2 Constant modulus property	14
2.2 Analysis of interference signal	15
2.2.1 Randomly modulated periodicity	15
2.2.2 Statistical significance testing for randomly modulated periodicity .	20
2.2.3 Methods of estimating fundamental period in randomly modulated periodic signals	23
2.2.4 Summary	27
3 Blind and semi-blind signal processing	28
3.1 Blind signal processing methods and restricted applicability	28
3.2 Semi-blind signal processing methods using special properties of system signals	29
3.2.1 Constant modulus algorithm: a telemetry-based property restora- tion scheme	30
3.2.2 A multichannel semi-blind source separation method using envelope property of telemetry and interference	36

3.2.3	A single channel semi-blind source extraction method based on interference properties	39
3.3	Practicability and performance evaluation of semi-blind schemes	43
3.4	Summary and Conclusion	49
4	Reference signal-based processing schemes	50
4.1	Inferior channel estimation	50
4.2	Straightforward signal estimation	51
4.2.1	Cascade interference cancellation/equalization	52
4.2.2	Joint interference cancellation/equalization	58
4.3	Practicability and performance evaluation	61
4.4	Summary and conclusion	68
5	Interference avoidance techniques via transform domain filtering	70
5.1	A review on transform domain filtering issues	70
5.2	Application of transform domain median filtering	71
5.2.1	Simulation and experimental results	77
5.3	Hybrid schemes	82
5.3.1	Mud CIR extract via combined NCMF and CLEAN algorithm	83
5.3.2	Combined NCMF and adaptive diversity combining schemes	87
5.4	Overall performance evaluation	94
5.5	Summary	98
6	Conclusion and outlook	100
A	MIMO-CMA derivation	102
B	Simulation channels	104
B.1	Simulation channel A	104
B.2	Simulation channel B	105
B.3	Simulation channel C	106
	List of Figures	107
	List of Tables	112
	Bibliography	113

List of Abbreviations

Abbreviations

ACF	Auto-Correlation Function
ASK	Amplitude Shift Keying
AWGN	Additive White Gaussian Noise
BCPM	Binary Continuous Phase Modulation
BER	Bit Error Rate
BHA	Bottom Hole Assembly
BPSK	Binary Phase Shift Keying
BSE	Blind Source Extraction
BSS	Blind Source Separation
CCF	Cross-Correlation Function
CFR	Channel Frequency Response
CIR	Channel Impulse Response
CM	Constant Modulus
CMA	Constant Modulus Algorithm
CMF	Conditional Median Filter
CPM	Continuous Phase Modulation
DC	Direct Current
DF	Decision Feedback
DFT	Discrete Fourier Transformation
ECR	Energy Capture Ratio
EGC	Equal Gain Combining
FC	Fat-Chirp
FFT	Fast Fourier Transformation
FIR	Finite Impulse Response
FSK	Frequency Shift Keying
HOS	Higher-Order Statistic
IDFT	Inverse Discrete Fourier Transformation
IFFT	Inverse Fast Fourier Transformation
ISI	Inter-Symbol Interference
KM	Known Modulus
LMS	Least Mean Square
LMSE	Least Mean Square Error
LP	Linear Prediction
LS	Least Square
MC	Multichannel
MF	Median Filter
MIMO	Multi-Input Multi-Output
MMSE	Minimum Mean Square Error

Abbreviations

MPT	Mud Pulse Telemetry
MRC	Maximum Ratio Combining
MRE	Mutually Referenced Equalizer
MSE	Mean Square Error
MWD	Measurement-While-Drilling
NCMF	Normalized Conditional Median Filter
PCM	Pulse Code Modulation
PDF	Probability Distribution Function
PN	Pseudo-Noise
PPM	Pulse Position Modulation
PSD	Power Spectral Density
PSK	Phase Shift Keying
RE	Relative Error
RLS	Recursive Least Square
RMP	Randomly Modulated Periodic
RMS	Root Mean Square
SC	Signal Coherence
SCD	Spectral Correlation Density
SIMO	Single-Input Multi-Output
SINR	Signal-to-Interference-Noise-Ratio
SIR	Signal-to-Interference-Ratio
SISO	Single-Input Single-Output
SMI	Sample Matrix Inversion
SMNR	Signal-to-Modulation-Noise-Ratio
SNR	Signal-to-Noise-Ratio
SOS	Second-Order Statistic
SS	Signal Subspace
TB	Training-Based
TD-AS	Time-Domain Averaging Subtracting
TS	Training Sequence
VO	Valve-Off
ZF	Zero-Forcing

Chapter 1

Introduction

As a basis of this work, an introduction to drilling technology used in the oil and gas industry and telemetry systems will be given in this chapter. Specifically, the characteristics of the environment used for telemetry application is reviewed. The major problem statement, state of the art and motivation of this research will be presented. Finally the overview of the dissertation is illustrated.

1.1 Drilling technology

Supplying reliable energy is a life prerequisite. Fossil fuels such as oil and natural gas produce most of the world's energy and therefore there is an appreciable market for petroleum oil. Petroleum deposits referred to as reservoirs are trapped in earth layers with different stone characteristics, therefore they have to be recovered efficiently by drilling oil holes known as boreholes. The term *drilling technology* denotes techniques and related systems for excavating oil or gas from the reservoir. General principles of drilling technology are described briefly [78].

The primary system of oil platforms used to find geologic reservoirs as well as to create borehole in the ground is *Drilling rig*. The drilling rig refers to as all the drilling machinery and devices that are used to excavate and extract oil from the ground [24]. There are many types of drilling rigs capable of applying different drilling technologies and excavating of thousand meters boreholes. The equipment associated with a rig is to some extent dependent on the type of rig but typically includes at least some of the components illustrated in **Fig. 1.1** and explained subsequently.

A rig is basically a crane, on the *hook* of which the *drill string* is mounted, and together with *travelling block* and *drilling line* constitutes the hoisting system, which facilitates the lowering and lifting of the drill string into and out of the wellbore. The drill string is referred to as a column of *drill pipes*, in which drilling fluid can be pumped via the mud pumps down through it and circulated back up the annulus. A steel tower known as *derrick* is used for lifting and positioning the drill string and pipe laying above the wellbore and containing the machinery for turning the drilling bit around in the borehole. As the drill string goes deeper into the ground, new piping has to be screwed on the top of the drill string to keep the whole system working. At the end of the drill string, *drilling bit* is placed that breaks apart and crushes the rock formations. To provide the drill bit working at an optimum rate, it has to be pushed with a certain degree of pressure relative

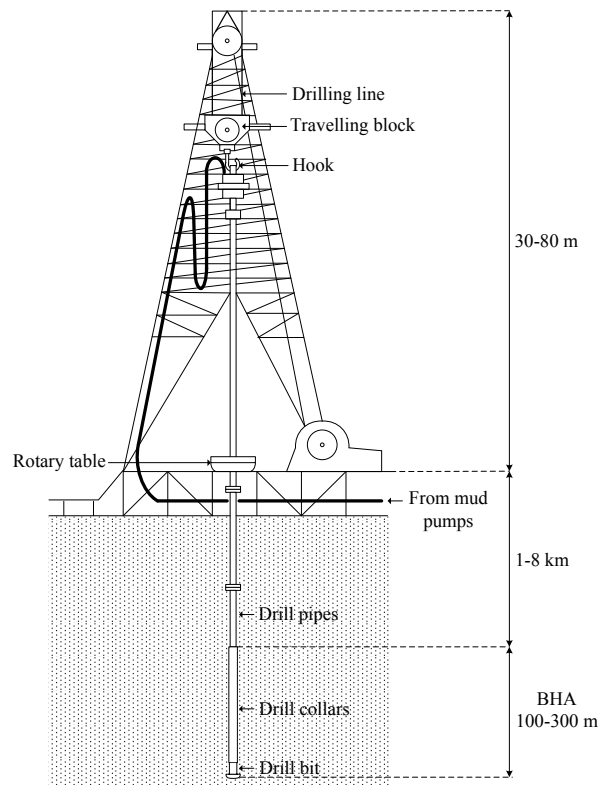


Fig. 1.1: Drilling rig

to the stone under it. Heavy, thick-walled drill pipes known as *drill collars* are used to apply weight to the drill bit [7, 24]. To drill a borehole, a mechanical device on a drilling rig provides torque which is needed to rotate the drill string. The axial motion of drill string and thus the weight on bit is controlled by the position of travelling block on the surface. The form of the drives is dependent on the system design and can be a *rotary table*, located under the working platform, or a *top drive*, suspended in the hook. A motor called *mud motor* located close to the drill bit is used for fast drilling. Large mud pumps circulate mud through the drill string and up the casing annulus, for cooling, removing the cuttings and lubricating the drill bit during the drilling task. Depending on the borehole depth, large quantities of mud are required for the drilling process. Therefore a rig has usually more than one fluid pump (three pumps are usual). In addition, directly above the drill bit and the optional motor, there are the down hole tools which allow us especially to control the drill bit and send up the borehole geometry and formation properties. Together with the drill bit and collars, they constitute *the Bottom Hole Assembly (BHA)* [7, 78].

The success of wellbore drilling operations highly depends on various real-time information about formation properties, wellbore geometry, drilling system orientation and mechanical properties of the drilling process, obtained by multiple sensors placed close to the drill bit. Therefore, in drilling technology, real-time telemetry is an important requirement to analyze and explore the well, operate the rig and reduce the costs. Utilizing *Measurement-While-Drilling (MWD)* system responds to this demand and serves as a specific feature of current techniques for drilling oil and gas wells to optimize the drilling process. The term MWD denotes the process of up-linking information between the surface and downhole. For example, the operator requires feedback from sensors located at the bottom of the hole in order to control the direction of the drill bit and ensure that the drilling proceeds

in a correct way [47].

There are several data telemetry methods developed for MWD operations, e.g. electromagnetic waves transmitted through the earth, acoustic waves travelling in the drill string, electric current transmitted through cables mounted in the pipes and pressure waves travelling in the mud column. The difference between these methods can be expressed in terms of the telemetry channel they use, the volume of information they can handle per unit time, and the distance the information can be transmitted. The latter method is generally known as *Mud Pulse Telemetry* (MPT) and due to its high reliability is by far the most applied technology in drilling operations. Achieved data rates by MPT are relative low; in return, MPT offers great reach in mud-filled boreholes. This work is carried out for the MPT systems, which is investigated in the next section [47, 24].

1.2 MPT system

The concept of *telemetry* is understood to be a process of gathering and transmitting data from downhole tools in the BHA to surface evaluation tools or computers.

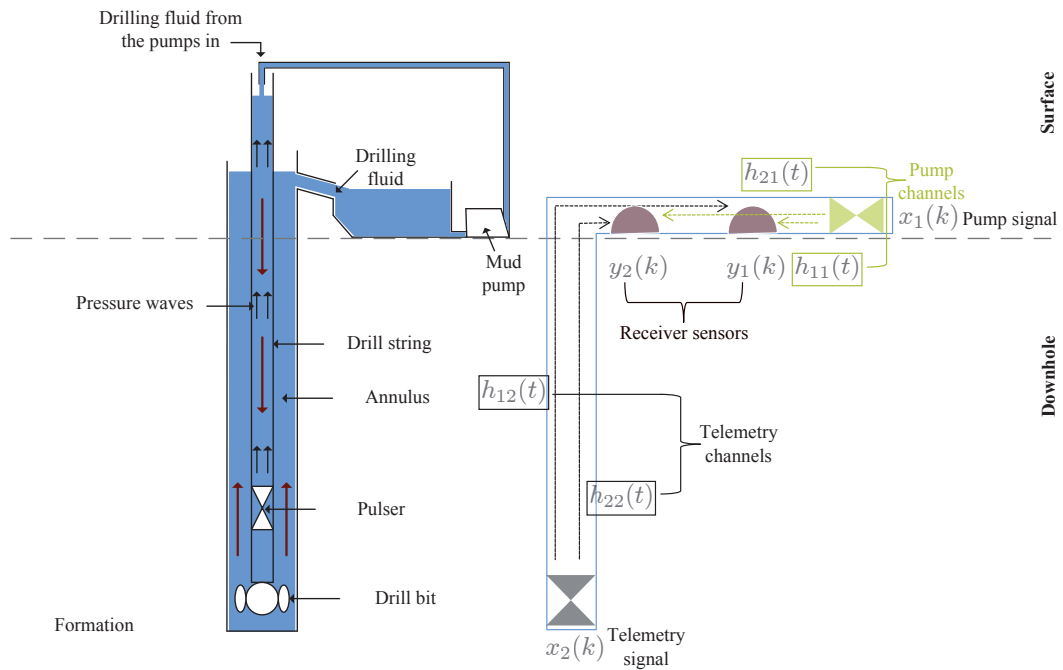


Fig. 1.2: The figure to the left depicts the general concept of MPT system. The figure to the right shows idealized MPT system model used to analyze the performance of mud pulse telemetry

As mentioned, the MPT is the most successful among the telemetry systems. Its basic principles are described precisely next.

Fig. 1.2 shows the general concept of an MPT system and idealized MPT system model used in the analysis of the mud pulse telemetry performance. The mud typically circulates

through the borehole to lubricate the drill and removes cuttings as well. Pumps generate and circulate the drilling fluid (mud) in the drill string through the nozzles in the drill bit and upwards in the annulus towards the surface. The long arrows indicate the flow of the drilling fluid. A valve pulser is located near to the drill bit, which generates pressure waves according to the information to be transmitted. There are two kinds of valve pulser, namely poppet and the shear valves which change the mud pressure by opening and closing the valve. The difference between these valves lies in the direction of the valve motion [25]. The telemetry pressure waves travelling in the drill string are depicted by two adjacent small arrows. The surface receiver system consists of sensors, which measure the pressure fluctuations, and signal processing unit. On the surface, the telemetry signal is measured by pressure transducers and processed by the signal processing unit to recover the telemetry signal and thereby information from downhole. In this regard, MPT system is a typical communication system (see **Fig. 1.2**).

The transmitter of the MPT system includes compression, encoding and modulation units. First of all, the amount of data to be transmitted is reduced by data compression. Afterwards, the compressed data are encoded so that the pulser can generate pulses representing these data. The encoding can be performed in the form of either pulse code modulation (PCM) or pulse position modulation (PPM). The encoded data are referred to as the baseband data. Finally the baseband data are modulated by a carrier to carry the transmission in higher frequencies. There are several modulation schemes such as amplitude shift keying (ASK), frequency shift keying (FSK), phase shift keying (PSK) and also continuous phase modulation (CPM) [11, 24]. After the modulation, the data or telemetry signal is ready to be transmitted.

At the surface receiver, the transmitted data through the channel is measured by pressure transducers and converted in electric signals, which can be processed to reconstruct the transmitted signal. For this, the surface receiver requires demodulator, decoder and decompression units. Similar to any kind of communication system, the common problem in data transmission in MPT is that besides the telemetry signal, various interfering signals such as the pressure fluctuations generated by the mud pumps and being referred to as the pump signal in this work¹, the excitation noise caused by the rotation of drill string and mud motors or the drilling dynamics caused by torsional oscillation of the drill string are also received at the pressure transducers. Because the pump signal pressure can be much higher than the telemetry signal pressure and pump frequencies are distributed over the entire telemetry spectrum, the pump signal is a key factor to deteriorate the communication quality in MPT [24].

The transmission bandwidth is limited up to 100 Hz due to the strong attenuation of higher frequencies by the mud and 40 bit/s is the highest data rate, which can be achieved for data transmission through the mud. The distortion caused by the communication channel is another problem to be dealt with; especially for high data rate transmission there will be severe Inter-Symbol Interferences (ISI). Therefore, high data rate and robust mud pulse telemetry is a challenging task due to the difficulty in characterizing the mud channel and the strong interference inherent to the mud pulse telemetry system. A reliable estimation of the channels for such kind of system, in which the training sequence is immersed in strong interference, seems to be a big challenge. This problem and other related issues will be discussed in the sequent chapters.

Sample measured data from test boreholes as well as commercial ones, called field-test

¹ In bore technique, the pump interference is also known as pump noise.

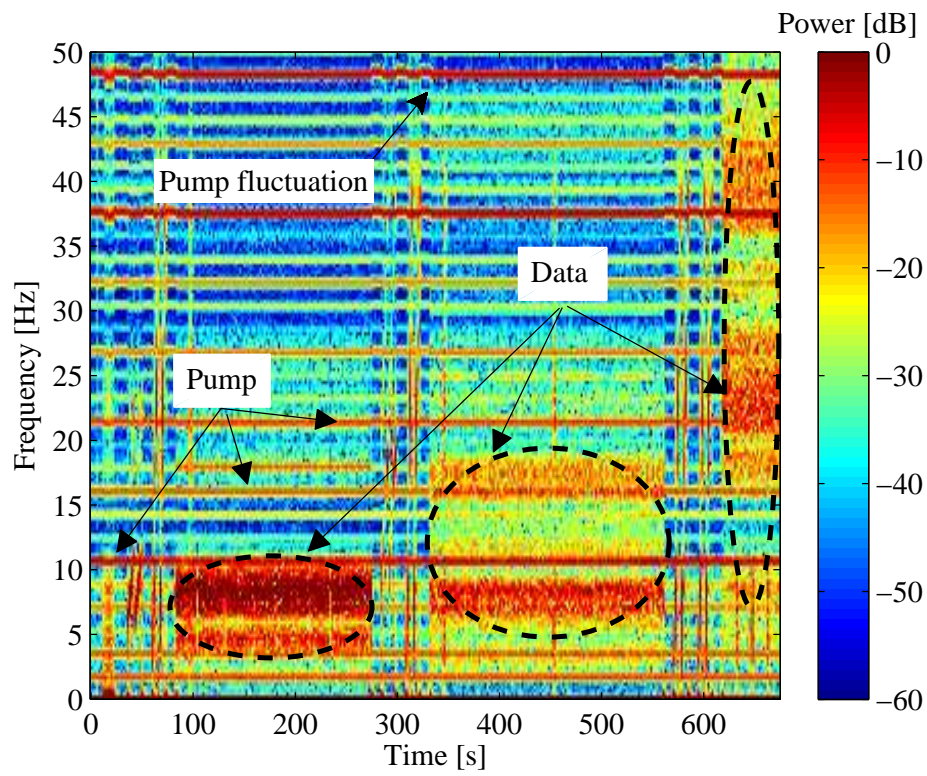


Fig. 1.3: Spectrogram of a field-test data recorded at a test borehole (horizontal lines show harmonic pump signal and labeled areas bandpass data signal)

data, facilitate analyzing the interfering signals, especially the pump signal, the behavior of the transmission channel, and reliable performance evaluation of developed algorithms. **Fig. 1.3** shows the time-frequency representation of a field-test data recorded at a test borehole.

The data telemetry in real commercial boreholes becomes more challenging due to higher number of pumps involved in drilling task and fluctuations of the pump signal caused by instable behavior of the pumps. In addition, the signal strength is much weaker and other interference sources can appear as well. **Fig. 1.4** shows the time-frequency representation of a field-test data recorded at a commercial borehole, which confirms this statement.

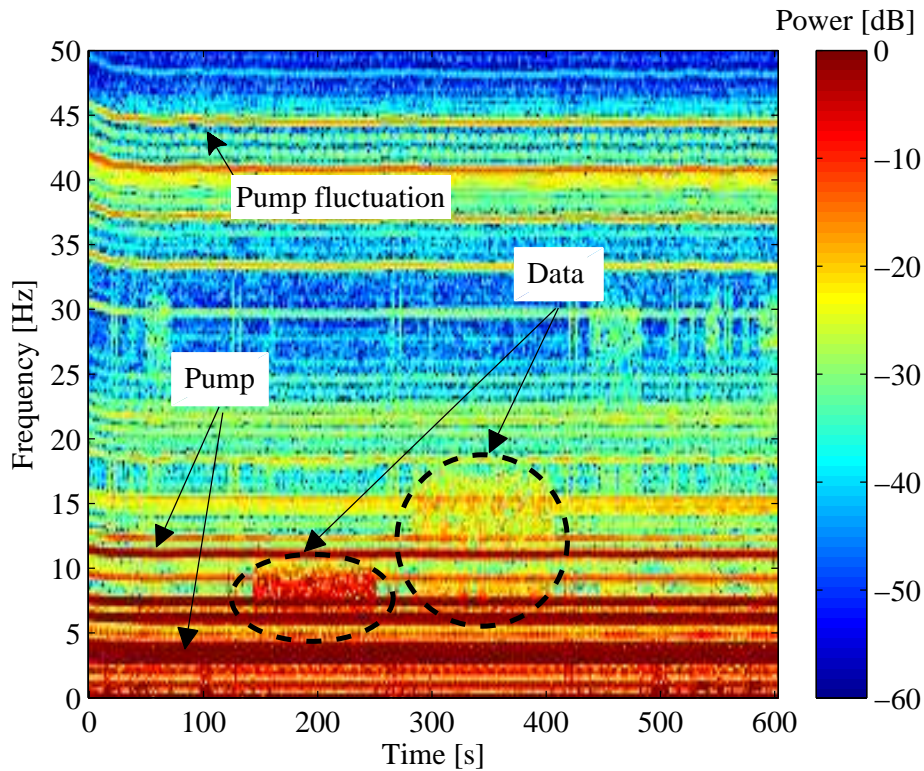


Fig. 1.4: field-test data recorded at a commercial borehole (horizontal lines show harmonic pump signal and labeled areas bandpass data signal)

1.3 Motivation and scope

Observation of the field-test data in the preceding section confirms that major distortions of the telemetry signal in an MPT system are caused by the mud pump, which called pump signal. The power of the pump signal is much stronger than the telemetry signal and is a strong interferer in the operation frequency of the MPT system. Moreover the pump signal exhibits multiple harmonics characteristic. The shape and period of the pump signal are unknown and can vary with time. The pump signal changes with the required flow rate

at the borehole, which is unpredictable². Considering this fact to assume that the pump signal is known is not realistic. The pump signal can be regarded as an ergodic process in the prescribed application. Also the pump signal can be treated as co-channel interference, arising from frequency reuse, for the telemetry signal. Considering that usually more than one pump is involved in drilling operation, dealing with the pump signal poses a great challenge in MPT.

In MPT systems, the communication channel (mud flow in drill string) is somewhat unusual. The drilling fluid is oil- or water-based and has the property of being thixotropic³[95]. Characterization of the channel has, up to now, been very difficult. The drill well can be quite long (12-14 km). Therefore the pressure pulse is strongly attenuated. Due to the reflections in the drill string and at the surface, the pulse signal suffers from multipath distortions as well. ISI arisen due to delay spread is a major limitation in MPT system and has to be also dealt for telemetry signal recovery. Another problem is the fact that the underlying pressure level varies with time as the control system on the mud pumps regulates the flow rate. The operator controlling the drilling can also adjust the flow rate as the drilling process requires it. The channel properties might be subject to some variations because of changes in mud characteristics and underlying pressure level. Due to the fact that the drilling velocity is very low, the mud channel can be considered as time-invariant. Therefore the effect of Doppler shift and Doppler spread in the transmitted signal is not significant and can be neglected.

Concerning the abovementioned effects, the received signals by two sensors are a mixture of different signals (telemetry and pump signals). The mixture is weighted and delayed corresponding to the multiple paths through which a mud pulse propagates to the receivers (see **Fig. 1.2**). Such a kind of mixture is called convolutive mixture and modeled as

$$\begin{aligned} y_1(k) &= h_{11}(k) * x_1(k) + h_{12}(k) * x_2(k) + v_1(k) \\ y_2(k) &= h_{21}(k) * x_1(k) + h_{22}(k) * x_2(k) + v_2(k) \end{aligned} \quad (1.1)$$

where $x_i(k)$, $i \in \{1, 2\}$ are the pump and telemetry signals respectively. $y_i(k)$ are the corrupted received signals and $v_i(k)$ is zero-mean additive white Gaussian noise (AWGN). $h_{i1}(k)$ represent the pump channels and $h_{i2}(k)$ the telemetry channels. To recover the telemetry signal, the signal to interference ratio (SIR) of the received signal has to be increased. This can be achieved by interference suppression. Several techniques have been investigated to suppress the pump signal, as discussed later.

In short, the common problem in the MPT applications is that the telemetry signal pressure is subject to the much stronger pump interference pressures in the whole operation frequency of the system. Additionally, distortions caused by the telemetry channel are required to be equalized, particularly in high data rate telemetry scenarios. The absence of a reference signal for the pump interference, instable behavior and the need for multiple pumps in most drilling tasks make efficient and robust data telemetry more challenging during the regular operations. Concerning these matters, developing reliable and feasible data recovery techniques for real-world drilling environments are dealt throughout this dissertation.

² Flow rate is typically fairly constant over long periods of time but may changes at any time due to the requirements of the drilling process.

³ Thixotropy is the property of certain fluids which form a gelled structure under normal condition, but flow over time when agitated or stressed [34].

1.3.1 State of the art in MPT systems

In former years, MPT systems have been further developed in terms of communication protocols and signal processing issues. The communication protocol has a further impact on the robustness and telemetry efficiency. Several proposals to describe the communication protocol have been proposed, but there is no standard specified for the MPT application. It is of great importance to consider the practicability and feasibility of the utilized protocol in real-world drilling scenarios. The data transmission protocol used in this work is specified by a startup sequence and meets the demands prescribed by the MPT application. The startup sequence includes a valve-off (VO) period, at which the valve pulser is inactive and a training sequence (TS) for telemetry signal and chirp signals proposed for synchronization.

It must be noted that such kind of training sequence is transmitted once with the exception of short synchronization chirps. In other words, no training sequence is available during the regular operation for the system related signals. The processing technique developed for data telemetry in the MPT system has been studied considering this matter. The most robust and efficient technologies require installing additional sensing elements at the pumps or employing two receiver sensors to remove the pump signal from the received signal. The concept of these techniques is briefly described as follows:

- The first technique is a pump cancellation approach based on magnetic detection and requires the pump strobe sensors to be installed in certain positions at pumps. According to the operational procedure reported in [24, 47], the successive pump strobes patterns are collected, averaged and extracted from the measured signal. To provide the pump patterns the pump strobe sensors are to be utilized at each active pump. These sensors register the magnetic changes, when the pump piston is moving under them. One pump strobe sensor is required for each pump. Usually three pumps are involved in the drilling task. This technique is quite simple for a single pump but requires high installation costs and expenses [24].
- The second technology based on a two-receiver structure is more attractive because of both economical reason and efficiency. According to this approach [24], the interference cancellation is performed by processing the signals of two receivers that are installed in certain positions at the surface of the borehole. Since the reconstruction of the pump signal is unwanted, to separate the telemetry signal from the pump signal, it is not needed to estimate the whole channels of the mixing system in **Eq. 1.1**. Using the principle of superposition $\tilde{x}_1(k) = h_{11}(k) * x_1(k)$ allows to estimate the channels between the receiver sensors $\hat{h}_{21}(k)$ during the VO phase according to

$$y_2(k) = \tilde{h}_{21}(k) * y_1(k) . \quad (1.2)$$

Based on this estimation, the pump signal can be subtracted from the measured

signal as

$$y_2(k) - y_1(k) * \hat{h}_{21}(k) = \underbrace{\left(h_{22}(k) - \hat{h}_{21}(k) * h_{12}(k) \right)}_{h(k)} * x_2(k) + v_2(k) - \hat{h}_{21}(k) * v_1(k)$$

equivalent to

$$\begin{aligned} h_{11}(k) * y_2(k) - y_1(k) * \hat{h}_{21}(k) &= \underbrace{\left(h_{11}(k) * h_{22}(k) - \hat{h}_{21}(k) * h_{12}(k) \right)}_{h(k)} * x_2(k) \\ &+ h_{11}(k) * v_2(k) - \hat{h}_{21}(k) * v_1(k) . \end{aligned} \tag{1.3}$$

In the second phase, the distortions caused by $h(k)$ are to be equalized. The equalizer estimation is performed during the training sequence phase. The estimation of the channel equalizer is done by minimizing the difference between the originally transmitted training sequence and the received equalized training sequence called error. By minimizing the mean square error, the Wiener-Hopf-Equation is derived. Stable fast recursive least square (RLS) algorithm is applied for determining the coefficient of a Wiener filter. Such kind of algorithm is numerically stable and exhibits fast convergence characteristic. Another advantage of the algorithm is being sample based, so the filter coefficient can be updated with every sample of the received training sequence [24].

The drawback of this method is that the pump cancellation is based on the initial estimation of $\hat{h}_{21}(k)$ during valve-off. By employing the superposition law, the pump signal can be removed during the regular operation. There is no possibility to update the initial estimation of the pump channel for this method. There is no efficient parameterized signal model for the pump signal. In the case of changes in the pump characteristic during the normal operation, the initial estimation becomes inaccurate and accordingly the detection performance decreases. To have an update for the initial estimation, the pulser has to be switched off, which makes tracking more complicated and cost ineffective [24].

The conclusion is that the existing processing techniques are reliant on either additional sensors of cost-intensive installation or the initial estimation during the VO phase which results in erroneous detection of telemetry data during the regular operation.

1.3.2 Open issues

As the background has shown, several open issues remain to be solved for the telemetry problem in the MPT system. In this context, the above mentioned two-receiver sensor structure has to be optimized for the tracking purpose. Notice that no training sequence is available for the system signals or the training sequence is only available as a part of system signals. Under these circumstances, an optimization of the communication quality in MPT is required. These requirements motivate a couple of fundamental research issues summarized as follows:

- Reliable tracking to maintain the system efficiency during the regular operations

- Optimal receiver arrangements being of structural efficiency and high performance in the scheme of two-receiver structure
- Efficient suppression of pump interference without any need of knowledge on MPT system signals and requirement on installing additional sensors
- Practically relevant estimation strategies, which based on the channel estimation and subsequent equalizer identification or on the straightforward equalizer estimation

1.4 Dissertation overview

The research objective presented in this thesis is primarily concerned with reliable suppression of the interference (pump signal) during regular operation and equalization of the distortions caused by the multipath in the channel. In this context, both blind and training based sequential as well as joint estimation schemes are proposed to develop robust receiver satisfying requirements of the MPT system.

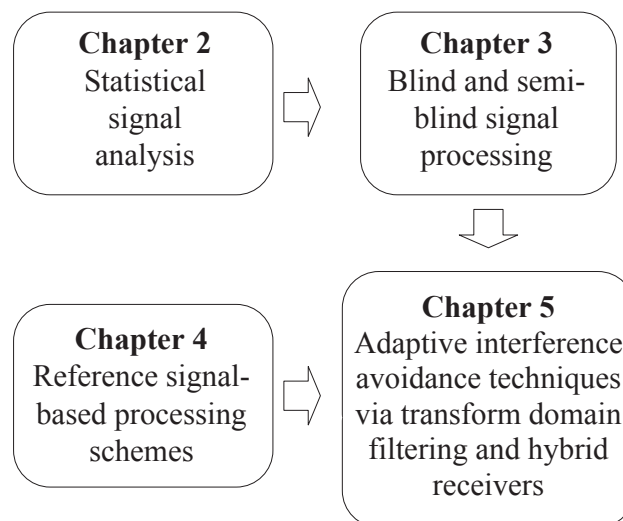


Fig. 1.5: Overview of the dissertation.

The overview of this dissertation in the respective chapters and the dependencies among them are illustrated in **Fig. 1.5**.

Chapter 2 describes statistical characteristics of system signals and methods for statistical signal analysis, which serves as a basis for developing reliable and relevant signal processing algorithms. The statistical properties of both telemetry and interference pump signals are studied. In the same chapter, it is also shown how an estimate of fundamental period of the pump signal can be obtained. This estimation provides a priori information required for semi-blind estimation algorithms in subsequent chapters.

In Chapter 3, the most common and efficient blind signal deconvolution technologies are applied to the telemetry problem for the MPT system. The advantages and drawbacks of

such kind of estimation methods are illustrated. The deficiencies of the algorithm working totally blind emphasize the necessity of exploiting some a priori knowledge for the algorithm design. A semi-blind source extraction approach based on the statistical property of the interference is presented. In addition, a new semi-blind source separation scheme is proposed, which utilizes the information on modulus or envelope of both telemetry and pump interference. Furthermore the applicability of semi-blind methods in the context of releasing the received signal from the interference is discussed.

In Chapter 4, different training-based algorithms are investigated, which serve as a reliable estimation approach using a training sequence. Furthermore, such kind of algorithms facilitates tracking by applying a decision feedback approach, where the detected data is used in turn as a training sequence to update the estimation.

Chapter 5 presents an effective scheme in the sense of adaptive removal of interference without utilizing any a priori knowledge, called transform domain median filtering. This scheme combined with training-based as well as semi-blind algorithms is presented. The advantages of combined schemes in terms of optimal combining and equalization using available receiver diversity (two-receiver system) are discussed. In addition, the combination of transform domain median filtering and CLEAN algorithm to extract the channel impulse response of the mud communication medium is proposed.

Finally, Chapter 6 provides a general conclusion with the contributions of this thesis and some research issues for future work.

Chapter 2

Statistical signal analysis

Statistical signal processing has found a wide range of applications like audio, image and array processing or digital communications. It is considered as a reliable processing approach, where no training sequence for the signals exists or the training sequence is only available for a part of system signals. Furthermore, developing relevant signal processing algorithms demands the investigation of the statistical characteristics of MPT system signals. Therefore, this chapter first gives a description of underlying MPT system signals and then investigates their statistical properties. In addition, the concept of testing the statistical significance is reviewed and utilized to derive statistical properties of the interference signal. This chapter concludes with the methods of fundamental period estimation proposed for the interference signal, which provides a-priori knowledge for designing the algorithms in the subsequent chapter.

2.1 Analysis of telemetry signal

As stated in Chapter 1, the modulated telemetry signal is generated by the mud pulser. Among the modulation schemes applicable in MPT, binary phase shift keying (BPSK) is seen as a promising scheme. However the transmitter namely sheering valve is not able to open and close the valve instantaneously and accordingly to generate discontinuous BPSK signals in practice. To take the advantage of phase modulation, another bit-to-signal mapping scheme was developed. This modulation scheme is a modified version of BPSK modulation and can be described as a continuous phase modulation (CPM) thus called binary continuous phase modulation (BCPM)[37].

2.1.1 Digital modulation scheme

An overview of PSK and CPM modulation schemes serves as a useful background for better understanding of BCPM modulation scheme in the MPT system. The general baseband expression for CPM signal is given by [59, 43]

$$x_T(t) = e^{j\varphi_T(t)} , \quad (2.1)$$

where

$$\varphi_T(t) = \alpha_F \sum_{k=-\infty}^{\infty} d_k q(t - kT) \quad , \quad q(t) = \int_{-\infty}^t s(\tau) d\tau \quad . \quad (2.2)$$

T is the symbol duration, d_k a complex discrete valued transmitted symbol and α_F modulation constant. Moreover $s(t)$ and $q(t)$ represent respectively the the frequency- and phase impulse. The information carried by instantaneous frequency is given by

$$\omega_T(t) = \alpha_F \sum_{k=-\infty}^{+\infty} d_k s(t - kT) \quad . \quad (2.3)$$

The bandpass CPM signal is calculated by

$$x(t) = \cos \left(2\pi f_c t + \alpha_F \sum_{k=-\infty}^{+\infty} d_k q(t - kT) \right) \quad , \quad (2.4)$$

where f_c is the carrier frequency. Recall $\omega_T(t) = \frac{d\varphi_T(t)}{dt}$, a rotation of carrier phase by $\pm\eta\pi$ corresponds to a frequency deviation of $\frac{\eta\pi}{T}$ from f_c . $\eta = \frac{\Delta\varphi}{\pi}$ is defined as modulation index [59, 43].

The characteristics of CPM signal depend on the modulation constant and the frequency or phase impulse. For BCPM the modulation index equals 1. The explanations described as follows. The general baseband expression for PSK signal is given by [43, 11]

$$x_T(t) = \sum_{k=-\infty}^{+\infty} |d_k| e^{j\theta_{d_k}} s(t - kT) \quad . \quad (2.5)$$

Here d_k is a complex discrete valued transmitted symbol and $s(t)$ signal pulse shape. The bandpass PSK signal is calculated by

$$x(t) = \sum_{k=-\infty}^{+\infty} |d_k| s(t - kT) \cos(2\pi f_c t + \theta_{d_k}) \quad . \quad (2.6)$$

For BPSK $\theta_{d_k} \in \{-\pi, \pi\}$ or $d_k \in \{-1, 1\}$. For generation a BCPM signal, a transition signal with half the carrier frequency $\frac{f_c}{2}$ for one carrier period $\frac{1}{f_c}$ is transmitted to maintain the phase continuity and at the same time to provide $\Delta\varphi = \pm\pi$. A binary 1 generates a phase deviation of $+\pi$ from the carrier, while a 0 a phase deviation of $-\pi$. It is obvious that the transition at the beginning of each symbol would be dependent on the value of the previous symbol. In the case of identical adjacent signals, there is no phase change and no need for transmission of the transition signal. Otherwise we have to transmit the transition signal. In other words, the signal pulse shape is longer than the symbol duration T and lasts $T + \frac{1}{f_c}$. So this concerns a partial response and control ISI case. After the first carrier period of a symbol the pervious symbol has no influence on the signal [9, 25, 59]. An example of BPSK and BCPM modulated signal are illustrated in the **Fig. 2.1**. As mentioned, in the MPT system, a BPSK signal is modified so that the generated signal equals a BCPM signal. This is achieved by the special design of the signal pulse shape. The spectral efficiency of modulation scheme is an important criterion

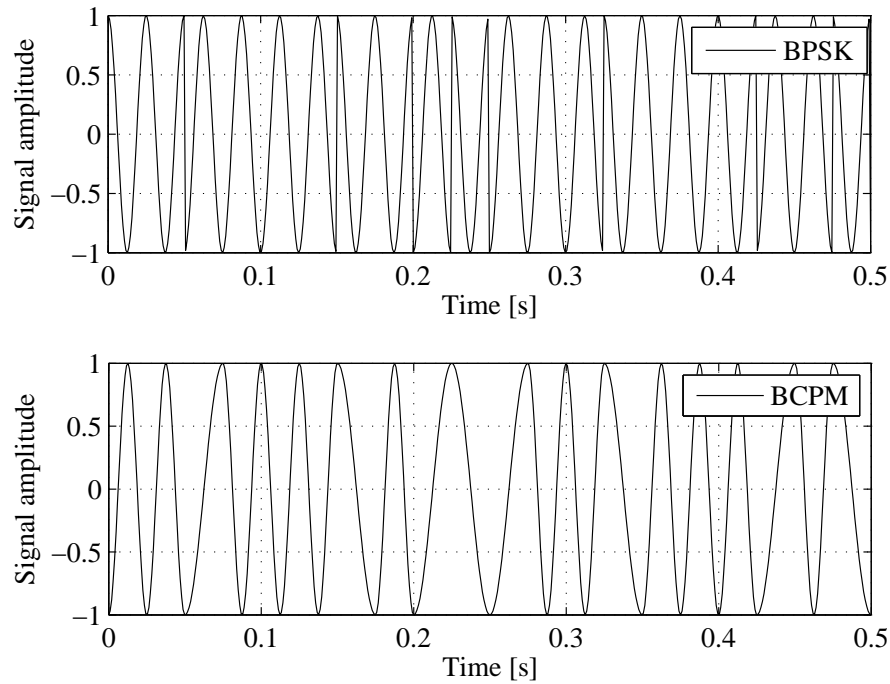


Fig. 2.1: Example of bandpass BPSK and BCPM modulated signal

to be considered. Since there is no phase discontinuity, BCPM signals, similar to CPM, have better spectral characteristics namely narrowband spectrum and low out of band fluctuation. Furthermore, for the case that equalization is necessary, in contrast to high order CPM modulation schemes, a linear equalization can be used for BCPM. The major characteristic of BCPM signal is described briefly in the following.

2.1.2 Constant modulus property

The applied modulation scheme for the telemetry signal is BCPM and similar to other phase modulated signals has the constant modulus (CM) property, also called constant envelope property. Such modulation schemes transmit a sinusoid of a constant analytic magnitude or modulus and of these signals, only the frequency or phase changes over the time. **Fig. 2.2** clarifies this property. The CM property can be utilized to reconstruct the telemetry signal in the absence of the training sequence. The main advantage of algorithms based on CM property lies in their simple implementation and efficiency, thus support the issues of this thesis [43].

Next to the CM property, BCPM exhibits cyclostationarity, due to its implicit periodicity. This can be related to its baud rate or/and carrier frequency [107]. Note that stationary signals have time-invariant second-order statistics, whereas cyclostationary signals have periodically time-varying second-order statistics. Although, this feature also provides the necessary knowledge for the reconstruction in the absence of the telemetry signals, the estimation approach is complicated, complex and offers a comparable performance with those using CM property [5]. Therefore, the concept of cyclostationarity is not considered in this dissertation.

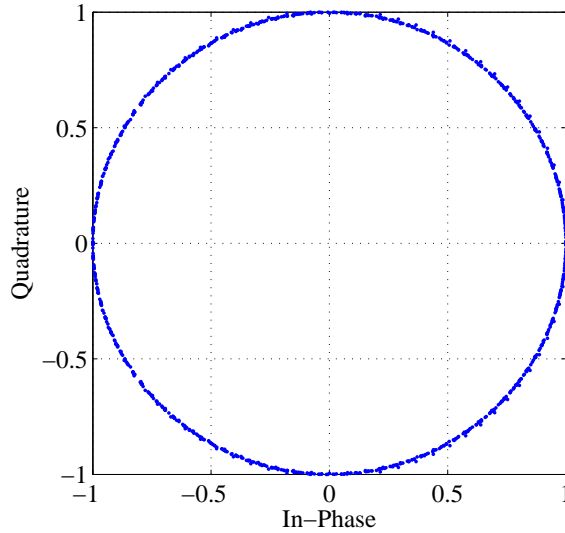


Fig. 2.2: Constant modulus/envelope property constellation

2.2 Analysis of interference signal

As stated, the pump signal is the main interference to be dealt with in MPT systems. In this context, the interference signal has to be analyzed exactly to derive its important characteristics. Interference properties are seen as a-priori knowledge, which can be utilized to develop efficient interference extraction and cancellation algorithms. Some examples of the pump signal recorded at a test borehole are illustrated in **Fig. 2.3**. The pump signal is generated by mud pumps and changes with the required flow rate at the borehole. In other words, it is generated by some nonlinear physical mechanism and has more or less stable inherent periodicity. The periodic pump signal is deterministic and predictable, but some variations, which are not deterministic, are also observable. Considering this fact, we can conclude that the pump signal belongs to a special class of signals, called randomly modulated periodic signals [71, 111, 16].

In the following the concept of randomly modulated periodicity is defined and the properties of this class of signals are addressed. Also the statistical analysis methods for such kind of signals are described. Finally using some pump signal measurements recorded at a test borehole, randomly modulated periodicity of the pump signal is confirmed.

2.2.1 Randomly modulated periodicity

The mathematical definition of a randomly modulated periodic (RMP) signal $x(t)$ of period T and K harmonic frequencies $f_k = \frac{k}{T}$ is given by [74, 71]

$$x(t) = s_0 + \frac{1}{K} \sum_{k=1}^K [(s_{1k} + u_{1k}(t)) \cos(2\pi f_k t) + (s_{2k} + u_{2k}(t)) \sin(2\pi f_k t)] \quad , \quad (2.7)$$

where s_0 is the DC part, and s_{1k} and s_{2k} are constant. The vector of modulation $\mathbf{u}(t) = \{u_{1k}(t), u_{2k}(t) : k = 1, \dots, K\}$ are of zero mean $E[u_{1k}(t)] = E[u_{2k}(t)] = 0$ and jointly

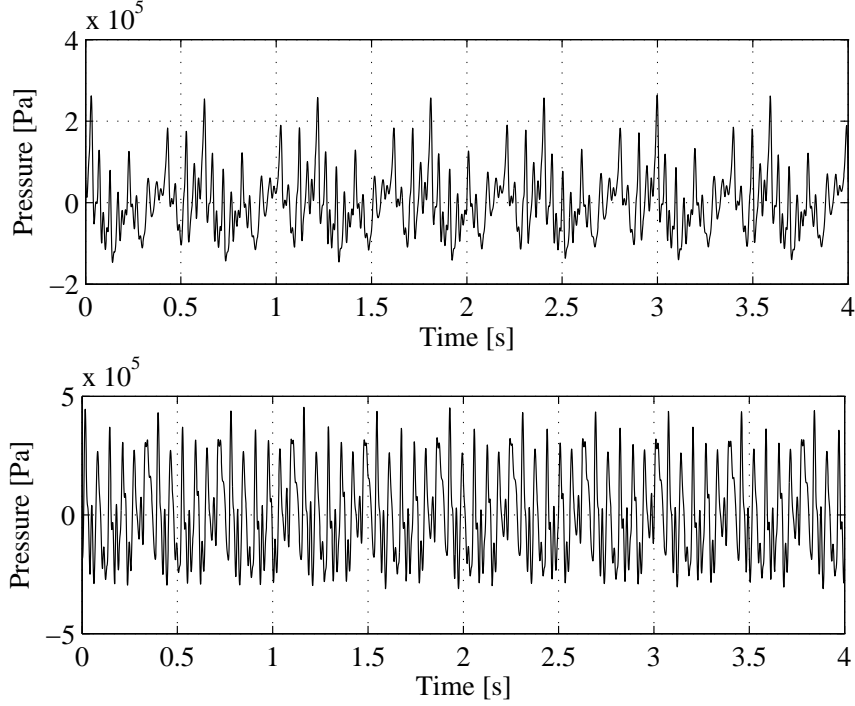


Fig. 2.3: Example measurements of pump signal

dependent random processes with finite moments, which satisfy the following conditions [71]:

- Periodic block stationary: The joint distributions of $\{\mathbf{u}(t_1), \dots, \mathbf{u}(t_m)\}$ and $\{\mathbf{u}(t_1 + T), \dots, \mathbf{u}(t_m + T)\}$ are equal for all $0 < t_1 < \dots < t_m < T$.
- Finite dependence: $\{\mathbf{u}(t_1), \dots, \mathbf{u}(t_m)\}$ and $\{\mathbf{u}(t'_1), \dots, \mathbf{u}(t'_m)\}$ are independent of each other if $t_m + D < t'_1$ for some positive D and for all $t_1 < \dots < t_m$ and $t'_1 < \dots < t'_m$.

The signal can be expressed as $x(t) = s(t) + u(t)$, where

$$s(t) = s_0 + \sum_{k=1}^K [s_{1k} \cos(2\pi f_k t) + s_{2k} \sin(2\pi f_k t)] \quad , \quad (2.8)$$

and

$$u(t) = \sum_{k=1}^K [u_{1k}(t) \cos(2\pi f_k t) + u_{2k}(t) \sin(2\pi f_k t)] \quad . \quad (2.9)$$

The mean of $x(t)$ defines the periodic part $s(t)$ and the zero mean stochastic part $u(t)$ is a real-valued non-stationary process [71, 74]. **Fig. 2.4** illustrates the periodic and stochastic parts of the pump signal recorded at a test borehole. As seen, the pump signal is characterized by both periodic and stochastic parts. In case of having more pumps to provide the required flow rate in the borehole, we will have a sum of RMP signals referred

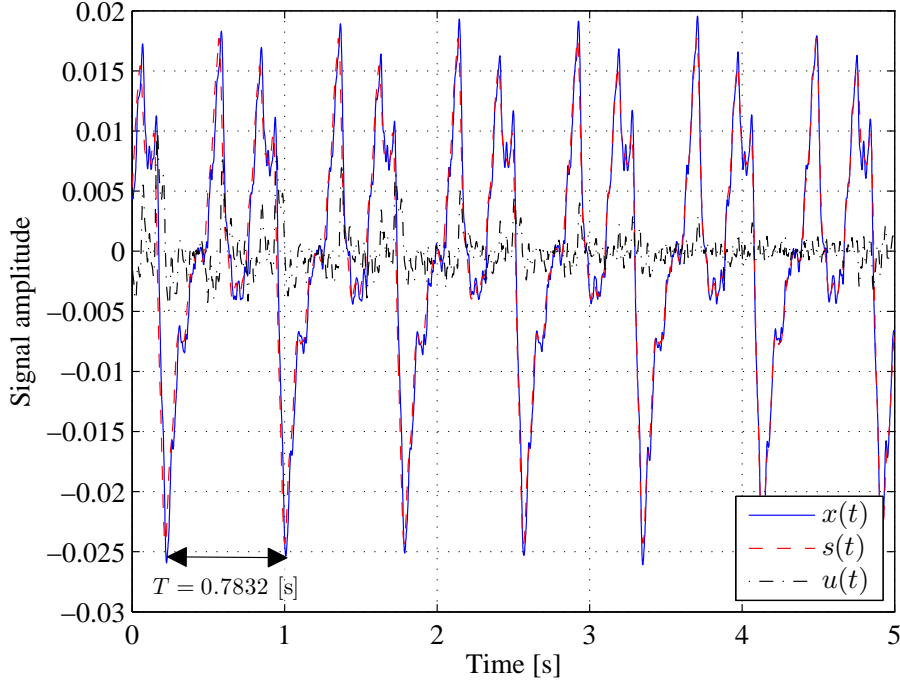


Fig. 2.4: Illustration of periodic $s(t)$ and stochastic $u(t)$ components of a sample pump signal $x(t)$

to as cumulative RMP signals and described by

$$x(t) = \sum_{p=1}^{N_p} x_p(t) , \quad (2.10)$$

where

$$x_p(t) = s_0 + \frac{1}{K} \sum_{k=1}^K [(s_{1k,p} + u_{1k,p}(t)) \cos(2\pi f_{k,p}t) + (s_{2k,p} + u_{2k,p}(t)) \sin(2\pi f_{k,p}t)] \quad (2.11)$$

and N_p denotes the number of pumps. **Fig. 2.5** illustrates a cumulative RMP signal, recorded at a test borehole and generated by two pumps.

Note that the first condition in the above definition means that $E[u(t_1)u(t_2)] = E[u(t_1 + T)u(t_2 + T)]$ if $|t_1 - t_2| < T$, but the equality is not necessarily valid if $|t_1 - t_2| \geq T$, in other words if t_1 and t_2 are in different blocks. Therefore, period block stationary is different from cyclostationary or covariance stationary [108]. The period block stationary is a subclass of cyclostationary processes. It is useful to introduce the cyclic auto correlation function and spectral correlation density functions. Recalling the conditions made on RMP signals, the auto correlation function of signal $R_x(t, \tau) = R_x(t + T, \tau)$, $|\tau| < T \forall t$ can be represented using Fourier series as [112]:

$$R_x(t, \tau) = \sum_{\alpha} R_x^{\alpha}(\tau) \exp(j2\pi\alpha t) , \quad (2.12)$$

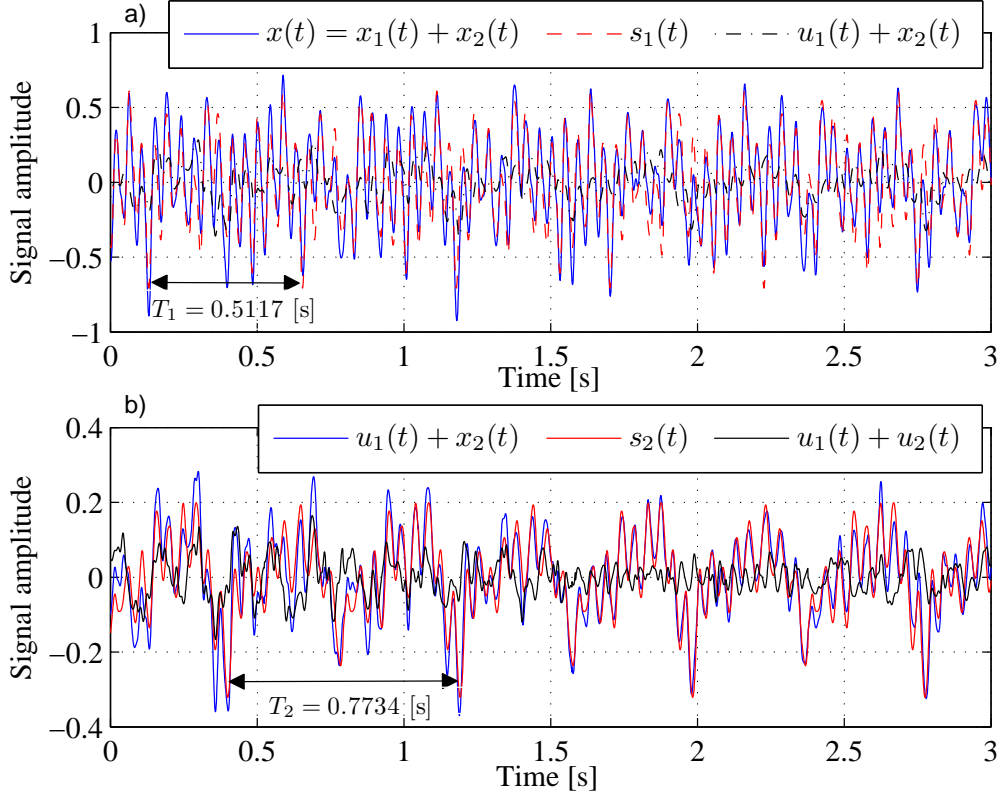


Fig. 2.5: RMP signal generated by two pumps: a) Illustration of two pumps cumulation $x_1(t) + x_2(t)$, periodic part of the first pump $s_1(t)$ with the fundamental period of $T_1 = 0.5117$ s and stochastic part of the first pump $u_1(t)$ together with the second pump signal $x_2(t)$, b) Illustration of stochastic part of the first pump $u_1(t)$ together with the second pump signal $x_2(t)$, periodic part of the second pump $s_2(t)$ with the fundamental period of $T_2 = 0.7734$ s and stochastic parts of two pumps $u_1(t) + u_2(t)$

where $R_x^\alpha(\tau)$ is the Fourier coefficients, known as cyclic auto correlation function and α its cyclic frequency. Spectral correlation density function (SCD) or cyclic spectrum $S_x^\alpha(f)$ is the Fourier Transformation of the $R_x^\alpha(\tau)$. The spectral correlation of a sample pump signal with a fundamental frequency of $f_1 = 1.25$ Hz is illustrated in **Fig. 2.6**. The spectral correlation is placed around the zero frequency and cyclic frequency of $\alpha = 2.5$ Hz, which equals the fundamental frequency multiplied by two. In terms of the central limit theorem, the second condition in the above definition guarantees that the summation of several frames of the received signal can be well approximated by a Gaussian random variable. In other words, if $D \ll T$ then $u(t)$ can be approximated by a stationary process within each period [71, 74].

After we introduced the concept of randomly modulated periodicity, the next step is to provide a measure of the amount of random variation relative to the underlying pure periodicity. Such a measure to quantify this variability is the signal coherence (SC) function. In order to define the signal coherence, the observed signal is segmented into M frames, each frame being of length T [94]. T is the period of the periodic component and assumed

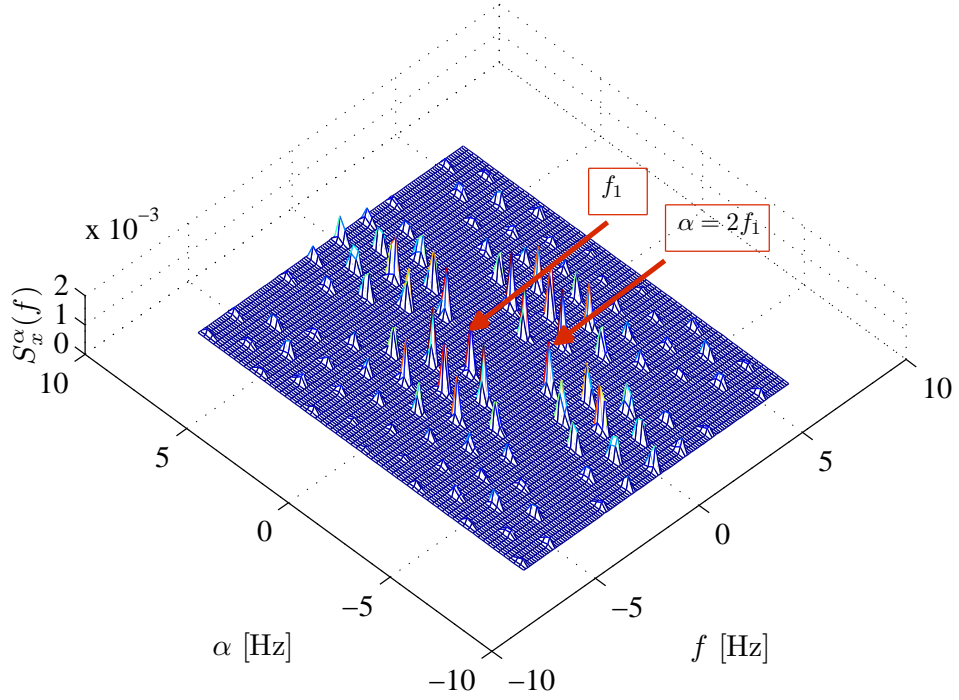


Fig. 2.6: Cyclic spectrum of a sample pump signal with a fundamental frequency of $f_1 = 1.25$ Hz and cyclic frequency of $\alpha = 2.5$ Hz

to be known at first. From now on, a time discrete description is used. Note that the signal bandwidth extends the highest harmonic f_K due to the modulations. To avoid aliasing, the sampling frequency must be greater than $2f_K$. If the sampling interval $T_s = \frac{1}{2f_K}$, $T = NT_s$ has N discrete samples $x(t_n)$ and $K = \frac{N}{2}$. The observed signal at time t_n in the m -th frame is $\{x((m-1)T + t_n), n = 0, \dots, N-1\}$ and the discrete Fourier transformation of this signal is given by [71, 74, 29]

$$\begin{aligned} X_m(k) &= \sum_{n=0}^{N-1} x((m-1)T + t_n) \exp(-j2\pi f_k t_n) \\ &= s_k + U_m(k), \quad s_k = \frac{1}{2}(s_{1k} + js_{2k}) . \end{aligned} \quad (2.13)$$

and

$$U_m(k) = \sum_{n=0}^{N-1} u_m(t_n) \exp(-j2\pi f_k t_n) . \quad (2.14)$$

The signal coherence function measures the variance of $X_m(k)$ about its mean s_k . This depends on the variance of $U_m(k)$. By the assumption of weakly stationary $u_m(t_n)$, it follows that:

$$\sigma_u^2(k) = E [|U_m(k)|^2] . \quad (2.15)$$

Now, the signal coherence function for each Fourier frequency can be defined by

$$\gamma_x(k) = \sqrt{\frac{|s_k|^2}{|s_k|^2 + \sigma_u^2(k)}} . \quad (2.16)$$

The term $U_m(k)$ is also called modulation noise. We define the signal to modulation noise (power) ratio (SMNR) as $\rho_x(k) = |s_k|^2 \sigma_u^{-2}(k)$. Thus $\gamma_x^2(k) = \frac{\rho_x(k)}{\rho_x(k)+1}$ is an increasing function of SMNR. The SMNR can be used to estimate signal characteristic [74, 61].

2.2.2 Statistical significance testing for randomly modulated periodicity

The randomly modulated periodicity of the pump signal must be verified and the concept of statistical significance testing can be used for this demand. It is supposed that an observed data meets the null hypothesis or another alternative hypothesis here RMP. Based on probabilities specified for each hypothesis in a decision rule, the validity of these hypotheses can be approved. The decision of rejecting the null hypothesis is referred to as a statistically significant result [89, 39]. More convenient is to use the equivalent test statistic (e.g. χ^2 -, t -, and F -test) instead of calculating probabilities [85]. Therefore the well-known test statistic developed for detecting hidden periodicity in data with random amplitude and modulation is applied. This test is also feasible to verify randomly modulated or varying periodicity existing in the observed data. First of all, it has to be ensured that there is no other deterministic or stochastic trend present in the data to be tested. Before performing the test statistic an estimation of s_k and $\sigma_u^2(k)$ should be done in advance. In this context, it is supposed that the fundamental period T is known and the signal over M such periods is considered, where $\{(m-1)T + t_n, n = 0, \dots, N-1\}$ is the m -th period. The unbiased estimate of the signal $\hat{s}(t_n)$ can be obtained by [71, 74]

$$\hat{s}(t_n) = \frac{1}{M} \sum_{m=1}^M x((m-1)T + t_n) , \quad (2.17)$$

and

$$\hat{s}_k = \sum_{n=0}^{N-1} \hat{s}(t_n) \exp(-j2\pi f_k t_n) \quad (2.18)$$

is the k -th DFT of $(\hat{s}(0), \dots, \hat{s}(T-1))$.

From the definition $x((m-1)T + t_n) = s((m-1)T + t_n) + u((m-1)T + t_n)$, follows

$$\hat{u}((m-1)T + t_n) = x((m-1)T + t_n) - \hat{s}(t_n) . \quad (2.19)$$

The k -th DFT component of $(u((m-1)T), \dots, u((m-1)T + T-1))$, is given by

$$\hat{U}_m(k) = \sum_{n=0}^{N-1} \hat{u}((m-1)T + t_n) \exp(-j2\pi f_k t_n) . \quad (2.20)$$

Accordingly, an estimation of the variance $\hat{\sigma}_u^2(k)$ is derived by

$$\hat{\sigma}_u^2(k) = \frac{1}{M} \sum_{m=1}^M \left| \hat{U}_m(k) \right|^2 . \quad (2.21)$$

Now, the test statistic can be preceded by evaluating these estimations. In terms of \hat{s}_k and $\hat{\sigma}_u^2(k)$ estimates, three kinds of processes are identifiable accordingly [73, 26]:

- if $\hat{s}_k = 0$ and $\hat{\sigma}_u^2(k) \neq 0$, then the process is random with no periodic structure.
- if $\hat{s}_k \neq 0$ and $\hat{\sigma}_u^2(k) = 0$, then the process is periodic (deterministic) plus stationary and ergodic noise.
- if $\hat{s}_k \neq 0$ and $\hat{\sigma}_u^2(k) \neq 0$, then the process is a randomly modulated periodic process. This means that some variation in the periodic structure about \hat{s}_k will remain, reflecting variation in the phase and amplitude of the spectral density function.

Randomly modulated periodicity hypothesis is verified by applying the test statistic on many measurements of the pump signal obtained from a test borehole. For example, the result of randomly modulated periodicity test is demonstrated in **Fig. 2.7**.

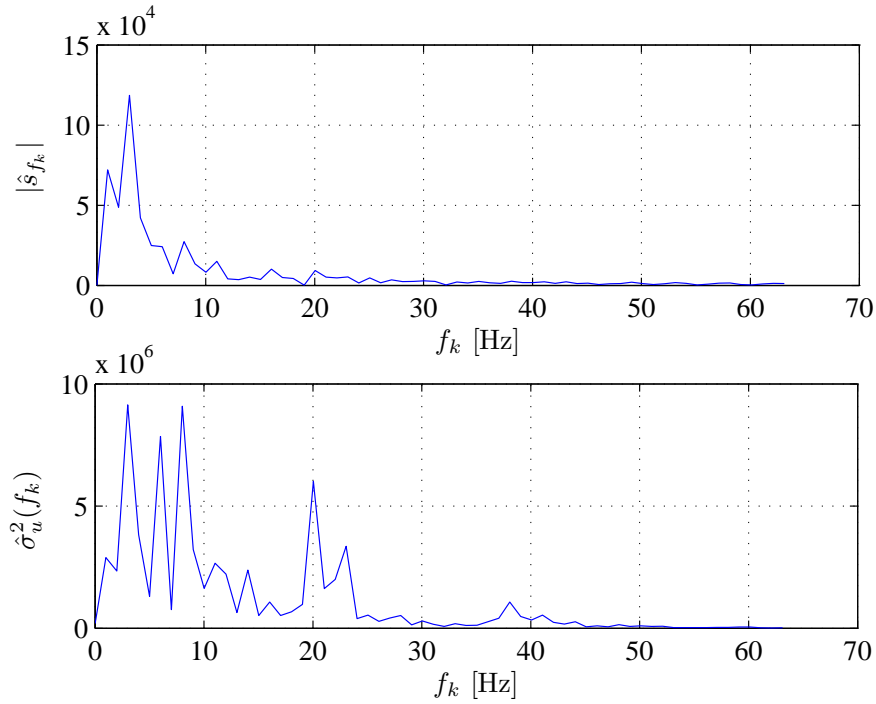


Fig. 2.7: Verification of RMP for a sample measurement of the pump signal

Having the estimations of both \hat{s}_k and $\hat{\sigma}_u^2(k)$, the signal coherence function can be also obtained by

$$\hat{\gamma}_x(k) = \sqrt{\frac{|\hat{s}_k|^2}{|\hat{s}_k|^2 + \hat{\sigma}_u^2(k)}} , \quad (2.22)$$

which again confirms the varying periodicity present in the pump signal as seen in **Fig. 2.8**.

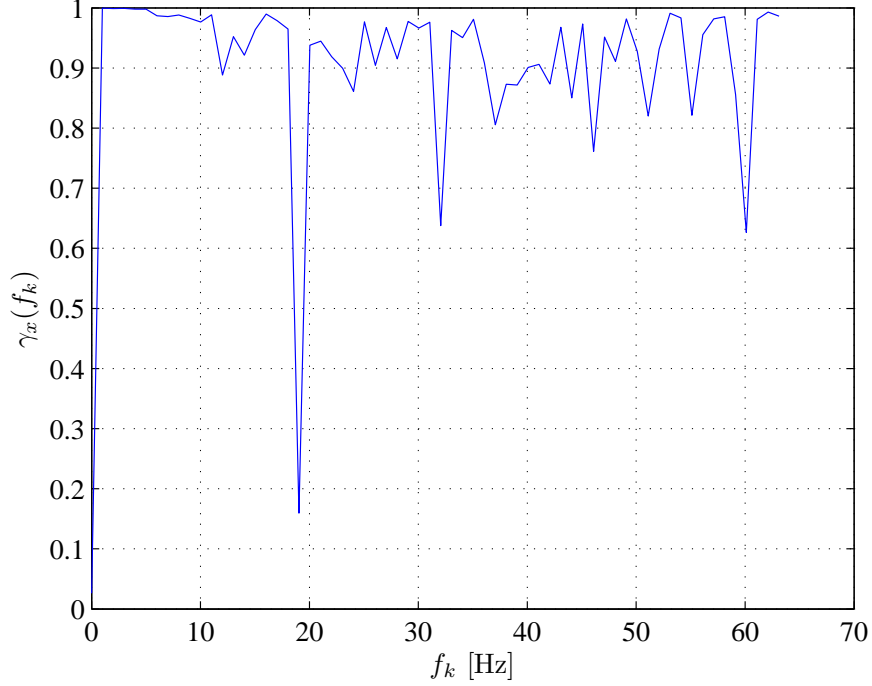


Fig. 2.8: Signal coherence estimate for a sample measurement of the pump signal

Next to the SC function, the estimate of SMNR given by

$$\begin{aligned} Z(k) &= \frac{M}{N} \frac{|\hat{s}_k|^2}{\hat{\sigma}_u^2(k)} \\ &= \frac{M}{N} \hat{\rho}_x(k) \ , \end{aligned} \quad (2.23)$$

provides the necessary statistical measure to perform test statistic for the stochastic part of pump signal. We precede by evaluating the distribution of $Z(k)$. If the stochastic term, modulation noise, is stationary, then the distribution of each $Z(k)$ is approximately distributed as Chi-Square $\chi_2^2(\lambda_k)$, where $\lambda_k = \frac{M}{N} \hat{\rho}_x^2(k)$. A sample measurement of the pump signal is used to analyze the distribution of each $Z(k)$. The result in **Fig. 2.9** illustrates an estimate of the distribution for a sample $\hat{Z}(k)$ and verifies the stationary modulation noise hypothesis.

Since $\chi_2^2(\lambda_k)$ are asymptotically independently distributed over the frequency band, the distribution of the sum statistics given by [73, 86]

$$\hat{S} = \sum_{k=1}^K \frac{M}{N} \hat{\rho}_x(k) \ . \quad (2.24)$$

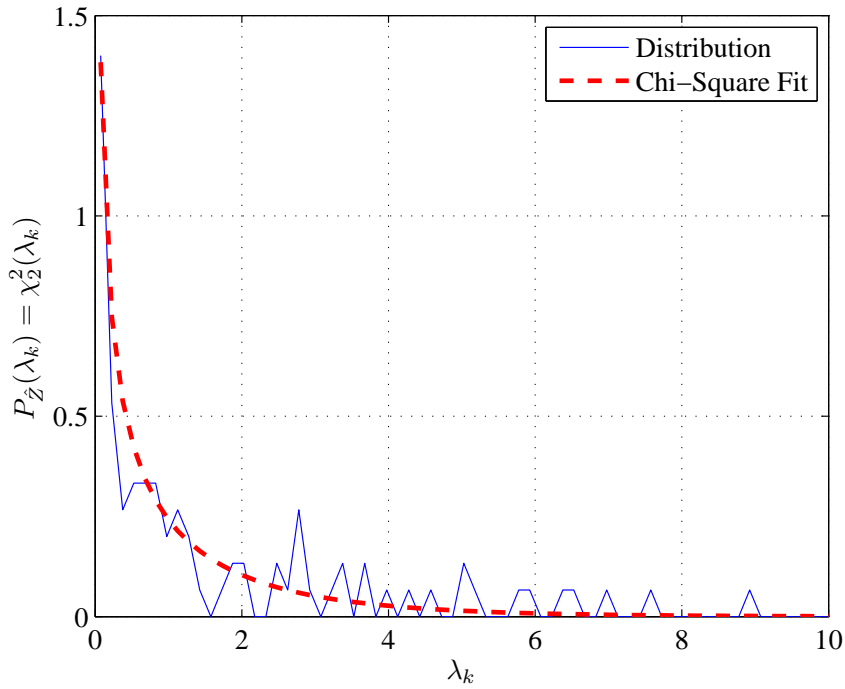


Fig. 2.9: Illustration of the modulation noise stationarity verified by the Chi-Square distribution of a sample $\hat{Z}(k)$

is approximately Chi-squared $\chi_K^2(\lambda)$ for large values of M , where $\lambda = \sum_{k=1}^K \lambda_k$. Note that \hat{S} provide not only the statistical measure for the above mentioned test statistic, but also can be used to detect the periodicity present in the signal [72]. This issue is discussed in more detail in the following.

2.2.3 Methods of estimating fundamental period in randomly modulated periodic signals

So far, it is assumed that the fundamental frequency or period of RMP signal is known, which does not hold in practice. Whereas many methods exist to estimate the fundamental period, only a few of them can be used for special class of signals considered in this thesis. In this context, two schemes are proposed to obtain the fundamental period of RMP signals.

The principles that some a-priori knowledge can be used to perform blind adaptation by maximizing some relevant correlation function [57, 41] is used here but in a different way. The first of these is to find the maximum correlation between two signals, with constraints, by applying the least mean square (LMS) scheme. These two signals are the received signal $x(t)$ and a delayed version of it, used to calculate the mean square error (MSE) as follow:

$$e = E [|x(t) - x(t - \tau)|^2] \quad . \quad (2.25)$$

The range of delays depends on the pump type applied in the field and is documented

in the instructions manual. An estimate of the fundamental period can be obtained by calculating e_i for each delay τ_i and finding the least mean square error (LMSE) according to

$$\hat{T} = \arg \min_i e_i . \quad (2.26)$$

The performance of this approach is tested on measurements produced by one pump with variable flow rate (see **Fig. 2.10**). **Fig. 2.11** demonstrates capability of the algorithm to estimate and track the fundamental period of the pump in **Fig. 2.10**. The estimation efficiency depends on the accuracy of constraints in specifying the range of delays or the length of estimation window. Long sized estimation windows not only increase the processing time but also result in false detection of the fundamental period.

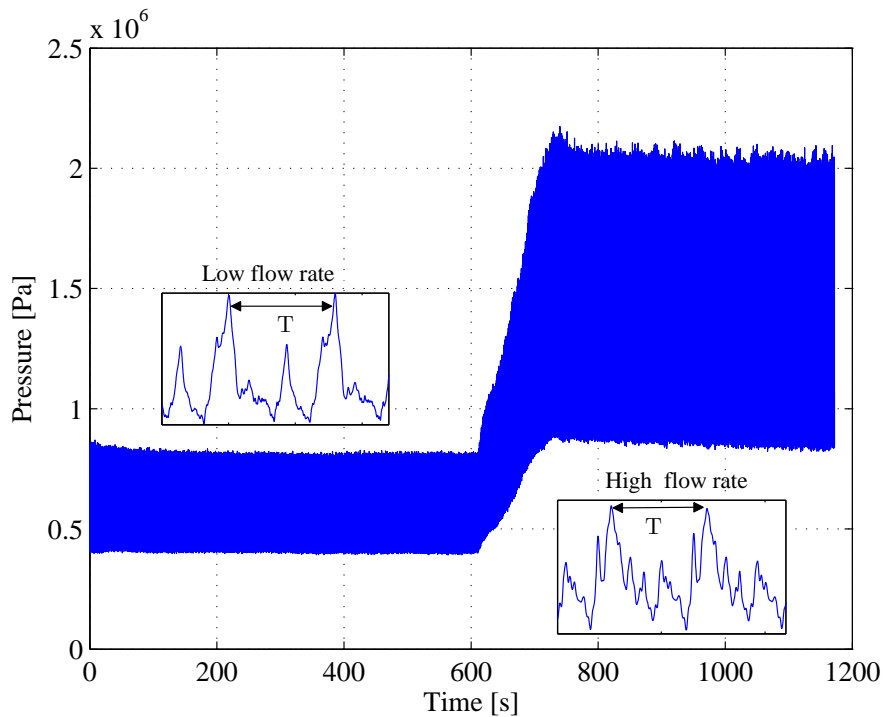


Fig. 2.10: A sample pump signal measurement with variable flow rate

The second principle is to apply the Chi-squared statistics for detecting the presence of a hidden periodicity in the signal [73]. Traditionally, for the estimation a sweep of trial fundamental frequencies is made over the frequency band to find the maximum value of sum of modulation noise in frequency domain \hat{S} . The frequency, at which the maximum yields, delivers the estimate of the fundamental period. Here, a range of trial fundamental periods $T_i \in \{T_{min}, T_{max}\}$ instead of a sweep of trial fundamental frequencies, is used for the straightforward estimation. Now, the estimation process can be done by estimating \hat{S}_i for each trial period T_i and finding the maximum as described by

$$\hat{T} = \arg \max_i \hat{S}_i . \quad (2.27)$$

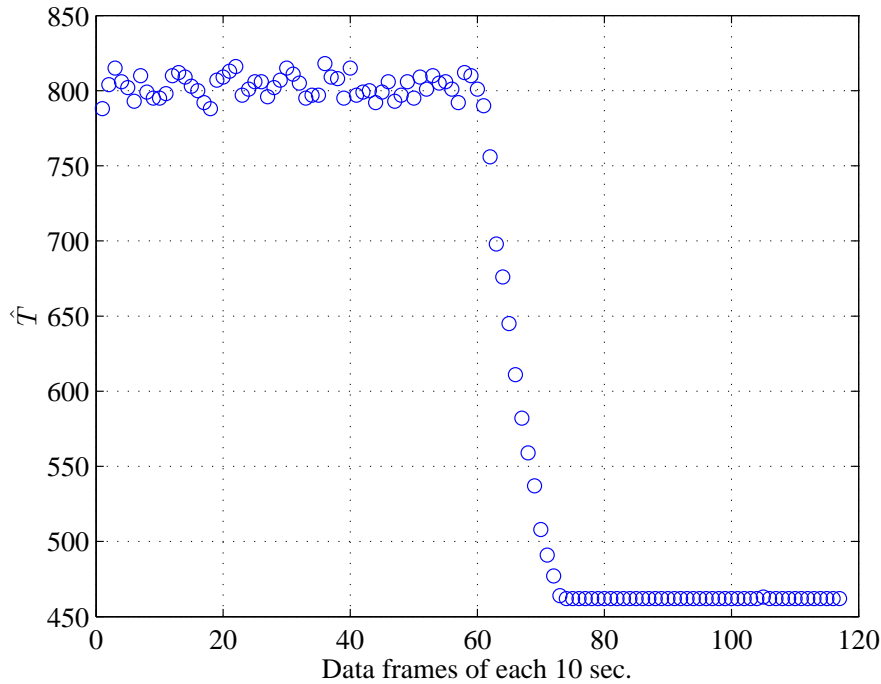


Fig. 2.11: Estimation/tracking results of fundamental period for a sample pump signal measurement with variable flow rate

The estimation result can be approved by calculating the p -value¹ tail probability of the maximum. If the p -value of the maximum S is small enough, then we can claim that the signal is RMP and its fundamental frequency is detected correctly.

All described methods have their own advantages and drawbacks. Whereas the second approach promises successful detection of single and multiple pump fundamental periods even in the presence of the telemetry signal and other noise signals, the first scheme offers simple implementation and comparable efficiency, but its applicability is limited to the detection of the fundamental period of a single pump signal.

The estimation performance of the approach based on Chi-squared statistics is tested using some pump signal measurements. Note that the measurements are performed with a constant flow rate. At first, the fundamental period is obtained for sample measurements consisting of the pump signal and measurement noise (AWGN). The estimation results in terms of frequency/counts of the maximum illustrated in **Fig. 2.12** verify the presence of periodicity giving an estimate of fundamental period. Also the estimation is performed for sample measurements of the pump signal generated by two pumps plus measurement noise. According to the estimation results shown in **Fig. 2.13** the periodicity is caused by two RMP processes giving an estimate of their fundamental periods.

Finally **Fig. 2.14** shows the estimation result of the fundamental period for the case that the measured signal is a convolutive mixture of the telemetry and pump signals. For this experiment the telemetry to pump signal ratio is -10 dB and the carrier frequency and

¹ The p -value measures, how much statistical evidence exists. For example, the p -value of a test of hypothesis is the smallest value that might lead to reject the null hypothesis or to support the alternative hypothesis [31].

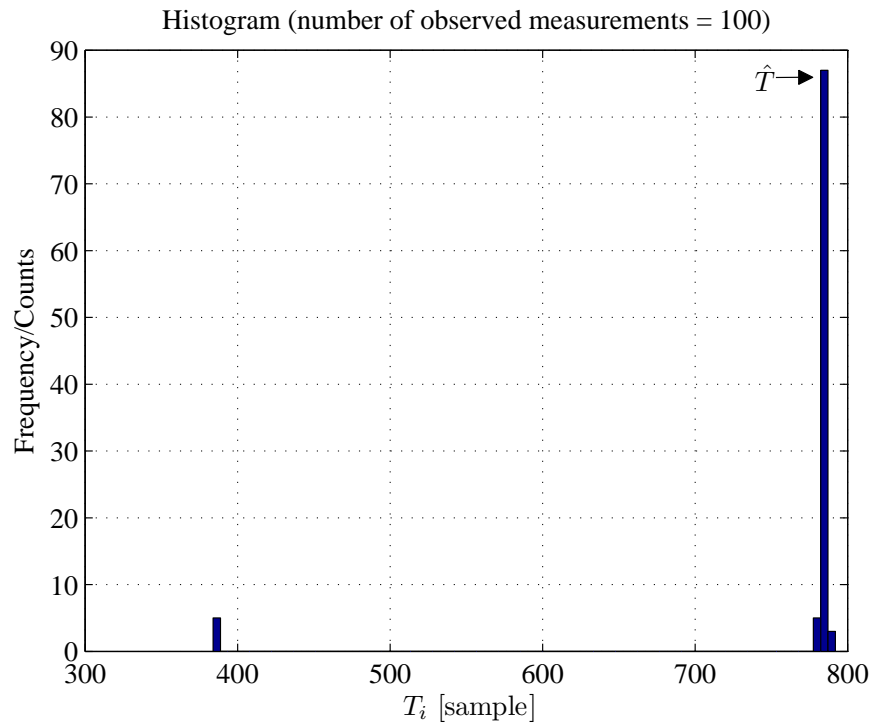


Fig. 2.12: Estimation of the fundamental period for a sample measurement of the pump signal

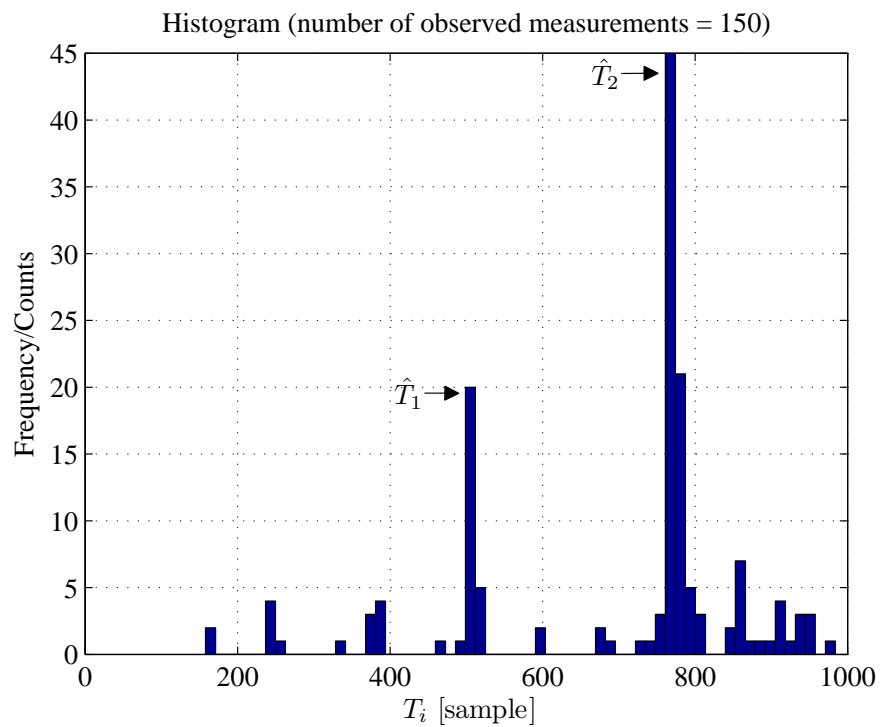


Fig. 2.13: Estimation of the fundamental periods for a sample measurement of the pump signal generated by two pumps

data rate are 9 Hz and 3 bit/s respectively.

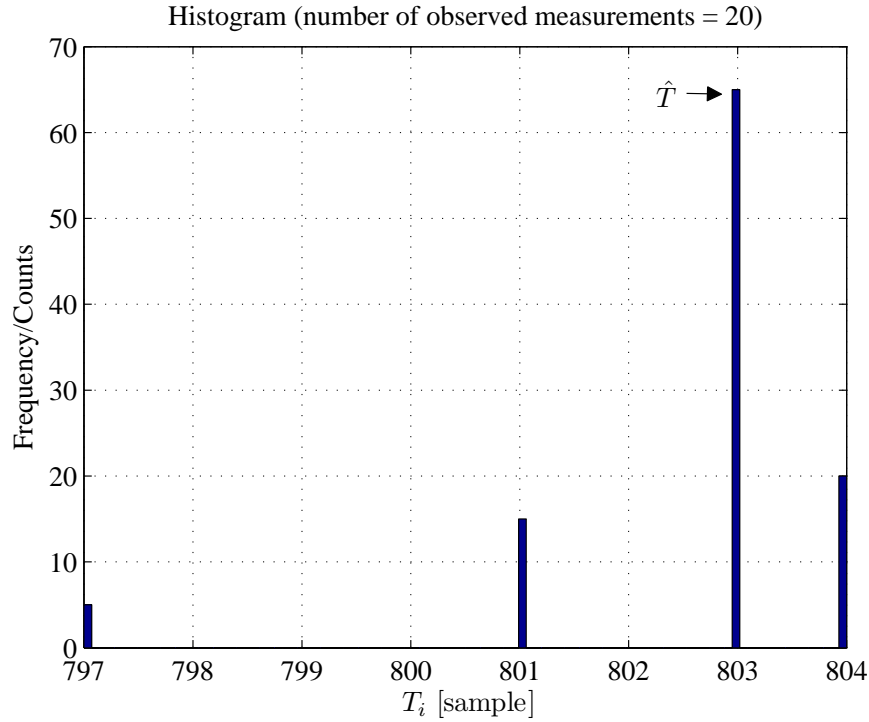


Fig. 2.14: Estimation of the fundamental periods for a sample measurement of the pump signal from the convolutive mixture of telemetry and pump signals

2.2.4 Summary

The modulation scheme and statistical property of the telemetry signal is reviewed in this chapter. It has been shown that the interference pump signal is a RMP signal and has deterministic periodic and stochastic random parts. Based on this investigation the estimation methods of fundamental period of RMP pump signal are proposed and evaluated. Whereas the measurements evaluation has shown the effectiveness of proposed methods in providing a reliable estimation, both schemes have an estimation delay of at least 10 s. Therefore it is a challenging task to provide a continuous estimate of the fundamental period as well as to track its fast fluctuations. Although both schemes can be applied for estimating the pump fundamental period, the trade-off between estimation accuracy and estimation delay has to be taken care of.

The estimate of the interference fundamental period and the knowledge on important characteristics of both telemetry and interference signal provides some basis for developing signal extraction and separation algorithms in Chapter 3. This includes the algorithm design based on the single and/or two-receiver structures.

Chapter 3

Blind and semi-blind signal processing

As stated, little or no priori information on the MPT system and related signals is available. When starting the project related with this dissertation the utilized protocol was specified by a startup sequence, including no training sequence for the telemetry signal. Even though such kind of facility is meanwhile embedded in the startup sequence, it is not supported during the regular operation. Moreover by using a blind approach, there is no need for training sequence, and thus the transmission data rate can be increased. From the signal processing point of view, blind source separation and extraction algorithms are seen as the enabling technology needed to solve the underlying signal detection problem. Therefore, this chapter gives at first a brief introduction on the concept of blind signal processing and demonstrates its feasibility constraints in the MPT application. Apart from that, the investigations in Chapter 2 lead to the development of semi-blind methods, which will be dealt with in this chapter. In this context, two consecutive strategies are proposed, in which both telemetry and interference characteristics are utilized. Consequently, via measurements obtained from test boreholes, the performance and practicability potential of the proposed schemes for telemetry signal estimation purposes in the MPT scenario is demonstrated and compared.

3.1 Blind signal processing methods and restricted applicability

Blind techniques which follow a separation or extraction¹ procedure find application in the scenario, where each received signal at a sensor array contains a mixture of signals from different sources and is processed to recover the source signals from the mixed observation. The term blind refers to that the characteristics of the transmission medium and the source signals are not known a priori. There are various areas, where blind processing technology is utilized, e.g. biomedical signal processing, speech processing, data communications, and sonar and radar technology. In many cases, it is desired to recover all source signals or at least one from the received mixtures. Moreover, it may be desired to find out how the source signals are mixed to obtain information about the transmission medium [68]. As mentioned in Chapter 1, an MPT system can be considered as a convolutive mixture of telemetry and pump signal. Therefore the problem of separating and

¹ Parallel or serial signal recovery

extracting a convolutive mixture is considered. Note that estimating the mixing process in general introduces not only the ill-posed estimation problem² but also the instable matrix inversion problem [79]. Therefore, recovery of the signals based on blind estimation of the mixing process is not advantageous especially in practical application. In the MPT scenario, since the main objective is to recover the telemetry signal, it is sufficient to estimate the separation or extraction filters. In general, there are two estimation criteria based on second-order statistics (SOS) and higher-order statistics (HOS) [17]. The estimation task requires some assumption on the source signals. The general assumption is that the source signals are independent of each other or at least uncorrelated, in addition to the assumption on the spatial diversity required in convolutive mixtures [62, 28, 106]. The estimation methods based on HOS minimize second and fourth-order dependence among the source signals and additionally require the condition of non-Gaussianity for successful separation of the underlying signals [79, 2, 3]. Among several HOS estimation methods kurtosis is a popular measure of non-Gaussianity.

Several blind estimation methods based on SOS and HOS have been developed and applied to audio separation tasks [96, 50, 83]. Among them a frequency-domain SOS-based scheme employing non-stationarity and a time-domain HOS-based method using least square kurtosis fits also to the MPT system [17, 18]. It is useful to note that the SOS-based estimation using cyclostationary belongs also to relevant schemes but the performance is poor [79]. The key concepts of these methods are described in [17, 18]. Main issues such as performance evaluation of the proposed algorithms in terms of SIR, the choice of optimal separation filter length and convergence are studied. The results are shown that the SOS-based scheme is stable, but suffers from slow convergence. In contrast, the HOS-based scheme converges very fast, but is instable and thus not suitable for practical applications. More important is the poor performance of both schemes in very low SIR scenarios of MPT, where the estimation of telemetry signals includes some residual pump signal [17, 18].

Therefore, blind estimation technologies using either SOS or HOS are not feasible for reliable signal recovery in the MPT applications. It is reasonable to apply algorithms utilizing additional a priori information about the characteristic of the system signals, which will be discussed in more detail in the following.

3.2 Semi-blind signal processing methods using special properties of system signals

The inefficiency and moderate performance of totally blind schemes provide the motivation to further investigate semi-blind signal processing issues in MPT application scenarios. The term semi-blind denotes that a priori information about the transmitted signal is available and can be utilized for signal recovery. Such a kind of algorithm comes from the field of mobile communications, where the transmitted signal is modulated and thus has some special features in contrast to audio signals. Based on the special properties of MPT system signals investigated in Chapter 2, semi-blind estimation methods are proposed in this chapter. The constant envelope property of the telemetry signal motivates

² Ill-posed problems refer to as problems which solution either is not unique or does not depend continuously on the data. If a problem is ill-posed, then it is challenging to obtain a numerical solution [77].

investigation of constant modulus algorithm (CMA). According to the ability of CMA of correcting the multipath and co-channel distortions on constant modulus (envelope) signals, their application in the mud pulse environment is investigated. According to the Multi-Input Multi-Output MIMO structure of MPT system, this chapter gives an introduction on constant modulus (CM) array filtering. Accordingly a MIMO decorrelation CM array filtering, which utilize both CM telemetry property and knowledge about the pump fundamental period, is proposed and its efficiency in terms of joint source separation and channel equalization is demonstrated. Based on the investigation in Chapter 2, it is possible to provide an estimation for fundamental period of the pump signal. Having such knowledge, leads to the development of a semi-blind signal extraction approach. Afterwards, the efficiency and practicability of this approach in the context of MPT applications is demonstrated. This chapter concludes with a performance comparison of the semi-blind signal processing methods.

3.2.1 Constant modulus algorithm: a telemetry-based property restoration scheme

One of the most famous algorithms for semi-blind signal reconstruction is the class of constant modulus algorithms (CMA's). One issue would be to apply the CMA for adjusting a finite impulse response (FIR) filter adaptively in such a manner that the output of the filter provides a corrected received signal. Another issue would be the application of CMA for separation of co-channel signals by an adaptive array [52, 32]. Since distortions of the telemetry signal is mainly caused by the co-channel pump signal, the first issue is briefly reviewed, which serves as a background for the main investigation of the second issue in this section. In this context, the key concept of CMA is described. Afterwards the algorithm performance in terms of convergence and stability is investigated via both simulations and field-test data.

3.2.1.1 Key concept

The class of CMA is usually based on an instantaneous gradient-search routine for minimizing a stochastic cost function, which penalizes the modulus deviation of the received signal $y(k)$ with respect to the known modulus of the transmitted signal $x(k)$, which is assumed to be scaled so that $|x(k)| = 1$. The block diagram of **Fig. 3.1** shows the general structure of the CMA.

Referring to the notation in **Fig. 3.1**, the cost function is defined by [69, 52]

$$J = \frac{1}{4}E \left[(|z(k)|^2 - 1)^2 \right] . \quad (3.1)$$

Here E denotes statistical expectation and the filter output $z(k)$ (complex in general) is expressed by $z(k) = Y^T(k)\mathbf{w}(k)$, where $Y(k) = [y(k) \ y(k-1) \ \cdots \ y(k-L+1)]^T$, $(\cdot)^T$ denotes transpose and $\mathbf{w}(k)$ is a $L \times 1$ vector including the filter coefficients at the time instant k . The filter coefficients are adjusted so as to minimize the cost function using a stochastic gradient decent method:

$$\mathbf{w}(k+1) = \mathbf{w}(k) - \mu \nabla_{\mathbf{w}} J \quad (3.2)$$

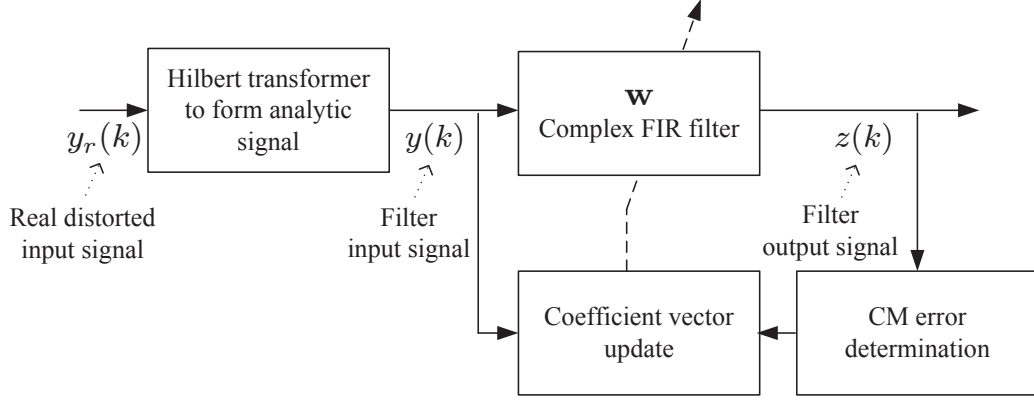


Fig. 3.1: General structure of the constant modulus adaptive algorithm

with

$$\begin{aligned}
 \nabla_{\mathbf{w}} J &= \frac{1}{2} E \left[(|z(k)|^2 - 1) \nabla_{\mathbf{w}} (\mathbf{w}(k)^H Y^*(k) Y^T(k) \mathbf{w}(k)) \right] \\
 &= E \left[(|z(k)|^2 - 1) Y^*(k) Y^T(k) \mathbf{w}(k) \right] \\
 &= E \left[(|z(k)|^2 - 1) z(k) Y^*(k) \right] .
 \end{aligned} \tag{3.3}$$

Here μ is the step size, $(\cdot)^*$ and $(\cdot)^H$ are complex conjugate and complex conjugate transpose operators. The adaptation algorithm which minimize the cost function mentioned above with respect to \mathbf{w} is obtained by replacing the true gradient $\nabla_{\mathbf{w}} J$ with an instantaneous gradient estimate $\hat{\nabla}_{\mathbf{w}} J = (|z(k)|^2 - 1) z(k) Y^*(k)$ as follows [52, 12]:

$$\mathbf{w}(k+1) = \mathbf{w}(k) - \mu (|z(k)|^2 - 1) z(k) Y^*(k) . \tag{3.4}$$

The CMA is typically applied on the equivalent baseband signal (after demodulation), or with complex filter coefficients before demodulation. Under real system consideration prescribed by the application scenario, it is desirable that the CMA accepts real data input and real filter coefficients. On this account, a version of CMA employing real arithmetic is also considered, whereas the analytical received signal is generated and used for the updating of the filter coefficients. In the context of real CMA, the constant modulus refers as the constant envelope. The cost function for the real CMA case can be written as [69]

$$J = \frac{1}{4} E \left[(|z_+(k)|^2 - 1)^2 \right] ; z_+(k) = z(k) + j\hat{z}(k) , \tag{3.5}$$

where $z_+(k)$ denotes the analytical description of the received signal and is generated by means of Hilbert Transformation [63]. The update equation for real CMA is expressed by

$$\mathbf{w}(k+1) = \mathbf{w}(k) - \mu (|z_+(k)|^2 - 1) z(k) Y(k) . \tag{3.6}$$

Since some modulation schemes e.g. BPSK modulated signals have the constant envelope property at least at the baud intervals, envelope is measured only at the baud intervals, known at the receiver [33, 53]. In other words, a cognitive constant envelope correction is conducted, due to the fact that some information available at the receiver, namely transmission data rate and sampling rate, are used in the adaptation process.

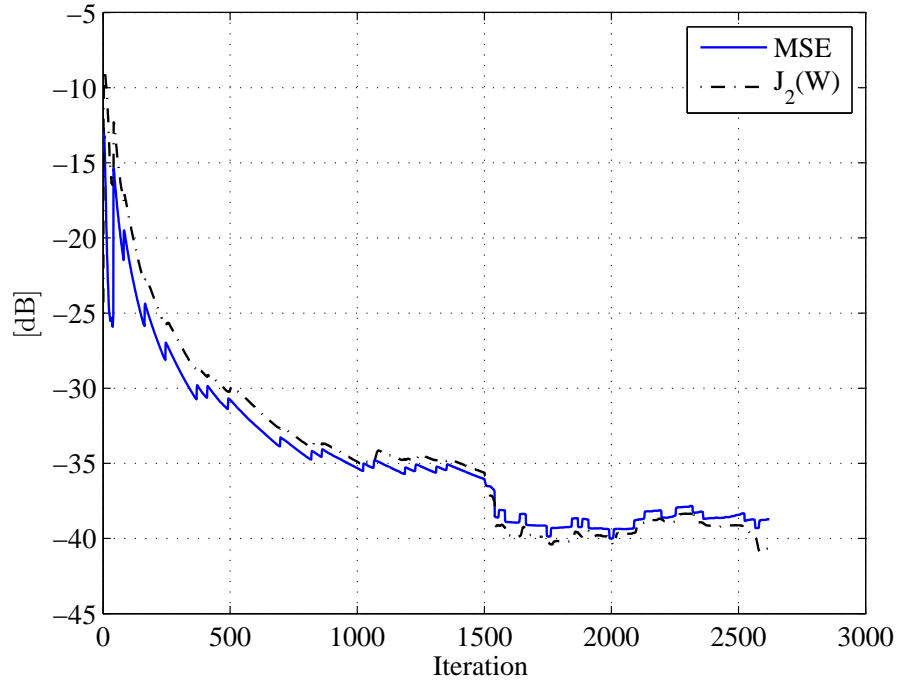


Fig. 3.2: Error course in MSE and cost function of CMA

Usually mean square error (MSE) between the transmitted signal and the estimated version is used as the measure of the performance. This is impossible in real application scenarios, where the transmitted signal is unknown. Thus the cost function in **Eq. 3.5** serves as a measure of CMA performance [23]. In case of global convergence, the course of error in MSE equals to the one in CMA cost function (see **Fig. 3.2**).

3.2.1.2 CMA Performance in terms of convergence and stability

In this section a brief summary of CMA performance to compensate the disrupted signal by multipath and additive interference is presented.

Multipath The ability of CMA to correct multipath distortions caused by the channel has been addressed in many papers [51, 14, 75], in which the scenario where the channel mostly consists of only a few paths is considered. The performance of CMA is channel-dependent. To verify this, the algorithm is simulated for frequency-flat and selective fading cases and the performance function J is plotted as a function of adaptation time in **Fig. 3.3**. As seen, the algorithm cannot effectively compensate the effect of multipath for different fading cases. The algorithm requires a few number of equalizer taps and indicates high convergence rate in frequency flat fading channels. In contrast, in frequency selective multipath channels, a higher number of equalizer taps is required and the convergence speed is low [52, 75].

More evaluation of the algorithm property is performed on a set of low data rate field-test measurements. The bit error rate (BER) results are analyzed in some cases. First, the CMA performance compared with the equalization method using a fat-chirp of 2 s

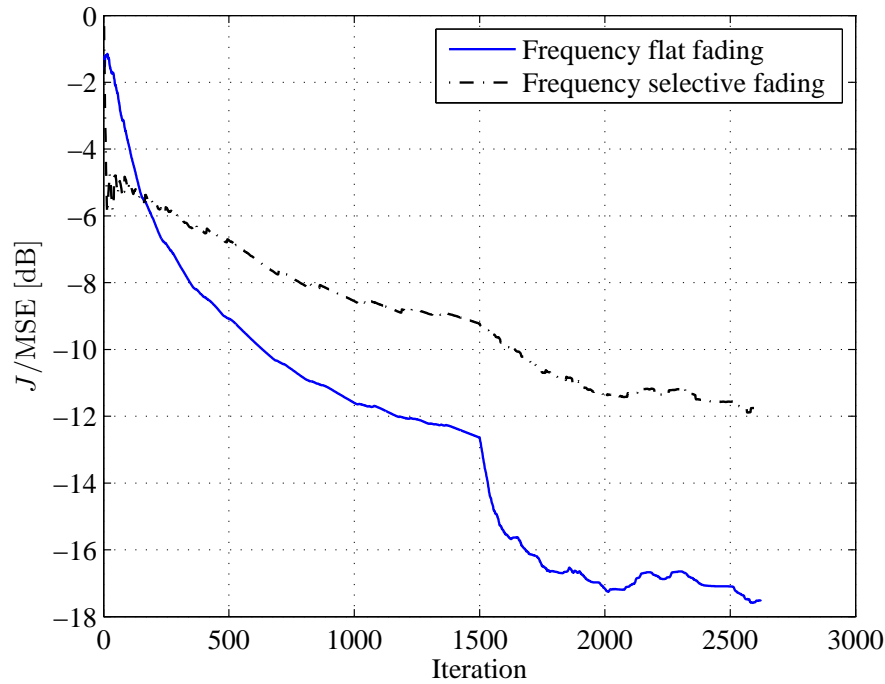


Fig. 3.3: Error course as a function of J vs. adaptation time for different fadings

duration as a reference signal to confirm whether or not CMA actually compensates for the channel effects. From the results in **Fig. 3.4** it is seen that the CMA algorithm delivers the same BER performance as the chirp-based one and even better for some field-test data. The reason for the poor performance of chirp-based equalization scheme is the insufficient chirp duration used for the training [98]. The second step in evaluating the CMA performance is to show how adaptation constant μ and filter length L adjustment affect the performance of CMA. The examination results are illustrated in **Fig. 3.4**. It can be observed that the algorithm is stable for very small step size/adaptation constant and it is unknown for what values of step size and equalizer length the algorithm becomes unstable [52, 75].

The advantages of CMA are the adaptive tracking and simple implementation. The drawbacks of CMA are the phase roll³ problem and appropriate choice of adaptation constant, which is a big challenge to practical applications.

Additive interference The concept of constant modulus approach can be used to deal with some kinds of interferences as well [52, 98]. Of particular interest are interferences caused by additive white Gaussian noise (AWGN) and pump signals. At first the behavior of CMA in the presence of AWGN at different SNRs is examined and illustrated in **Fig. 3.5**. As seen, the initial convergence performance is not affected severely by AWGN at the receiver, but the amount of modulus variation which can be reduced is limited. In other words, the residual error is increased at lower SNRs [52].

Examination of CMA's properties in the presence of pump signal (**Fig. 3.6**) shows that

³ The constant modulus processor can introduce an arbitrary phase shift to the signal of which the constant modulus criterion is still satisfied [52].

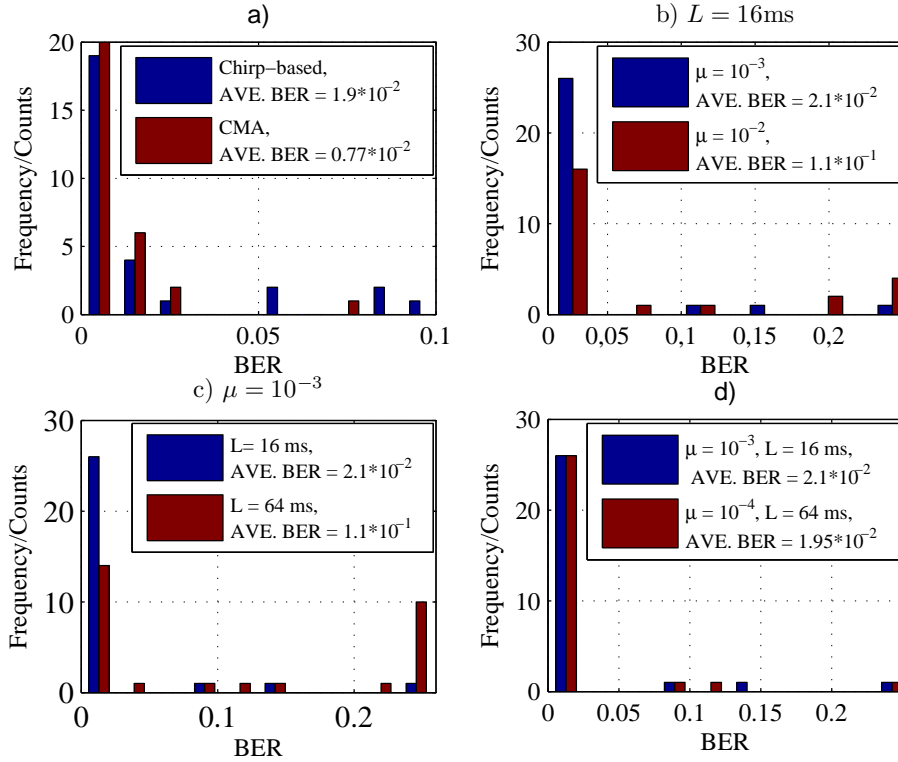


Fig. 3.4: Overall performance evaluation of CMA algorithm (a) BER comparison between the chirp-based equalization and CMA , b) , c) and d) the effect of step size and filter length adjustment on the BER performance)

not only the reduction amount of modulus variation, but also the initial convergence performance is affected at different SIRs [52, 54, 98].

The reason is that the underlying pump interference as shown in Chapter 2 consists of multiple sinusoidal interferers. Generally, for such interferers the CMA performance is constrained by signal capture effects due to the nonlinear nature of the algorithm. If the interferer becomes stronger than the desired signal, the algorithm tends to capture the interferer and reject the desired signal [52]. Therefore, applying CMA in realistic system scenarios like MPT with strong interferers requires external control and additional utilities, e.g. a prior information about the interference or multiple receiver structure to merge the CM concept with the spatial diversity scheme [109, 92, 54]. Another phenomenon to be noticed in this context is the notching compromise, where the algorithm avoids to completely notch out the interferer and attempts to compromise between reduction in modulus variation caused by the interferer and distortion of desired signal due to the notching [52].

Since the main target in MPT systems is to suppress the strong pump interference signal, in the following the issue of CM array filtering is addressed briefly and extended using additional knowledge of the pump signal.

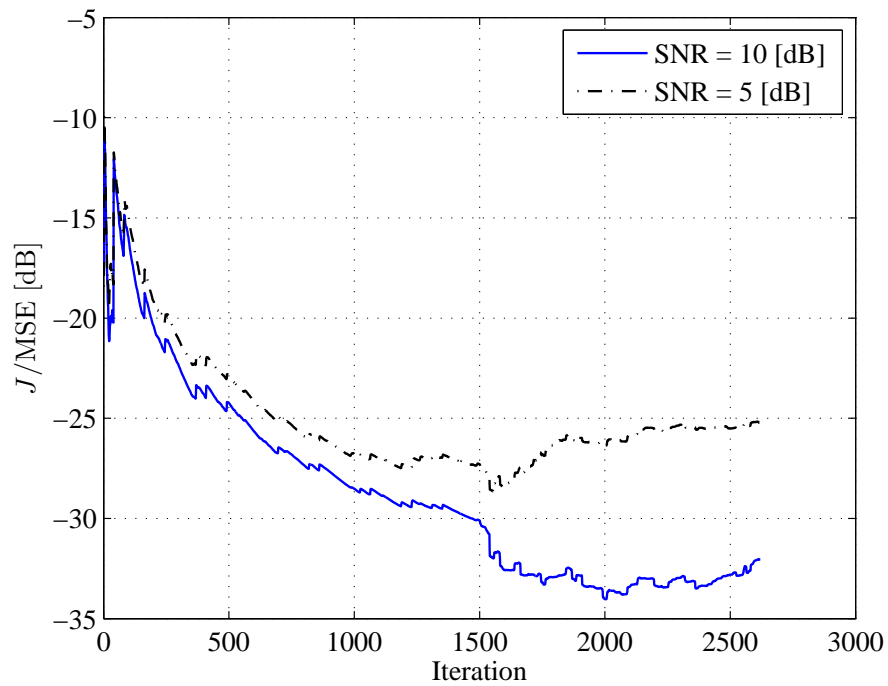


Fig. 3.5: Error course as a function of J vs. adaptation time in the presence of AWGN for different SNRs

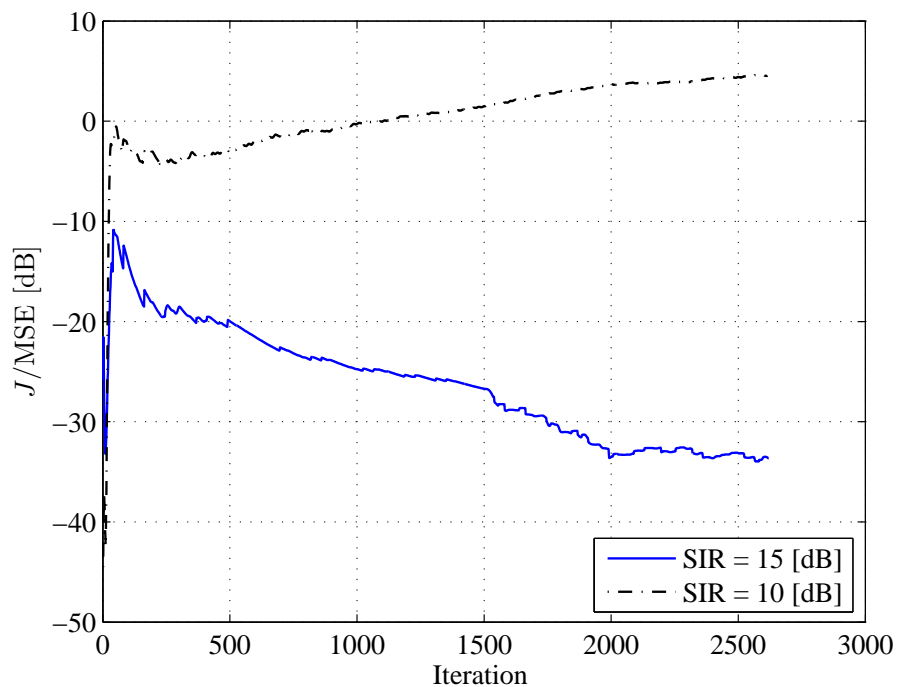


Fig. 3.6: Error course as a function of J vs. adaptation time in the presence of pump signal for different SIRs

3.2.2 A multichannel semi-blind source separation method using envelope property of telemetry and interference

As the background has shown, both multipath propagation and additive interference disrupt the constant envelope property of the received signal. In addition, the capability of CMA in capturing telemetry or suppression of the interferer depends on SIR, the filter initial condition and the adaptation constant. Of particular importance is the tendency of the algorithm in capturing the strongest signal. Based on the motivation in Subsection

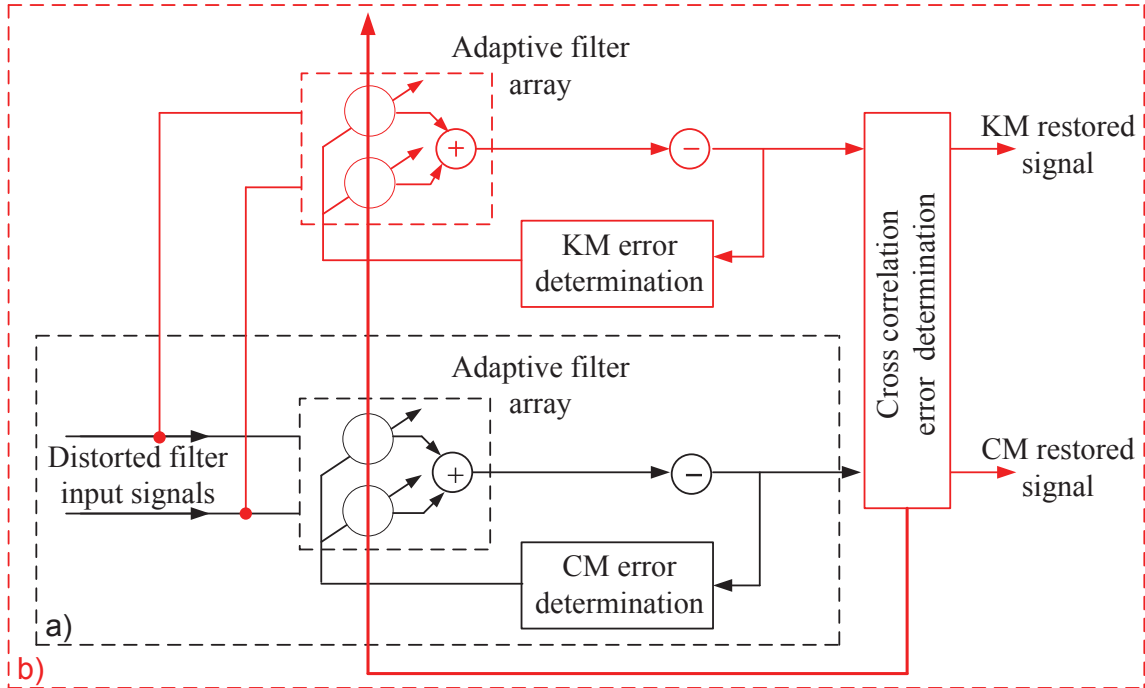


Fig. 3.7: Conceptual scheme: a) CM array filtering, b) Extended MIMO decorrelation filtering

3.2.1.2, an extended version of CMA is proposed by utilizing a two-receiver structure and specifying a new cost function [46, 52, 84]. As shown in Chapter 2 the main part of the pump signal namely deterministic part can be estimated. The details on the estimation procedure will be demonstrated in the sequel. Accordingly, we have an estimate of the pump signal envelope. The basic idea is introduced by a combined cost function, which on one hand penalizes the deviation from the constant modulus of the telemetry signal as well as known modulus (KM) of the pump signal and on the other hand minimizes the cross correlation between the reconstructed telemetry and pump signals [56, 53]. The proposed semi-blind source separation (BSS) approach can be seen as the extension of constant modulus array filtering and considered as a kind of joint interference rejection and signal reconstruction scheme [109, 23]. Multiple receiver array applications aim to find methods of training the array to have high gain towards the signal of interest, which is done blindly based on CM property of the signal of interest and where the array is adapted to minimize the deviation from the constant modulus [46, 4]. The concept of both CM array filtering and the extended MIMO decorrelation scheme is illustrated in Fig. 3.7.

For better understanding the mathematical description of the proposed scheme, the receiver structure is modeled as a linear 2×2 MIMO-system (see **Fig. 3.8**). We denote by

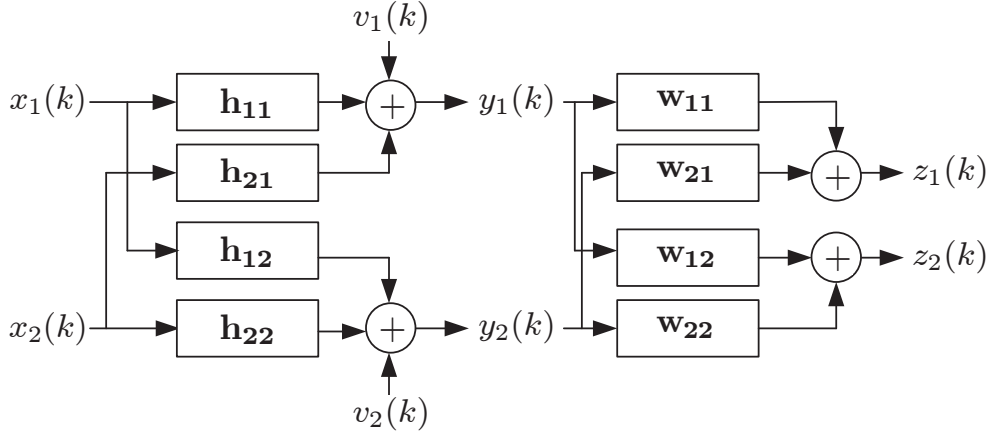


Fig. 3.8: linear 2×2 MIMO-system model of the extended MIMO decorrelation scheme

$x_j(k)$, $j \in \{1, 2\}$ the j -th transmitted signal. $y_i(k)$, $i \in \{1, 2\}$ are the corrupted signals at channel output i and $v_i(k)$ is zero-mean additive white Gaussian noise at the i -th receiver. $z_j(k)$ is the j -th equalizer output at time instant k . \mathbf{h}_{ij} , $j \in \{1, 2\}$, $i \in \{1, 2\}$ are $N \times 1$ vectors standing for the channel of length N from the input j to the output i . \mathbf{w}_{ij} , $j \in \{1, 2\}$, $i \in \{1, 2\}$ are $L \times 1$ vectors containing the equalizer coefficients of the i -th receiver to j -th equalizer output. The discrete-time signal received at the i -th receiver and the j -th equalizer output can be expressed as below respectively [56, 38, 20]:

$$y_i(k) = \sum_{n=1}^N \sum_{j=1}^2 h_{ij,n} x_j(k-n) + v_i(k) , \mathbf{h}_{ij} = [h_{ij,1}, \dots, h_{ij,N}]^T , \quad i \in \{1, 2\} , \quad (3.7)$$

and

$$z_j(k) = \sum_{l=1}^L \sum_{i=1}^2 w_{ij,l} y_i(k-l) , \mathbf{w}_{ij} = [w_{ij,1}, \dots, w_{ij,L}]^T , \quad j \in \{1, 2\} . \quad (3.8)$$

Since the telemetry signal has the constant envelope and the envelope of the pump signal $|A(k)|$ can be estimated, the cost function to be minimized can be expressed as [56, 38, 20]

$$J = E \left[(|z_1(k)|^2 - |A(k)|^2)^2 \right] + E \left[(|z_2(k)|^2 - 1)^2 \right] + 2 \sum_{l,n=1, n \neq l}^2 \sum_{\tau=\tau_1}^{\tau_2} |R_{ln}(\tau)|^2 , \quad (3.9)$$

where $R_{ln}(\tau)$ is the cross-correlation between the reconstructed telemetry signal $z_2(k)$ and the pump signal $z_1(k)$, defined as $R_{ln}(\tau) = E [z_l(k) z_n^*(k-\tau)]$. τ_1 and τ_2 are integers to include the available delays between the two signals. The first two terms of the cost function penalize the deviation from the modulus, while the last term penalizes the correlation between the reconstructed signals. The cost function J can be minimized using a stochastic gradient descent method as follows [12]:

$$\mathbf{W}(k+1) = \mathbf{W}(k) - \mu \nabla_{\mathbf{W}} J , \quad (3.10)$$

where μ is a positive step size and ∇ is the gradient operator. \mathbf{W} represents the matrix of equalizer coefficients given by

$$\mathbf{W} = \begin{bmatrix} \mathbf{w}_{11} & \mathbf{w}_{12} \\ \mathbf{w}_{21} & \mathbf{w}_{22} \end{bmatrix}$$

\mathbf{W} which minimize the cost function can be obtained by calculating

$$\nabla_{\mathbf{w}} J = \begin{bmatrix} \frac{\partial J}{\partial \mathbf{w}_{11}} & \frac{\partial J}{\partial \mathbf{w}_{12}} \\ \frac{\partial J}{\partial \mathbf{w}_{21}} & \frac{\partial J}{\partial \mathbf{w}_{22}} \end{bmatrix}$$

as follows, whereof a simplified description of $z_j(k) = \sum_{i=1}^2 Y_i^T(k) \mathbf{w}_{ij}$ with $Y_i(k) = [y(k) \ y(k-1) \ \dots \ y(k-L+1)]^T$ is used [56, 38, 20] (see **Appendix. A**):

$$\frac{\partial J}{\partial \mathbf{w}_{i1}} = 4E \left[(|z_1(k)|^2 - |A(k)|^2) z_1(k) Y_i^*(k) \right] + 4 \sum_{n=1, n \neq j}^2 \sum_{\tau=\tau_1}^{\tau_2} R_{jn}(\tau) E [z_n(k-\tau) Y_i^*(k)] \quad (3.11)$$

and

$$\frac{\partial J}{\partial \mathbf{w}_{i2}} = 4E \left[(|z_2(k)|^2 - 1) z_2(k) Y_i^*(k) \right] + 4 \sum_{n=1, n \neq j}^2 \sum_{\tau=\tau_1}^{\tau_2} R_{jn}(\tau) E [z_n(k-\tau) Y_i^*(k)] \quad (3.12)$$

The step size should be small; otherwise the algorithm might be instable. Note that, if more than one pump signal is involved in drilling process, the cost function has to be revised to consider sum pump signal envelopes.

The performance of both CM array filtering and the extended MIMO decorrelation approach in capturing the telemetry signal and rejecting the pump interference signal is examined on low data rate field-test measurements. Two cases considered here: the first, shown in **Fig. 3.9** is to examine a field-test data of high SIR and has demonstrated comparable performance of both schemes; the second is the evaluation of a field-test data having low SIR. As seen in **Fig. 3.10** the extended MIMO approach delivers an estimate of the telemetry signal, while CM array filtering capture the pump signal, which has a higher power.

Moreover the algorithm property in terms of convergence time is examined on field-test data of both high and low SIR. Here the detection performance is plotted as a function of time. As seen in **Fig. 3.11**, the convergence rate for the data with higher SIR is faster.

Further examination of the algorithm is carried out on high data rate field-test data. The frequency-domain presentation of the exemplary received and processed data in **Fig. 3.12** shows that the separation task is not achieved completely and residual pump signal is observable in the estimated telemetry signal.

Consequently, despite robustness and effectiveness of the proposed approach in interference rejecting over the conventional CM beamforming scheme, the ill convergence/divergence problem in high data rate scenarios is not solved. Availability of some a priori knowledge about the interference signal and its association in CM array filtering motivate the investigation in the next section.

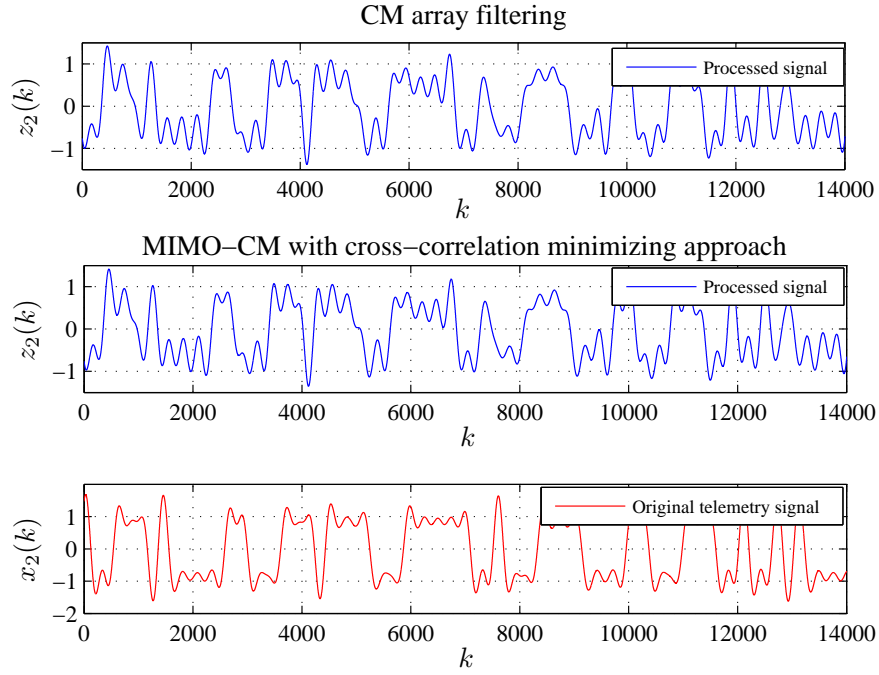


Fig. 3.9: Performance comparison of the CM array filtering and MIMO-CM methods in the presence of the pump signal for high SIR case (both methods capture the telemetry signal)

3.2.3 A single channel semi-blind source extraction method based on interference properties

RMP characteristic of the pump signal motivates the development of an interference cancelling scheme called time-domain averaging and subtracting (TD-AS). The observations of the pump signal have shown that the main part of distortions in the telemetry signal is caused by the periodic component of the pump signal. The idea is to estimate the periodic part of the interference for a certain observation time and extract it from the received signal. Afterwards either linear or nonlinear equalization methods (e.g. CMA) can be applied to equalize the inter-symbol interference introduced by the transmission channel. The first step is to determine the fundamental period of the pump signal known as averaging period T using one of two methods presented in Subsection 2.2.3. The second step is to select the duration of the received signal to be averaged, called averaging length M . The averaging length has to be selected correctly. If averaging length is too short, a part of the telemetry signal might be removed after the processing. Otherwise, the interference might not be removed effectively. So the effectiveness of the averaging depends on the signal to interference ratio (SIR) and the algorithm can be optimized by a coarse estimation of SIR. After determining the averaging period and averaging length, the observed signal is divided into M frames, each having the length of averaging period $T = NT_s$, $T_s = 1$. **Fig. 3.13** describes the system structure of TD-AS approach. An

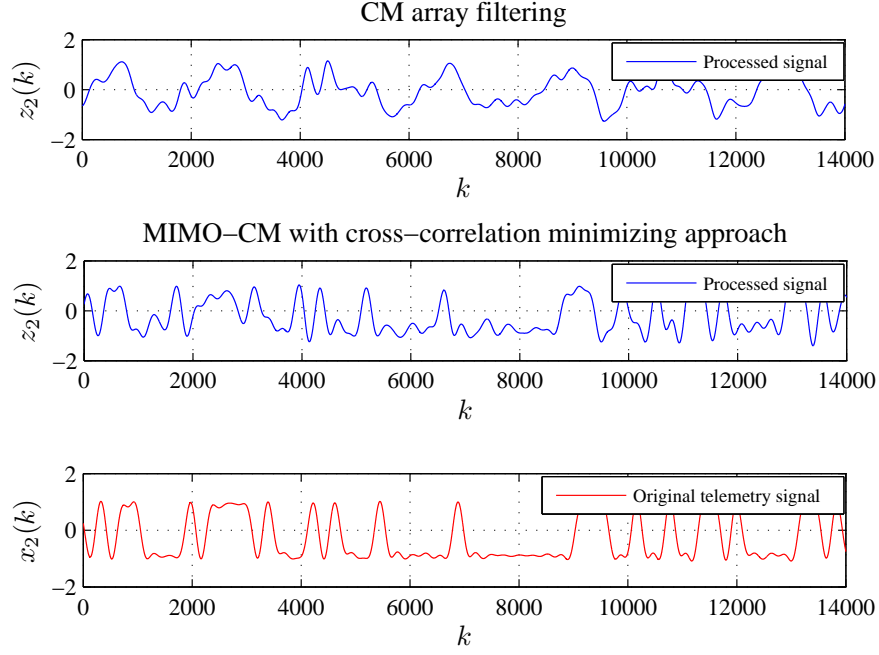


Fig. 3.10: Performance comparison of the CM array filtering and MIMO-CM methods in the present of the pump signal for low SIR case (CM-based array filtering captures the pump signal)

estimate of the deterministic part of the interference $\hat{s}(k)$ is obtained as follows

$$\hat{s}(k) = \frac{1}{M} \sum_{m=1}^M y(k + (m-1)N), \quad k = 0, \dots, N-1. \quad (3.13)$$

where $y(k)$ denotes the received signal at time instant k . By subtracting $\hat{s}(k)$ from $y(k)$, we can remove the main part of the interference and $z(k) = y(k) - \hat{s}(k)$ includes the telemetry signal affected by the mud channel and residual stochastic part of the pump signal. By equalizing $z(k)$ we can compensate the possible distortions of the signal caused by the transmission channel as well and detect the signal correctly. The best averaging scheme shown in **Fig. 3.14** is to build up the averaging from the previous and incoming neighborhood frames. In this way, the signal discontinuity caused by the time-domain subtraction can be eliminated or reduced. The semi-blind source extraction (BSE) scheme based on TD-AS is analyzed in some respects. The first step is to investigate how the averaging length affects the detection of the telemetry signal in the case of low SIR. The examinations are carried out on field-test data as well as simulated data. The evaluation result of a set of field-test data is illustrated in **Fig. 3.15**. It is seen that if the averaging is performed over $M = 21$ frames, the residual stochastic term of the pump signal is strong enough to cause the erroneous detection of the telemetry signal as shown in the labeled area of the figure. To demonstrate the performance dependency on SIR, the BER is plotted as a function of SIR for averaging lengths of different value. The results in **Fig. 3.16** show that the averaging length affects the algorithm performance at very low or very high SIRs. Besides, the averaging length specifies the width of area to be notched out. In

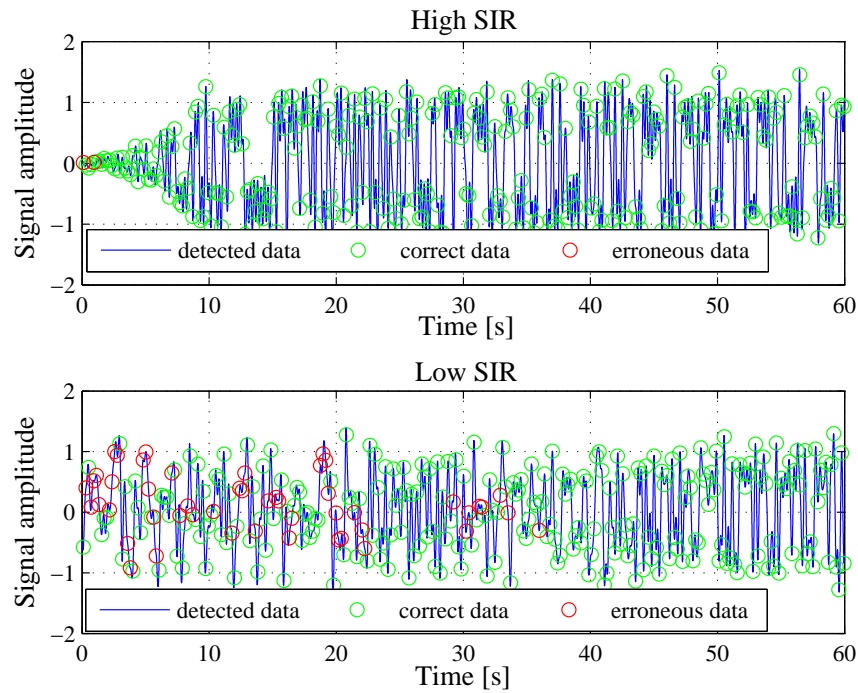


Fig. 3.11: Convergence time of MIMO-CM methods in the presence of the pump signal for high and low SIRs (the Convergence is faster at high SIR)

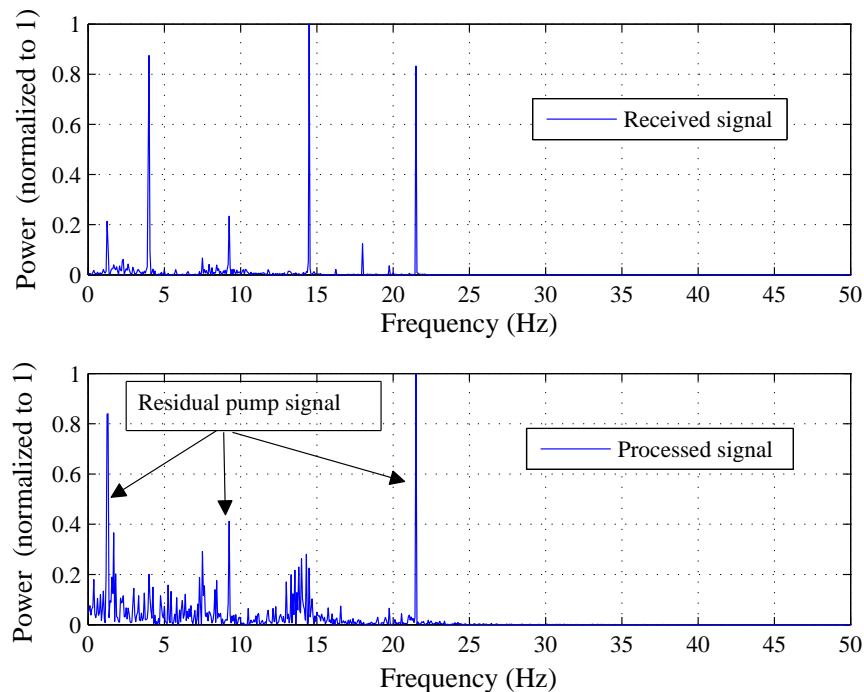


Fig. 3.12: Poor performance of the MIMO-CM approach for high data rate/wideband transmission

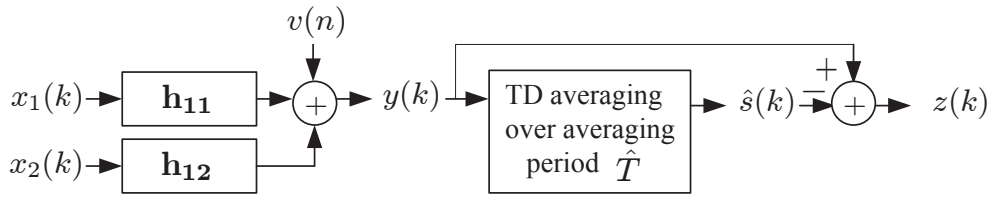


Fig. 3.13: TD-AS Concept

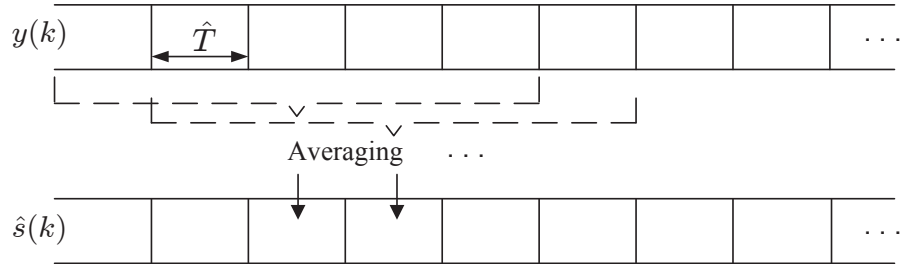


Fig. 3.14: Averaging procedure

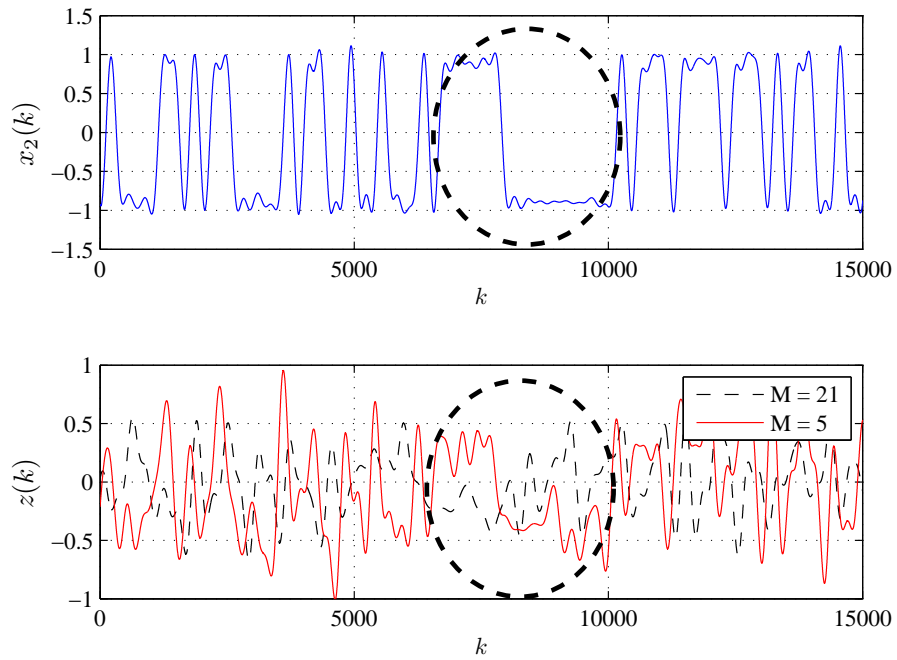


Fig. 3.15: Effect of averaging length on the detection performance in an example of field-test data

fact, for small values of averaging length notching process begins to distort the telemetry signal as well. In this regard, a coarse estimation of the SIR is useful for appropriate parameter configuration in TD-AS scheme.

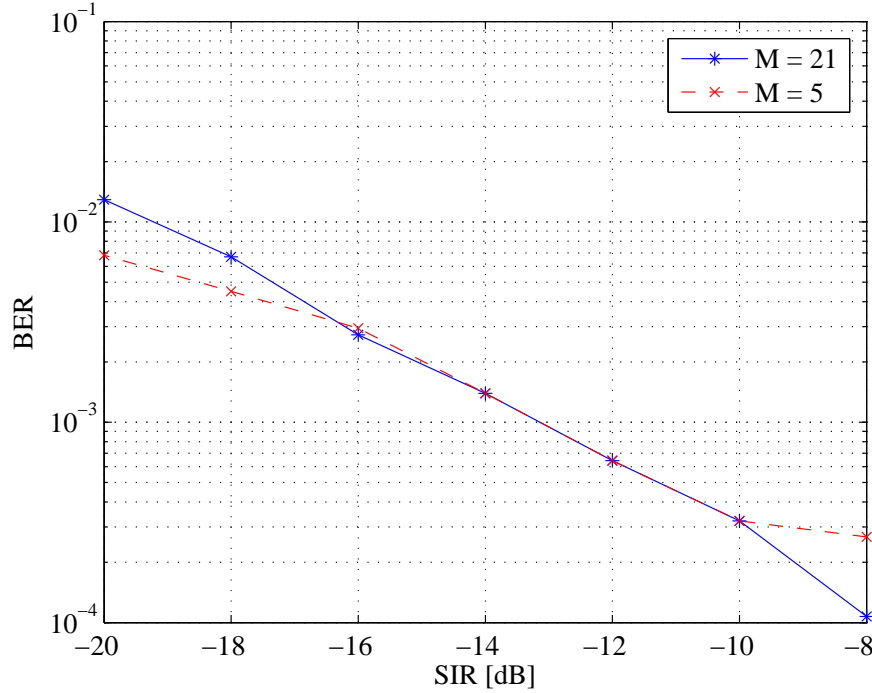


Fig. 3.16: Effect of averaging length on the simulative detection performance as a function of BER vs. SIR

The second step in examining of the algorithm's performance is to demonstrate whether or not the algorithm actually suppresses the pump interference signal. This is performed by testing the algorithm on a field-test data of a carrier frequency $f_c = 30$ Hz and data rate $R = 5$ bit/s. The estimated fundamental period is $\hat{N} = 585$ samples and $M = 21$ frames.

The frequency-domain baseband presentation of the received and processed signals illustrated in **Fig. 3.17** shows that the algorithm notches the main part of the interference. From the time-domain baseband presentation of the received and processed signals in **Fig. 3.18** it is seen that an apparent reduction in the amount of erroneous data detection can be achieved by the TD-AS method.

3.3 Practicability and performance evaluation of semi-blind schemes

To illustrate the performance of proposed algorithms in Subsections 3.2.2 and 3.2.3, we analyze both simulative and field-test data from test boreholes. These investigations also include evaluating the method using pump strobe sensors to get an assessment of the applicability of proposed methods in the MPT system. This section ends up by comparing the simulated results with the measured ones. However it is impossible to estimate the SIR during the regular operation, a rough estimate of SIR can be obtained during the startup sequence. The power of the pump signal can be measured during the valve-off period. Afterwards, the SIR can be calculated during a time slot equal to valve-off duration,

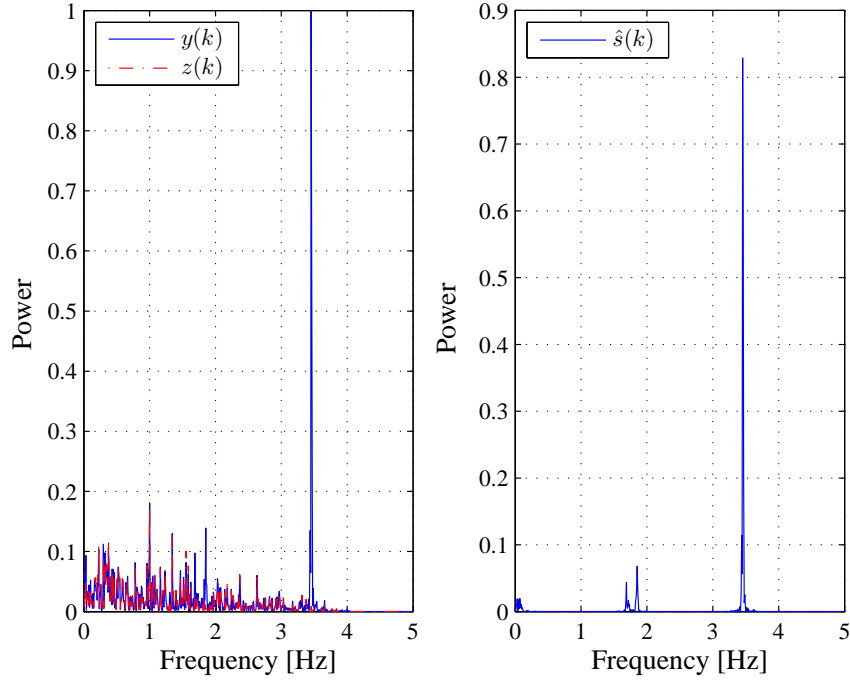


Fig. 3.17: Spectrum of the received sensor signal $y(k)$, the estimated periodic pump signal $\hat{s}(k)$ and the processed signal $z(k)$ in baseband

where a training sequence for the telemetry signal is transmitted as follows

$$\hat{SIR} = 10 \log_{10} \frac{E[y^2(k)] - E[y_{VO}^2(k)]}{E[y_{VO}^2(k)]}. \quad (3.14)$$

The SIR estimation shown in **Fig. 3.19** is performed for field-test data sets to be analyzed and provides some information about the frequency and amount of SIRs encountered in real MPT applications. Moreover, such information can be used for more realistic configuration of simulation parameters. As stated in Subsections 3.2.2 and 3.2.3 an estimate of the fundamental period of the pump signal is required by the proposed schemes. In this regard, the estimation method based on correlation maximization in 2.2.3 is applied to estimate the fundamental period for each field-test data set to be analyzed. The estimation is carried out during both valve-off and regular operation time. The results in **Fig. 3.20** provide not only an estimate of fundamental period but also illustrate the capability of the estimation method during regular operation. It can be seen that the estimation results are similar, except of trivial variation in sample.

In the first step, the simulative evaluation based on the MPT-system in **Eq. 1.1** is performed. Time-invariant frequency-flat fading channels are considered to model the channels of the MPT-system. AWGN and the pump signal represents the additive system interferences, which disrupt the telemetry signal at most and cause erroneous data detection. The aim of this simulation is to determine the efficiency of the proposed schemes in detecting a BCPM modulated telemetry signal with the carrier frequency of 40 Hz and a data rate of 40 bit/s for the case when the received signal is affected by randomly generated flat fading channels, Gaussian noise and interference pump signal. Therefore we perform for different media noise with the same SNR 100000 Monte-Carlo trials. The

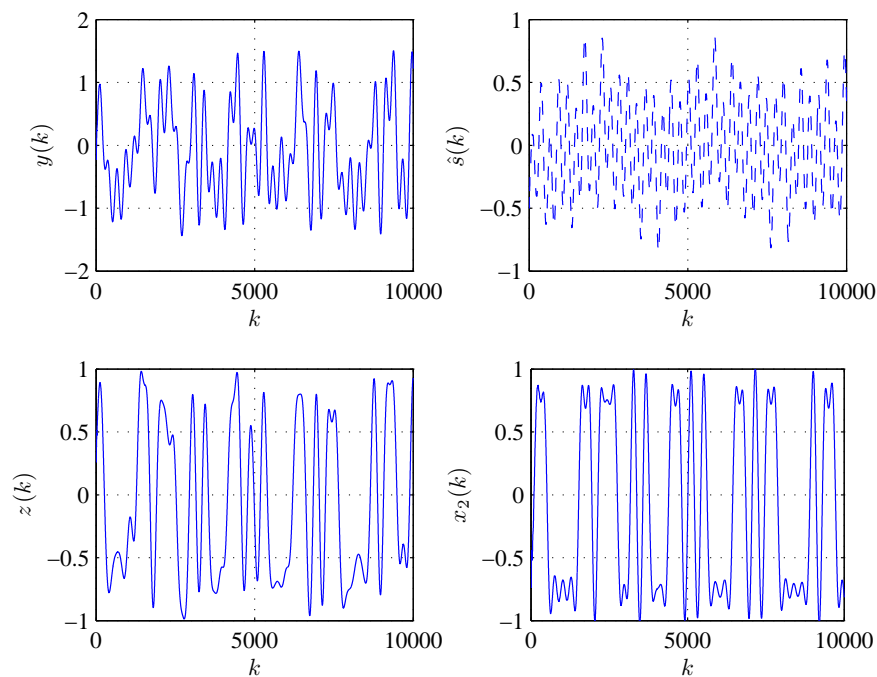


Fig. 3.18: Baseband presentation of the received signal $y(k)$, the estimated periodic pump signal $\hat{s}(k)$ and the processed signal $z(k)$ compared to the original telemetry signal $x_2(k)$

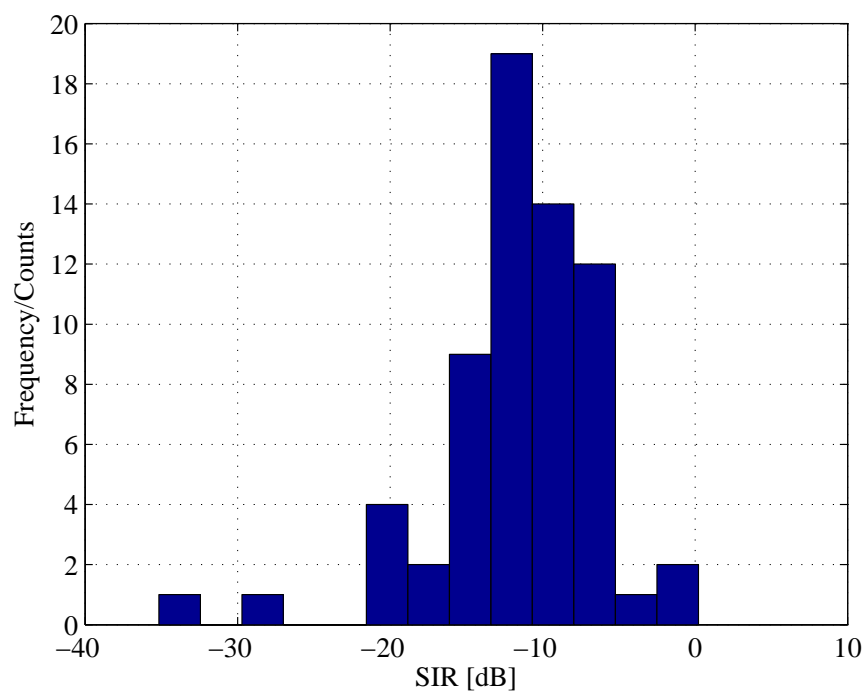


Fig. 3.19: SIR analysis of field-tests data sets

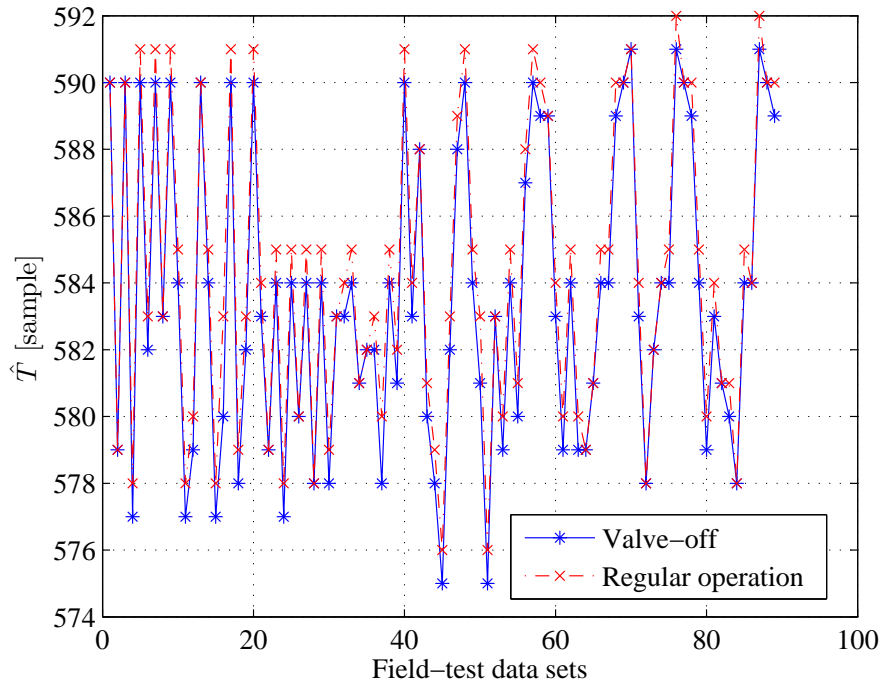


Fig. 3.20: Estimation results of fundamental period during valve off and regular operation

range of SNRs is from 0 dB to 30 dB. The pump signal recorded at the test borehole is used to model the interference, thus the simulations correspond with the real situations. Using the statistics on the value of SIR provided in **Fig. 3.19**, SIR of -15 dB is considered in the simulation and the results are thus related to a moderate situation.

The parameter setup for the proposed schemes are summarized in **Table 3.1**.

Sampling rate	$f_s = 1024$ [Hz]
Filter length	$L = 31$ [ms]
Range of delays	$\tau_1 = -20$ [ms] and $\tau_2 = -\tau_1$
Step size	$\mu = 10^{-4}$
Adaptation time	20 [s]
Averaging length	$M = 21, 5$

Table 3.1: Simulation parameter setup for the proposed semi-blind processing schemes

The simulation results are provided in **Fig. 3.21** as BER vs. SNRs and compared to the situation where no processing is performed as well as to the situation where the processing is carried out by the pump cancellation method based on pump strobe sensors. As expected, MIMO semi-blind source separation scheme yields best performance and helps not only in suppressing the pump interference signal but also in channel equalizing and de-noising the received signal from the Gaussian noise. Obviously, the BER results are improved as the SNR increases. From the BER results, no significant differences are

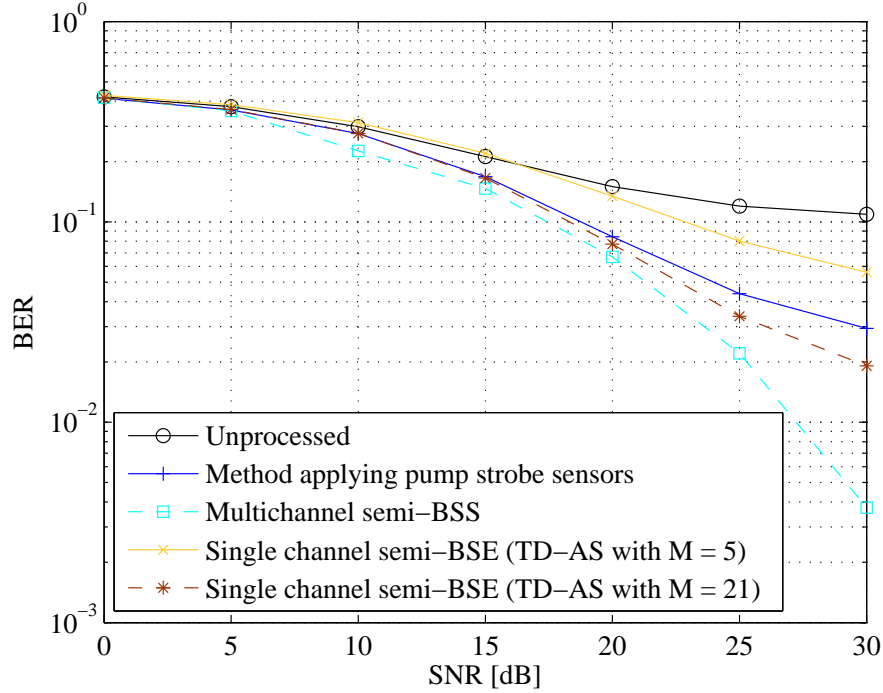


Fig. 3.21: Simulative performance analysis of the proposed semi-blind processing schemes in terms of BER vs. SNR at $SIR = -15$ dB

noticed between the TD-AS scheme with $M = 21$ and the approach based on pump strobe sensors.

In the second step, field-test data sets are analyzed to experimentally verify the performance of the algorithms as well as the applicability of the simulations regarding real situations. In this part, the BER count or frequency is used as the performance measure. 84 field-test data sets corresponding to 60000 bits are involved in the evaluation. A summary on evaluated field-test data is given in **Table 3.2** and the parameter configuration is the same as in **Table 3.1**.

Low data rate scenario	$R = 5$ [bps]	30000 bits
High data rate scenario	$R = 20, 25, 30, 35, 40$ [bps]	30000 bits

Table 3.2: Field-test data setup involved in the evaluation of semi-blind schemes

The evaluation results illustrated in **Fig. 3.22** are in accordance to the simulation ones. The performance is not significantly different from each other for all the discussed algorithms and all methods deliver almost comparable performance. Further field-test data based evaluations shown in **Fig. 3.23** indicates that a significant performance improvement can be achieved by combining single channel TD-AS and CMA schemes. The block diagram of **Fig. 3.24** demonstrates the structure of combining single channel semi-BSE based on the TD-AS and semi-blind CMA.

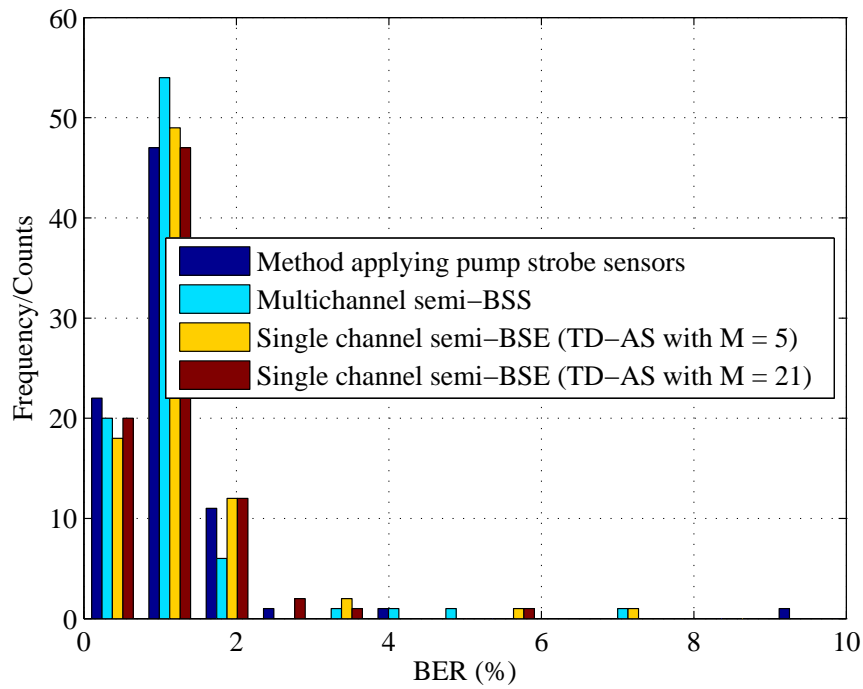


Fig. 3.22: Field-test data based performance analysis of the proposed semi-blind processing schemes

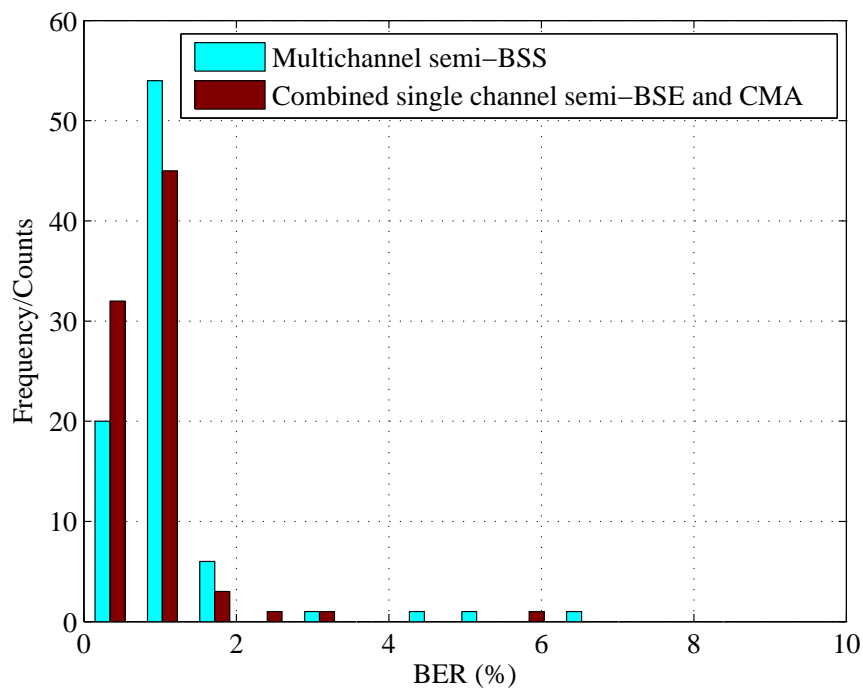


Fig. 3.23: Field-test data based performance comparison between the multichannel semi-BSS and the single channel semi-BSE followed by CMA

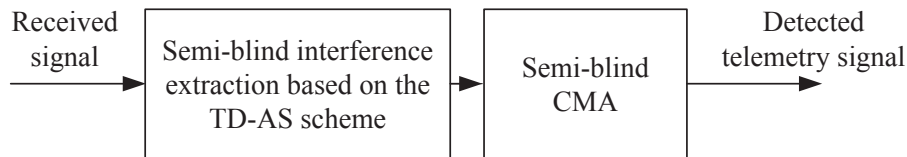


Fig. 3.24: Concept block diagram of combining single channel semi-BSE based on the TD-AS and CMA

3.4 Summary and conclusion

In this chapter, two semi-blind estimation schemes based on telemetry and/or interference properties were proposed mainly to support interference suppression encountered in MPT applications: one uses modulus/envelope properties of both telemetry and interference signals, and the other explicitly special properties of RMP interference signal. The application of both algorithms requires a-priori information about the fundamental period of the pump interference signal. Depending on the applied data rate, we can proceed from the narrowband or wideband system assumption. Accordingly, the amount of interference being taken in the transmission bandwidth is also varied. Both approaches are analyzed using simulation as well as field-test data measurements and compared to one that utilized pump strobe sensors installed at pumps to remove the pump signal. In the simulation part, the analysis was for a high data and AWGN system scenario using real pump measurements and flat-fading channels. In the second part, the measurements from the test boreholes include field-test data of different data rates possibly affected by the multipath mainly at high data rates. The results indicate that although MIMO semi-blind source separation method using envelope property of telemetry and interference yields best performance, it is less robust than the semi-blind source extraction method due to the possible divergence phenomenon especially for the wideband/high data rate transmission case. Another reason for choosing extraction scheme over the separation one, is its simple single receiver structure and significant performance improvement achieved by CMA post-processing. Next to this, additional research could further examine the latter in the context of two-receiver structure. Even though these methods work in real environments, estimating and specially tracking of required a-priori information about the interference signal not only introduces a big challenge to practical applications but also increases system complexity. Based on this investigation, an extension proposal capable of extracting interference without employing any a priori knowledge about the interference should be studied. Furthermore, the two receiver structure available in the MPT system architecture offers further research aspects to be dealt with in this dissertation.

Chapter 4

Reference signal-based processing schemes

The semi-blind signal processing schemes proposed in Chapter 3 demand a-priori information and show moderate performance. These decrease their usefulness in practical applications. Therefore, the training sequence facility embedded in the startup sequence is utilized for algorithm development. Since available technology based on the two-receiver structure is of economical and efficiency interests, this chapter concentrates on conceptualizing estimation schemes based on a reference signal combined with the two-receiver structure available in MPT. In this context, the reliability and efficiency of channel estimation is discussed. Afterwards, different receiver structures and estimation concepts are proposed to provide efficient estimation and tracking facility to update the estimation during the regular operation. Consequently, the efficiency and practicability of the proposed algorithms in estimating the telemetry signal is tested and compared using field-tests data acquired from different rigs.

4.1 Inferior channel estimation

It is difficult to reliably estimate the channel because of substantial strong pump interference inherent to the MPT system. However, for high signal to interference ratios it is still possible to achieve good channel estimation, but reliable channel estimation in MPT system, in which the reference signal is almost immersed in strong interference, is challenging.

The problem of reliable channel estimation can be dealt with either by removing the interference in advance and preceding the channel estimation or estimating the channel in the presence of interference [49]. The first approach is inefficient because of the concomitant distortion of the transmitted signal, which induces an inaccurate channel estimation/equalization as well. Different estimation methods based on the second scheme are also investigated and compared in [99]. Results reported in [99] demonstrate the limited and SIR-dependent performance of these methods as well. Moreover, due to the lack of a training sequence for the pump signal, it is not possible to exploit the structure property of MIMO channel offered by the MPT system architecture and accordingly the receiver structure is reduced to a Single-Input Multi-Output (SIMO) system. In addition, it is shown in [99, 49] that a layered equalization scheme, where the co-channel pump

interference is subtracted out from all received data and each received data is equalized thereafter, is much more efficient.

It should be noticed that, in the subsequent chapter a reliable method of channel estimation is developed to extract channel impulse responses (CIR), supporting simulation studies of this work. In this chapter a different estimation and detection approach for the MPT system with the two-receiver structure is proposed, where the focus is on cancelling the interference while simultaneously detecting the desired telemetry signal.

4.2 Straightforward signal estimation

Conventional interference cancellation is performed by feeding a reference of interferer to a receiver having structure as shown in **Fig. 4.2** [40]. Since no reference signal is available for the pump interference, the two-receiver structure of MPT system is utilized to fulfill the task of cancelling interference [24]. Two-receiver based interference cancellation technique presented in [24] was shown to be highly effective in suppressing the interference, working without any knowledge of the interfering signal and any pump strobe sensors. The major drawback of this scheme is the inability of adaptation. Therefore, the receiver structure has to be optimized to include both adaptive interference cancellation and channel equalization features. To this end, two kinds of adaptive receivers have been proposed. The first, called here cascade interference cancellation and equalization, has the

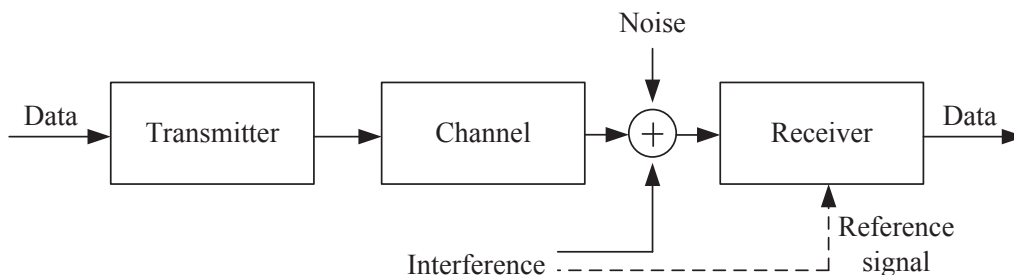


Fig. 4.1: Conceptual diagram of conventional interference cancellation in a communication system

same receiver structure as presented in [24, 80]. The second scheme, termed joint interference cancellation and equalization, involves a multichannel adaptive receiver algorithm. Both of these receiver algorithms utilize a reference signal to adaptively notch out the interferer and extract the telemetry signal. The adaptive processing can be accomplished by applying the well-known adaptive weighting schemes such as sample matrix inversion (SMI), least mean square (LMS), and recursive least square (RLS) [100]. The reference signal is usually provided by transmitting a training sequence known a priori to receiver. Such kind of signal is also referred to as temporal reference and can be a data signal or other appropriate signal such as chirps proposed for the synchronization [67, 42]¹.

¹ Knowledge on signal arrival direction is called spatial reference.

The current MPT system provides training sequence facility in the form of data signal as well as synchronization chirp. Providing a reference signal during the regular operation poses a great challenge. One possibility to form a reference signal after terminating the training sequence is the re-modulation of the demodulator decision i.e., the so-called decision feedback (DF) operational mode [67]. Provided decision error rates lower than 10^{-2} , the obtained reference signal is still of sufficient quality to allow efficient tracking [67]. An alternative approach to avoiding such errors is to deploy periodic training sequence e.g. synchronization chirp [67]. Thus both schemes proposed in this section are capable of tracking using the reference signal generation approaches.

In the next two sections, the discussion and the realization of both approaches are based on realistic MPT environment and communication channels.

4.2.1 Cascade interference cancellation/equalization

In this section, the two-receiver structure available in the MPT system and the special feature of startup sequence is utilized to perform traditional interference cancellation based on a reference signal [40]. As shown in **Fig. 4.2**, this scheme consists of a cascade arrangement of interference cancellation and equalization sections.

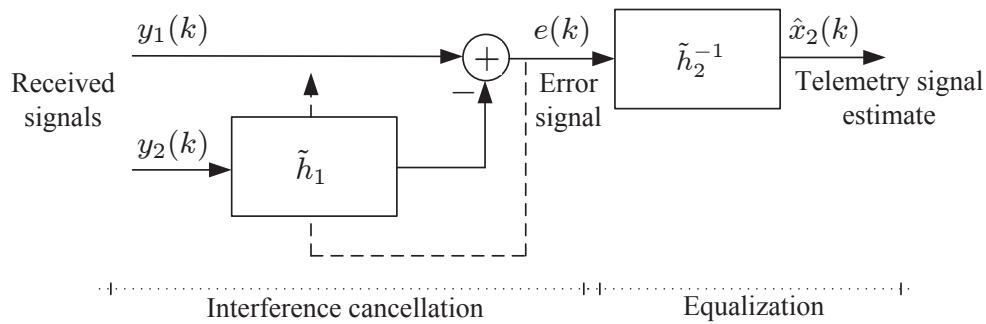


Fig. 4.2: Block diagram of the cascade interference canceller/equalizer

The interference cancellation algorithm is initially adjusted during the VO period of the startup sequence to notch out the interference. Residual signal distortions mostly caused by the communication channels are to be compensated at the equalization section. The equalizer initial adjustment is achieved using the training sequence of the startup sequence [24]. However, the cascade interference cancellation/equalization offers simple receiver architecture and low computational efforts, but suffers from two important problems [40, 70]. The first one is the interference adaptation. In other words, the adjustment of the interference cancellation section prescribes VO phase, which is not supported by the system during the regular operation. The second one, which limits the performance of the cascade interference cancellation/equalization during the regular operation, is the presence of the telemetry signal in both receivers [40]. In this case, not only the interference but also parts of the telemetry signal can be removed by the interference canceller and caused performance reduction of the system.

An alternative estimation scheme, called here joint adjustment of interference and equalization sections, is proposed to deal with tracking problems of the cascade structure. The initial adjustment of both interference and equalization sections is performed in the training phase, which in turn facilitates tracking during regular operation.

Recalling the mathematical description of the interference removal scheme based on two-receiver structure in **Eq. 1.3** the corresponding equations for the cascade receiver structure and adaptive joint estimation approach are derived as follow:

$$y_2(k) - \tilde{h}_1(k) * y_1(k) = \tilde{h}_2(k) * x_2(k) + \tilde{v}(k) , \quad (4.1)$$

or

$$y_2(k) = \tilde{h}_1(k) * y_1(k) + \tilde{h}_2(k) * x_2(k) + \tilde{v}(k) , \quad (4.2)$$

where $\tilde{h}_1(k) = \tilde{h}_{21}(k)$, $\tilde{h}_2(k) = h_{22}(k) - \tilde{h}_{21}(k) * h_{12}(k)$, $\tilde{v}(k) = v_2(k) - \tilde{h}_{21}(k) * v_1(k)$, and $y_1(k)$, $y_2(k)$ and $x_2(k)$ are the received and training signals respectively. $v_1(k)$ and $v_2(k)$ are zero-mean additive white Gaussian noise. It should be noted that **Eq. 4.1** is used to deliver the estimation for the telemetry signal, whereas **Eq. 4.2** can be used to estimate the parameters required by **Eq. 4.1**.

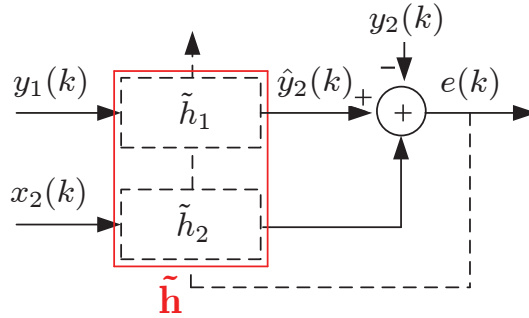


Fig. 4.3: Conceptual diagram of joint estimation for the cascade receiver structure

A simplified block diagram for the estimation strategy is illustrated in **Fig. 4.3**, where $\hat{y}_2(k)$ is the output of the adaptive filter and the difference $e(k) = \hat{y}_2(k) - y_2(k)$, between the received and filter output signals is applied to the adaptation algorithm. The vector representation is suited to demonstrate the adaptation procedure. Assuming that the filter length equals to L , the vector representation of $\hat{y}_2(k)$ at time index k is given by

$$\begin{aligned} \hat{y}_2(k) &= \sum_{l=0}^{L-1} \tilde{h}_1(l) y_1(k-l) + \tilde{h}_2(l) x_2(k-l) \\ &= \tilde{\mathbf{h}}^T \phi(k) , \end{aligned} \quad (4.3)$$

where $\tilde{\mathbf{h}} = \left[\tilde{h}_{1,0}, \tilde{h}_{1,1}, \dots, \tilde{h}_{1,L-1}, \tilde{h}_{2,0}, \tilde{h}_{2,1}, \dots, \tilde{h}_{2,L-1} \right]^T$ and $\phi(k) = \left[y_1(k), \dots, y_1(k-L+1), x_2(k), \dots, x_2(k-L+1) \right]^T$.

The filter coefficient are adjusted so as to minimize the performance function, which will be defined in the sequel, by employing simple adaptation algorithms such as standard RLS, which has good numerical stability [10]. Since the signal as well as environment characteristics could be time-variant, the use of an adaptive processing scheme is preferred. Recursive least square algorithm is a class of adaptive algorithms based on the least squares (LS) criterion, in which the cost function to minimize is a sum of squared errors given by [10, 110]

$$J_{LS}(k) = \sum_i^k \rho^i |e(k-i)|^2, \text{ for } 1 \leq i \leq k . \quad (4.4)$$

Since both current and all past inputs samples are involved in the estimation, the algorithm offers fast convergence at the cost of increased complexity. The forgetting factor ρ is purposed to assign different weighting for the current and previous errors in the cost function. The minimization of the the LS cost function is achieved by setting its gradient to zero ($\nabla_{\tilde{\mathbf{h}}} J_{LS}(k) = 0$) [110, 70].

$$\begin{aligned} \nabla_{\tilde{\mathbf{h}}} J_{LS}(k) &= \nabla_{\tilde{\mathbf{h}}} \sum_i^k \rho^i \left| y_2(k-i) - \tilde{\mathbf{h}}^T \phi(k-i) \right|^2 \\ &= \nabla_{\tilde{\mathbf{h}}} \sum_i^k \rho^i \left[y_2(k-i) - \tilde{\mathbf{h}}^T \phi(k-i) \right] \left[y_2(k-i) - \tilde{\mathbf{h}}^T \phi(k-i) \right]^* \\ &= \nabla_{\tilde{\mathbf{h}}} \sum_i^k \rho^i \left[|y_2(k-i)|^2 - 2\tilde{\mathbf{h}}^T \phi(k-i) y_2^*(k-i) + \tilde{\mathbf{h}}^T \phi(k-i) \phi^H(k-i) \tilde{\mathbf{h}} \right] \\ &= \sum_i^k \rho^i \left[-2\phi(k-i) y_2^*(k-i) + 2\phi(k-i) \phi^H(k-i) \tilde{\mathbf{h}} \right] \\ &= -2p(k) + 2R_{\phi\phi}(k) \tilde{\mathbf{h}} , \end{aligned} \quad (4.5)$$

where

$$R_{\phi\phi}(k) = \sum_i^k \rho^i \phi(k-i) \phi^H(k-i)$$

$$p(k) = \sum_i^k \rho^i \phi(k-i) y_2^*(k-i) .$$

The minimum of the LS cost function is obtained by

$$\tilde{\mathbf{h}}(k) = R_{\phi\phi}^{-1}(k) p(k) . \quad (4.6)$$

The LS solution can be obtained by rewriting **Eq. 4.4** in a recursive manner as follows:

$$J_{LS}(k) = J_{LS}(k-1) + |e(k)|^2 . \quad (4.7)$$

Accordingly $R_{\phi\phi}(k)$ and $p(k)$ can be calculated recursively by:

$$R_{\phi\phi}(k) = \rho R_{\phi\phi}(k-1) + \phi(k) \phi^H(k)$$

$$p(k) = \rho p(k-1) + \phi(k)y_2^*(k) . \quad (4.8)$$

The coefficient vector $\tilde{\mathbf{h}}$ can be calculated with a matrix inversion of $R_{\phi\phi}(k)$ by solving **Eq. 4.6**. To avoid the time consuming matrix inversion operation, the matrix inversion lemma (Haykin, 1996)

$$(A + BCD)^{-1} = A^{-1} - A^{-1}B(C^{-1} + DA^{-1}B)^{-1}DA^{-1}$$

is used [110, 24]. By replacing $A = \rho R_{\phi\phi}(k-1)$, $B = \phi(k)$, $C = 1$ and $D = \phi(k)^H$, $R_{\phi\phi}(k)^{-1}$ can be calculated with **Eq. 4.7** directly.

$$R_{\phi\phi}^{-1}(k) = \rho^{-1} (R_{\phi\phi}^{-1}(k-1) - G(k)\phi^H(k)R_{\phi\phi}^{-1}(k-1)) , \quad (4.9)$$

where $G(k)$, also known as Kalman gain vector or adaptation gain vector, is defined by

$$G(k) = \frac{R_{\phi\phi}^{-1}(k-1)\phi(k)}{\rho + \phi^H(k)R_{\phi\phi}^{-1}(k-1)\phi(k)} . \quad (4.10)$$

The adaption equations is derived by inserting **Eq. 4.9** and **Eq. 4.8** into **Eq. 4.6** as below:

$$\begin{aligned} \tilde{\mathbf{h}}(k) &= \rho R_{\phi\phi}^{-1}(k)p(k-1) + R_{\phi\phi}^{-1}(k)\phi(k)y_2^*(k) \\ &= \tilde{\mathbf{h}}(k-1) - G(k)\phi^H(k)\tilde{\mathbf{h}}(k-1) + G(k)y_2^*(k) \\ &= \tilde{\mathbf{h}}(k-1) - G(k) \left(\phi^H(k)\tilde{\mathbf{h}}(k-1) - y_2^*(k) \right) \\ &= \tilde{\mathbf{h}}(k-1) - G(k)e^*(k) \end{aligned} \quad (4.11)$$

An estimate of $\tilde{\mathbf{h}}$ delivers required update for interference cancellation as well as equalizer sections of the cascade system. Whereas the estimation for the interference cancellation section is fed directly to the system, the estimation for the equalization section has to be inverted to obtain the equalizer coefficient. This can be performed by a time- or frequency-domain approach. It must be noticed that different structure of detection and estimation procedures introduces a processing delay to the system as well.

On comparing the VO-based and training-based (TB) estimation schemes, the impulse response of the interference canceller and the equalizer output are considered. **Fig. 4.4** shows the interference canceller estimate based on both VO and training sequence at different data rates. It is seen that TB scheme delivers the same estimation result of the channel impulse response as the VO-based approach. Accordingly, the estimation accuracy of the interference canceller section is affirmed.

The efficiency of the equalizer section in reconstructing the distorted signal at different data rates is illustrated in **Fig. 4.5**. It is observed that the equalized signal exhibits fewer distortions, which is also a verification of the estimation accuracy for the equalizer section.

The spectrogram of the received and processed signals in **Fig. 4.6** and **Fig. 4.7** show the fact that despite of the joint estimation the algorithm still attempts to remove the desired telemetry signal. Under this circumstance the joint estimation scheme might also deliver erroneous results [40]. In other words, the solution is not unique.

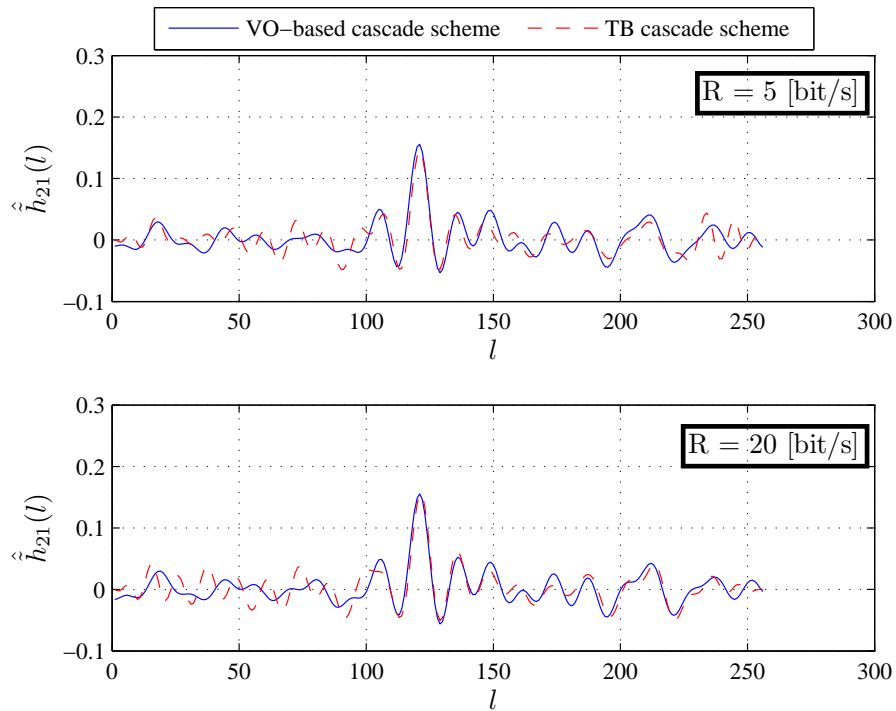


Fig. 4.4: VO-based and TB impulse response estimation of interference canceller for low and high data rate cases

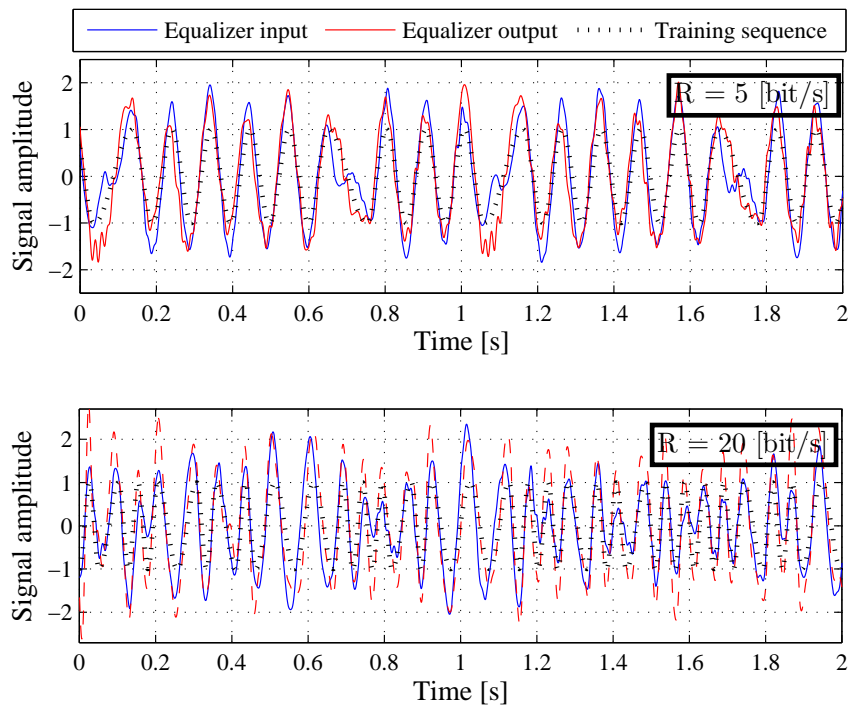


Fig. 4.5: Examining the functionality of the equalizer section for low and high data rate cases

This can be dealt with by parameter initialization during VO period, which can support

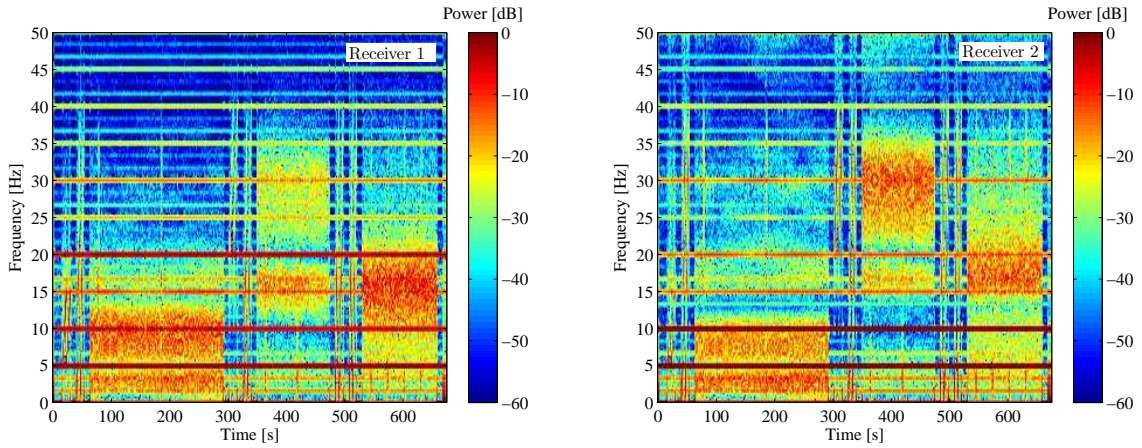


Fig. 4.6: Spectrogram of the unprocessed received signals

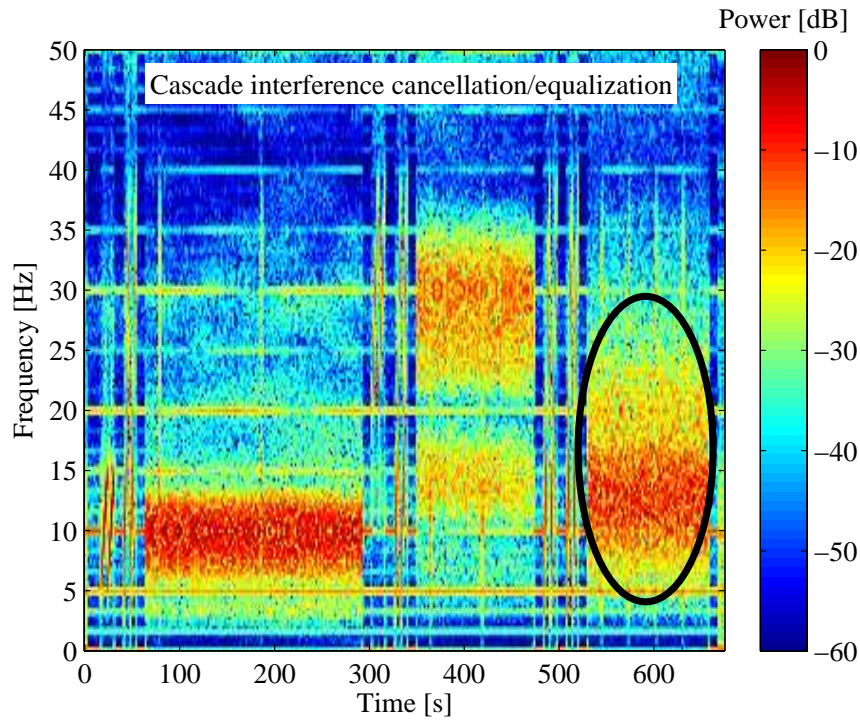


Fig. 4.7: Spectrogram of the processed signal using cascade interference canceller/equalizer

proper and faster convergence. To increase the estimation trustfulness a recursive scheme can be followed, where a part of training sequence is used to obtain an estimate of the equalizer and the equivalent channel impulse response. This estimation serves as a parameter initialization and assists to provide an update for interference canceller using another part of the training sequence. The idea is borrowed from turbo coding and is promising provided that the channels do not change rapidly. Accordingly, a recursive channel identification and telemetry signal estimation can be used to solve the channel identification with regular operation.

Another shortcome of the cascade scheme is that the performance of this method is highly dependent on the filter length. Thus a priori knowledge on the channel length is necessary for efficient work of this scheme.

4.2.2 Joint interference cancellation/equalization

The main issue to be discussed in this section is to mitigate signal distortion subject to channel and interfering signals jointly. The problems inherent in the cascade interference cancellation/equalization provide the motivation to reconsider the receiver architecture. An alternative is to use a joint interference cancellation/equalization structure [40, 81]. Such receiver arrangement does not exhibit basically the deficiencies of the previous structure. In this scheme both received signals are fed to the so-called multichannel adaptive

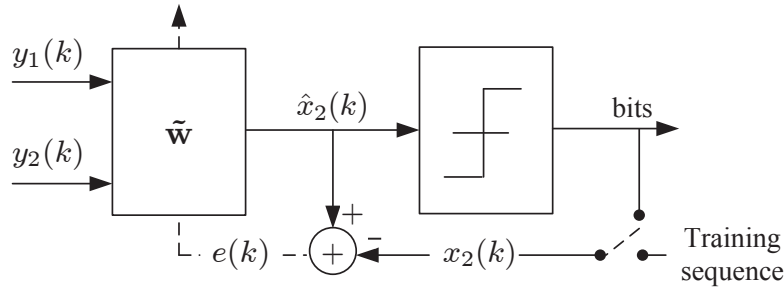


Fig. 4.8: Block diagram of the joint interference canceller/equalizer

equalizer and processed jointly to recover the desired telemetry signal. In other words, the space diversity reception available in the system offers deploying spatial signal processing technologies, where the signal of different receivers are combined to combat the channel effects due to multipath and reduce the potential interferences [55, 60, 48, 82]. To this end, two well-known schemes are proposed: diversity combining and adaptive arrays, also known as smart arrays. In this regard, the concept of optimal combining is introduced aiming to maximize the signal-to-interference-noise-ratio (SINR) at the receiver outputs [67, 55].

Traditionally adaptive arrays are deployed in environments featuring no fading and able to suppress an interfering signal, provided the angular separation between the interferer and signal of interest is large enough [55]. However in the MPT system similar to mobile radio systems due to the multipath the phase of signals is independent of each other, if the distance between the receivers/transmitters is greater than half of a wavelength [55]. Since the interference source (pump signal) is at the surface and the telemetry signal at the down hole, the aforementioned condition on the distance among the transmitters holds true in the MPT system. Thus, although the MPT environment differs from that of typical adaptive arrays system, application of adaptive arrays or optimal combining technologies is yet of distinct advantages [67, 55].

An extensive performance evaluation of optimal combining schemes for coherent detection of PSK signals subject to flat fading (Rayleigh channels) is given in [55]. The results reported in [55] include both analytical and simulative evaluations and illustrate the superior BER performance of the optimal combining over the traditional diversity combining schemes e.g. maximum ratio combining (MRC) with co-channel interferences. Accordingly the performance gain achieved by optimal combining is a factor of 5-10 [dB] [55, 87, 40]. Since the statistic of mud channels is not yet specified, it is extremely difficult to provide an analytical performance evaluation for optimal combining schemes in MPT

systems. Therefore, the performance evaluation is based upon simulation and field-tests data measurements obtained from different boreholes. The joint interference cancellation and equalization is referred to as the optimal combining scheme proposed in this work. The straight forward signal recovery of the joint scheme provides simplicity and directness for the tracking task. Similarly, the multichannel adaptive equalizer is initially adjusted during the training procedure. The multichannel adaptive equalizer can be tracked either by a decision feedback approach or using periodically transmitted signals (e.g. synchronization chirps). A block diagram of the proposed receiver is depicted in **Fig. 4.8**. The proposed scheme processes the received signals so as the telemetry signal components correlated with the temporal reference are enhanced and uncorrelated ones are removed. Therefore interference and noise can be suppressed in this way. Furthermore the proposed optimal combining scheme is able to reduce the effects of dispersive or frequency selective channels. This relies on the assumption that the autocorrelation functions of telemetry data and reference signals are close to each other [67].

Equalizer optimization based on adaptation criteria is a tradeoff between the structural complexity and the measure of communication quality generally in terms of BER. Concerning this matter, the MSE criterion in spite of simple adaptation structure results in inferior BER performance and accordingly is not qualified [87, 36]. To this end, the adaptation algorithm based on RLS criterion is also applied here to adjust the coefficient of multichannel adaptive equalizer. By specifying the error signal as $e(k) = \hat{x}_2(k) - x_2(k)$ with $\hat{x}_2(k) = \tilde{\mathbf{w}}^T \phi(k)$, $\phi(k) = [y_1(k), \dots, y_1(k-L+1), y_2(k), \dots, y_2(k-L+1)]^T$ the equalizer update equation is obtained as follow:

$$\tilde{\mathbf{w}}(k) = \tilde{\mathbf{w}}(k-1) - G(k)e(k)^* \quad , \quad (4.12)$$

where $\tilde{\mathbf{w}} = [\tilde{w}_{1,0}, \tilde{w}_{1,1}, \dots, \tilde{w}_{1,L-1}, \tilde{w}_{2,0}, \tilde{w}_{2,1}, \dots, \tilde{w}_{2,L-1}]^T$. Similarly $G(k)$ is defined by **Eq. 4.10**.

It should be noticed that the multichannel equalizer is a simplified version of the joint interference cancellation/equalization structure proposed in [40] and solely consists of feed forward transversal filters. The most important issue to be emphasized is that the processing procedure is identical for the involved signals in the joint scheme. To this end, the concept of receivers splitting into the reference and received signals in the cascade structure is abstracted in the joint structure [40]. The specification to be implied is that the multichannels have to provide new information about the interference or/and telemetry signals. The multichannel adaptive equalizer has the ability of rejecting narrowband interferences without any requirement on having reference for the interfering signals. Such equalization scheme employs available diversity in systems with parallel fading channels to reduce the effect of interference correlated from channel to channel [87]. In other words, available diversity required for fading protection is sacrificed in order to suppress the interference. Since the communication quality is mainly degraded by the pump interference, the arisen diversity loss is of less importance in the context of MPT multi-signal system.

A better performance can be achieved by increasing the number of receivers to attain additional channels at the cost of computational effort [55, 40]. However, providing the required diversity in the MPT system might be restricted. In one hand, due to certain housing of rigs, receiver placing is spatially limited. In the other hand, installing additional receivers results in additional costs and is financially less attractive.

The spectrogram presentation of the received signals in **Fig. 4.6** and the processed ones

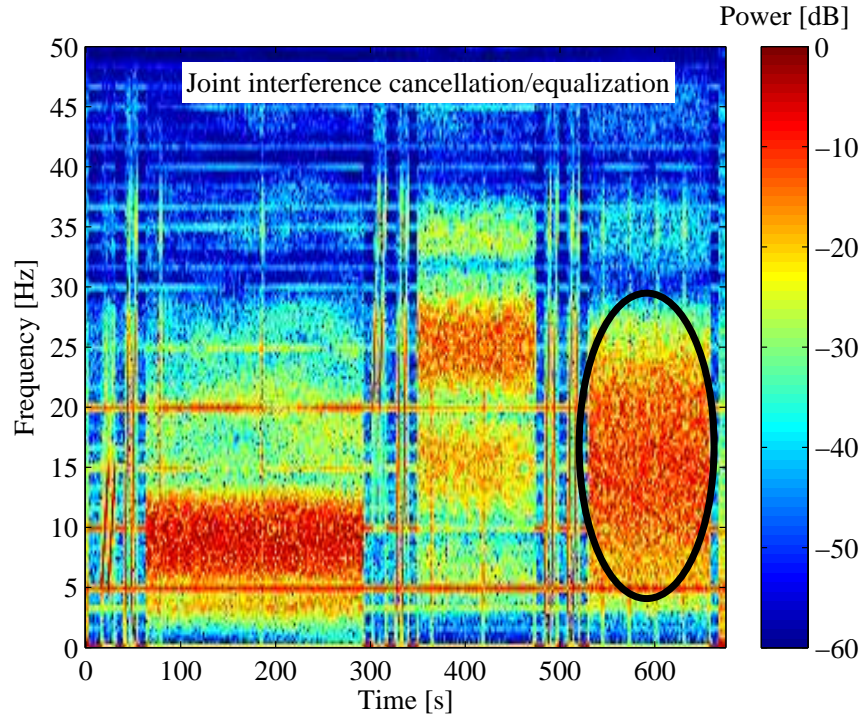


Fig. 4.9: Spectrogram of the processed signal applying optimum combining joint interference canceller/equalizer

in **Fig. 4.7** and **Fig. 4.9** shows the improvement of the signal strength and verifies the superior performance of the optimal combining scheme promised by the theory.

The convergence behavior of the joint multichannel scheme at different SIRs is analyzed. The results in **Fig. 4.10** show that the initial convergence performance is not affected seriously by SIR at the receiver, but the residual error is increased at poorer SIRs. In this regard, the amount of training sequence required for the estimation with a constant filter length can be reduced. This means less redundancy, higher data rate as well as fast tracking.

Efficient suppression of interferences whose power is much greater than that of the telemetry signals and/or those of large numbers might require applying larger filter lengths and accordingly larger amounts of reference signal. **Fig. 4.11** shows the convergence rate or the amount of training sequence required by the algorithm at different filter lengths.

As stated in previous chapters, more than one pump is involved in the drilling process. The consequence is twofold: increasing the number and the bandwidth of in-band interference. Thus examining the ability of the algorithm in rejecting multiple pump interfering signals is of great interest. On this account field-test data from a borehole running two pumps is considered. The spectrogram of the received and processed data in **Fig. 4.12** and **Fig. 4.13** shows that a distinct improvement of the signal strength (SINR) can be achieved.

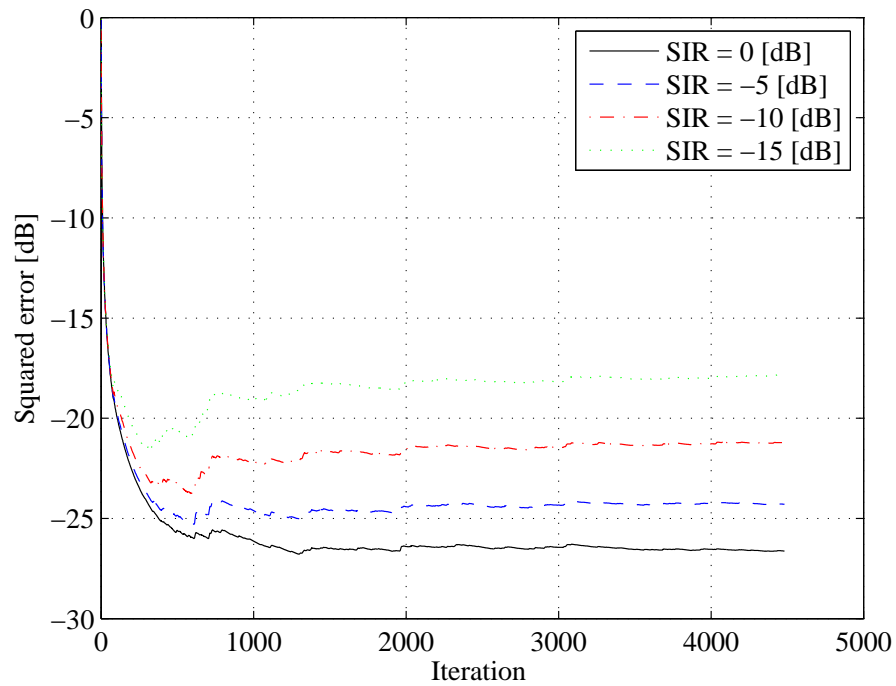


Fig. 4.10: Convergence evaluation of the joint multichannel scheme for different SIRs regimes

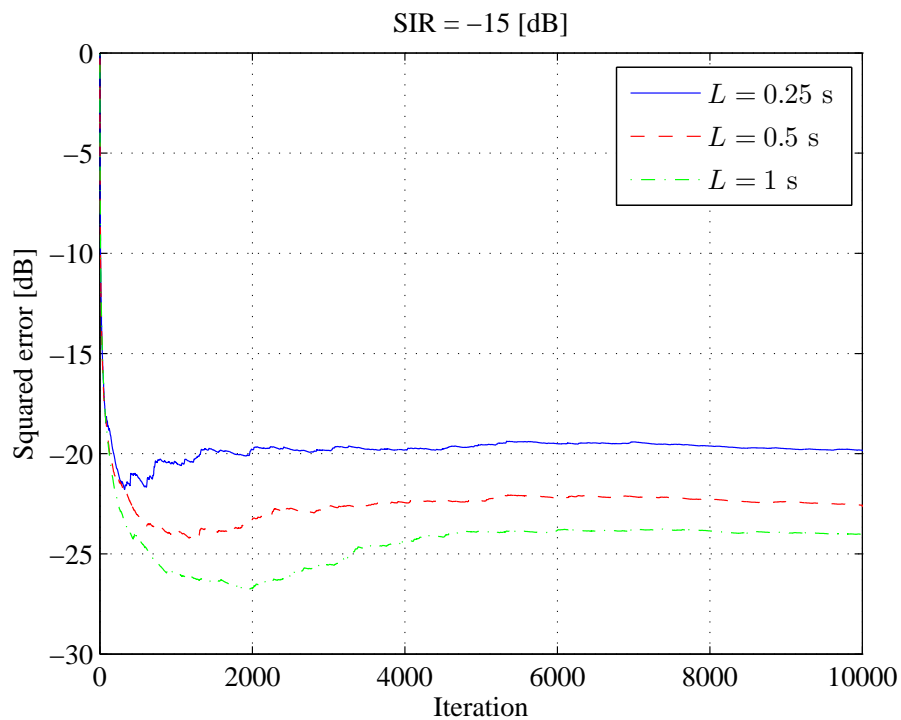


Fig. 4.11: Convergence evaluation of the joint multichannel scheme for different setup of filter lengths

4.3 Practicability and performance evaluation

The performance evaluations enclose both simulative as well as field-test data measurements.

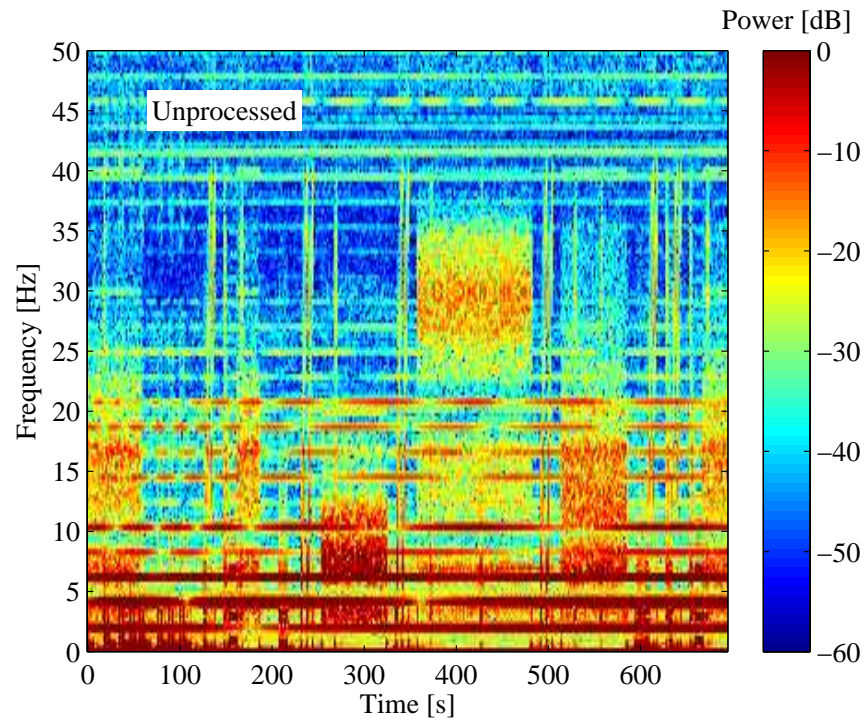


Fig. 4.12: Spectrogram of the unprocessed received signal distorted by a wideband two-pump interference

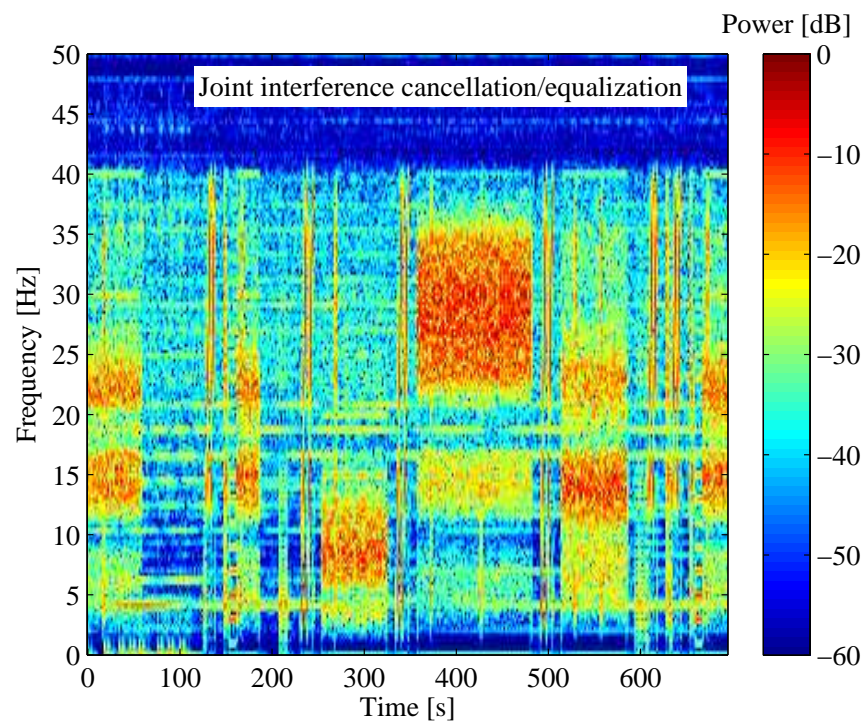


Fig. 4.13: Spectrogram presenting the ability of optimum combining joint interference canceller/equalizer in rejecting wideband two-pump interference

The first step in analyzing proposed algorithms in Sections 4.2.1 and 4.2.2 is to provide a comparative study on their stability and robustness. The aim of this study is to show whether a parameter readjustment is required for every measurement and/or rig environments. Such requirement makes the algorithms, even with a promising performance, unattractive for real MPT applications. Since the performance of the algorithms depends on the filter length setup, the BER vs. the filter length L is used to show the stability analysis. To evaluate the stability, sample field-test data of different data rates ($R = 5, 20$ bit/s) are considered.

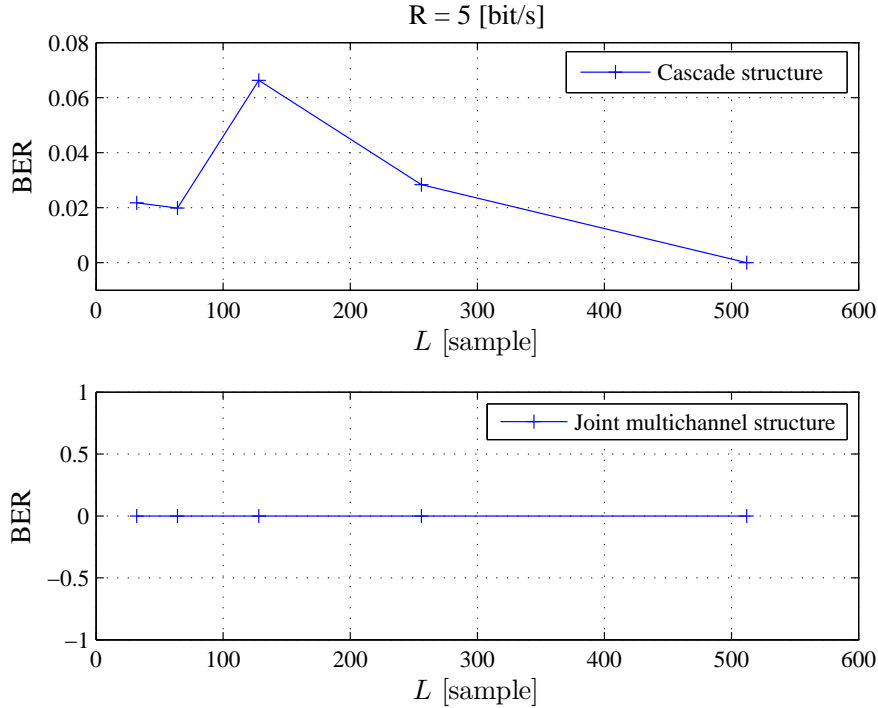


Fig. 4.14: Stability study of cascade and joint receiver structure on low data rate field-test measurements

The evaluation results are illustrated in **Fig. 4.14** and **Fig. 4.15**. The optimal filter length is specified by that given the lowest BER on the figures. It can be seen that the BER performance of the joint interference cancellation and equalization scheme for both high and low data rate cases is almost not affected by the filter length setup. However, the cascade interference cancellation and equalization scheme requires certain filter length adjustment to deliver best performance. Therefore, the results of stability analysis show the benefit of the joint scheme in MPT applications.

Initial performance study is carried out in a simulation environment, which offers more flexibility and precise algorithm study. The simulation environment is arranged according to the MPT system model presented in Chapter 1, with extracted CIRs from both test and commercial boreholes (see **Appendix. B.1** and **Appendix. B.2**). The related issues to CIR extract will be discussed in depth in the following chapter.

The aim of the simulations is to provide a quantitative/qualitative comparison of proposed

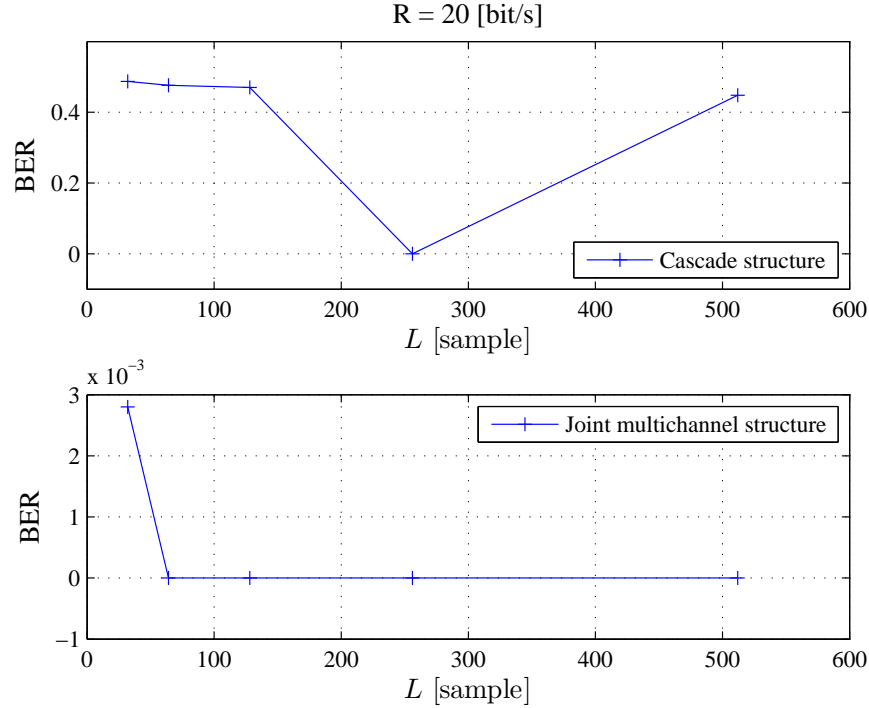


Fig. 4.15: Stability study of cascade and joint receiver structure on high data rate field-test measurements

algorithms in detecting a BCPM of $f_c = 40$ Hz and $R = 40$ bit/s at certain SIRs and SNRs. For different media noise (AWGN) with the same SNR, 100000 Monte-Carlo trials are performed. The range of SNR is from 0 dB to 35 dB. The pump signal measured at a test borehole is used to model the interference. Based on the investigation in Chapter 3.3, a SIR of -15 dB is considered. The training sequence and filters are of 13 s and 0.25 s duration respectively. The simulation results are provided in **Fig. 4.16** and **Fig. 4.17** as a function of BER vs. SNRs and compared with the situation where no processing is performed. Additionally the results are compared with the existing methods based on two-receiver as well as single channel and equal gain combining (EGC) equalization based on RLS. In EGC scheme the received signals are processed individually and then combined.

It can be seen that the joint scheme has a superior BER performance and offers a gain of about 10 dB over the other schemes, for both test and commercial boreholes scenarios. On comparing the joint scheme with the cascade one, it can be concluded that in the presence of noise the joint strategy is superior to that of cascade.

In addition to the simulations, field-test data acquired from different rigs are analyzed to examine the performance of the algorithms experimentally and to verify the simulation results. Here the BER frequency/counts is used as the measure of performance. 60 field-test data sets are involved in the evaluations. The evaluation results illustrated in **Fig. 4.18** are in agreement with the simulation results and verify the superior performance of the joint multichannel scheme. It should be noted that the filter length of TB cascade scheme has to be adjusted for each data set and accordingly is of less practicability.

According to theoretical analysis increasing the number of receivers can lead to a considerable performance improvement. To verify performance gain achieved by additional

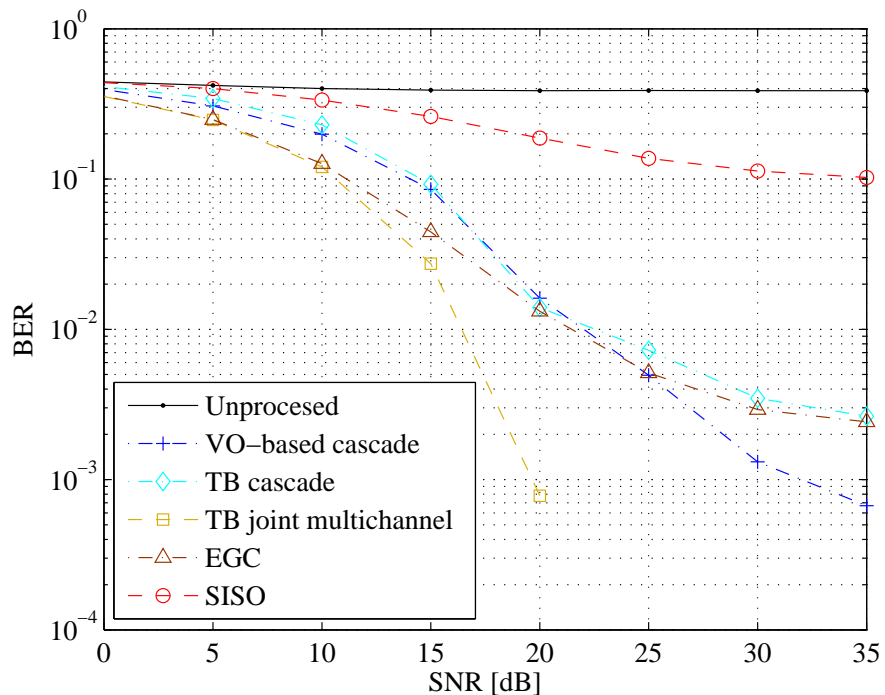


Fig. 4.16: Simulative performance analysis in terms of BER vs. SNR using CIRs obtained from a test borehole

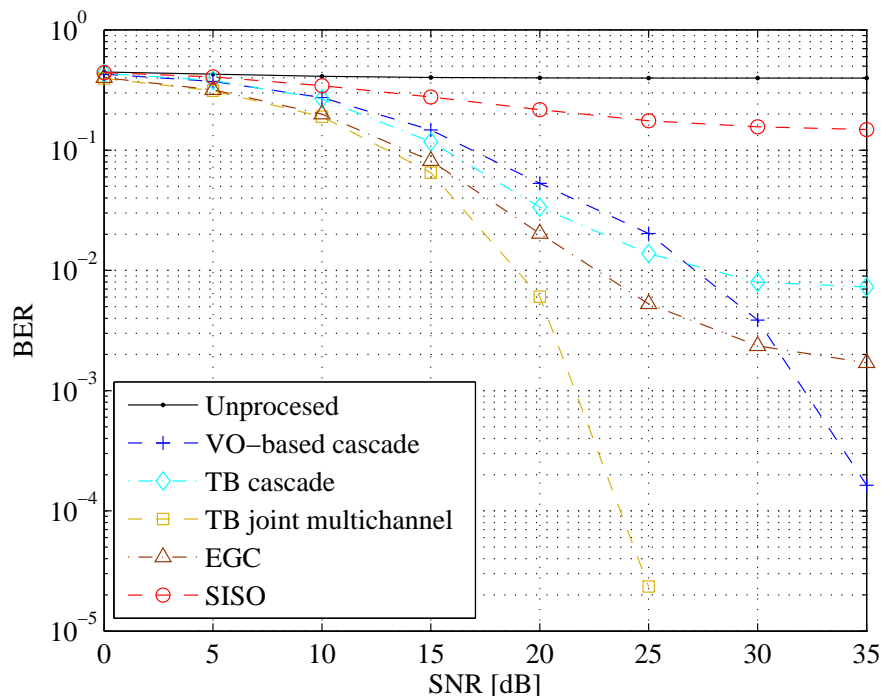


Fig. 4.17: Simulative performance analysis in terms of BER vs. SNR using CIRs obtained from a commercial borehole

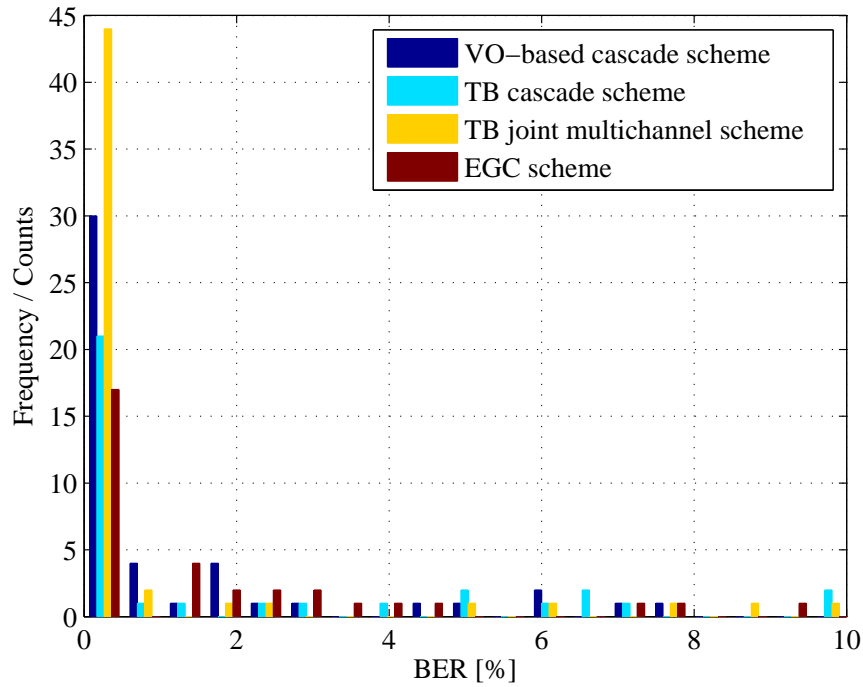


Fig. 4.18: Field-test data based performance analysis of the reference signal-based schemes

receiver installation in MPT applications a simulation environment of a three-receiver structure is arranged. The channel impulse responses are obtained from a commercial borehole with three-receiver structure (**Appendix. B.3**). Such simulations enable to deliver a performance comparison in a quantitative point of view. It should be noted that all evaluations are carried out with the same simulation setup. The evaluation is twofold: In **Fig. 4.19** the BER performance is plotted versus SNR and **Fig. 4.20** shows the performance gain in terms of BER vs. SIR. In both case a performance improvement of almost 6 dB can be achieved. Since there are not sufficient field-test records of three-receiver structures, the real data analysis is limited to a data set of different carrier frequencies and data rates. The evaluation results in terms of BER [%] and calculated SNR [dB] is given in **Table 4.1**. As seen the three-receiver structure outperforms any other optional two-receiver structures. The explanation for the inferior performance of three-receiver structure at $f_c = 40$ Hz and $R = 40$ bit/s is the higher ISI to be combated.

The final step in examining the joint multichannel scheme, so far the most promising scheme, is to evaluate the efficiency with different types of reference signals available in the MPT system. In the previous evaluations, the reference signal used in the evaluation is a training sequence of data symbols having the same carrier and data rate as the telemetry signal. Another possibility is to use the synchronization chirps so-called fat-chirps (FC) as the reference signal. The analysis is performed for field-test data recorded at different rigs and plotted in **Fig. 4.21** as a function of BER counts. The BER performance of fat-chirp-based scheme at higher data rates is lower than that of training-based (TB) as reflected in the results. The reason is twofold: First the available 0-40 Hz fat-chirp does not cover the whole spectrum at a higher data rate and as a reference signal is of less power comparing to the TB alternative. Second the autocorrelation function of FC is not as close to that of a telemetry signal and thus the assumption required to reduce the

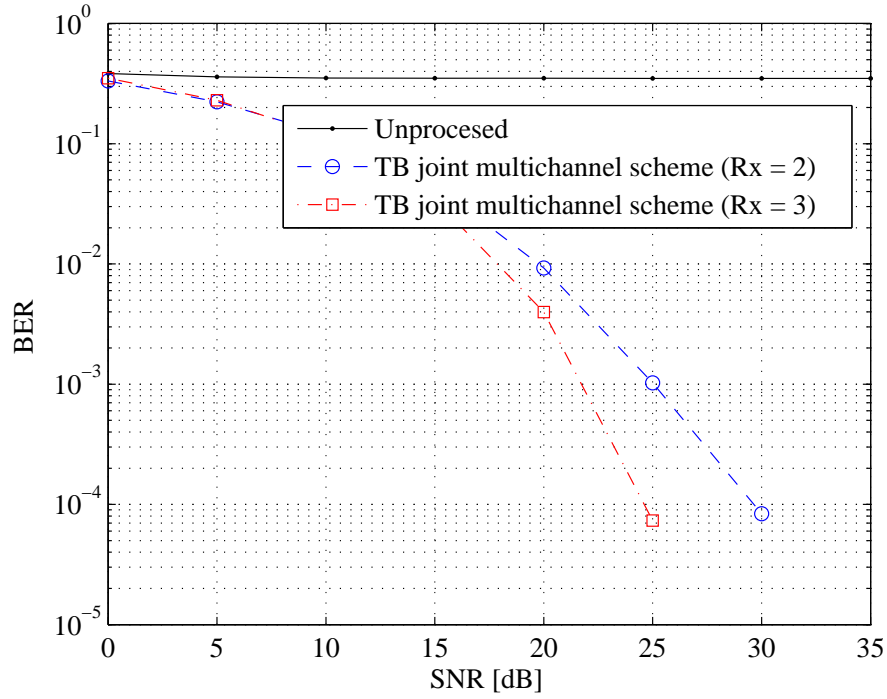


Fig. 4.19: BER vs. SNR for different spatial diversity in the presence of AWGN and pump interference with $SIR = -15$ [dB]

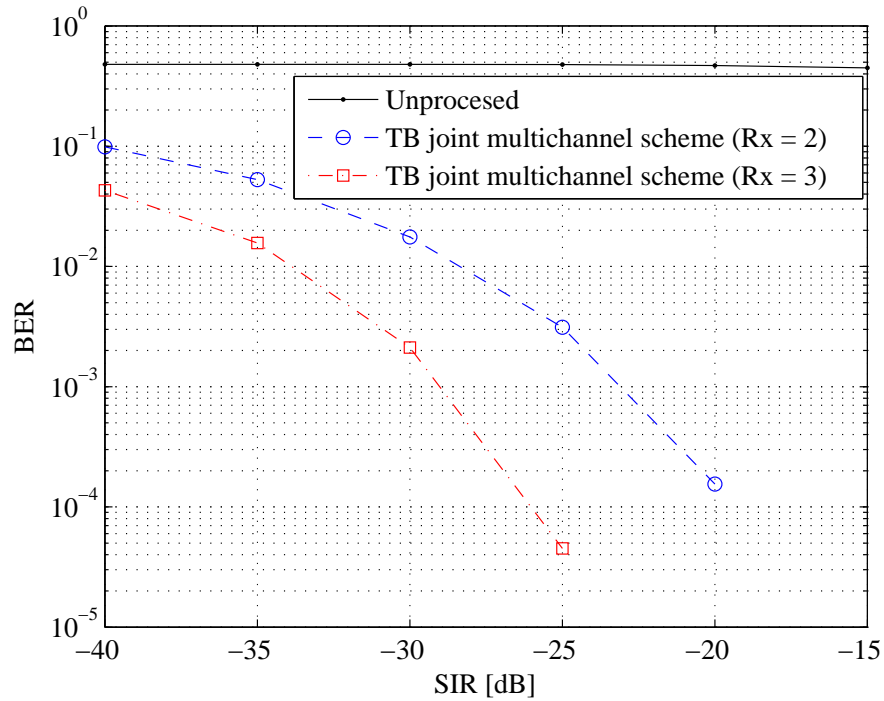


Fig. 4.20: BER vs. SIR for different spatial diversity in the presence of pump interference and a noise free channel

f_c [Hz], R [bit/s]	Rx {1, 2, 3}		Rx {1, 2}		Rx {1, 3}		Rx {2, 3}	
	BER	SNR	BER	SNR	BER	SNR	BER	SNR
9, 3	0	19.29	0	15.04	0	17.33	0	15.96
10, 5	0	15.33	0	12.64	0	15.24	1.84	5.85
15, 5	0	18.70	0	16.06	0	19.55	0	14.76
30, 10	0	20.79	0	17.66	0	20.80	0	17.27
20, 20	0	11.52	0.19	9.63	0.09	8.99	4.45	5.77
40, 40	12.59	4.10	13.54	3.58	6.91	4.43	12.88	3.57

Table 4.1: Performance gain due to spatial diversity in field-test data based evaluation

delay spread of the dispersive channel is not fulfilled. However a comparable performance can be still achieved with alternative reference signals. Moreover, a larger reference signal length can be offered utilizing both TB and FC possibilities.

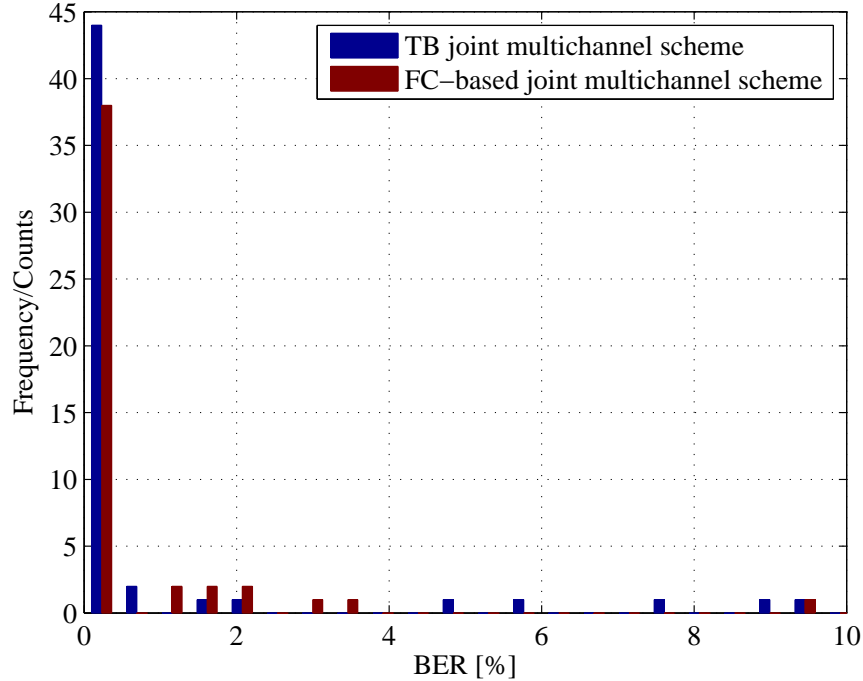


Fig. 4.21: Field-test data based performance evaluation of joint multichannel scheme with alternative reference signals

4.4 Summary and conclusion

In this chapter, the cascade and joint receiver architectures are presented and analyzed from different perspectives. Both approaches deploy a training sequence, transmitted for the telemetry data at the beginning of drilling operation, to adjust the receiver parameters

initially. Such receiver structures facilitate the parameter readjustment or the tracking task during the regular operation using the estimated signal as a new training sequence. The main achievement is to cancel the pump interference without requiring any kind of knowledge about the interference. The interference rejection ability is provided by the multichannel receiver structure. A simulative and real-data comparison of the proposed methods is conducted. It is shown that the joint interference and cancellation scheme has the best performance in terms of BER as well as stability. Based on this investigation, alternative interference avoidance algorithms will be presented in the next chapter, where neither multichannel receiver structure nor knowledge on the pump signal is required. Hence, the system performance can be improved by utilizing the multichannel receiver structure to perform channel equalization explicitly. In addition, it might be interesting to combine the algorithms proposed in this chapter and semi-blind schemes to improve the system performance as well as to support the tracking task.

Chapter 5

Interference avoidance techniques via transform domain filtering

The proposed approaches in the previous chapters principally aim the signal reconstruction without explicitly considering the cause of distortions. This chapter focuses on individual investigation and processing of signal distortions. As discussed, the pump interference of non-stationary character damages the telemetry data at most. Therefore, first of all the interference caused by the pumps is to be removed. Afterwards, ISI induced by the mud channel at high data rate transmission is to be equalized. The requirement to be fulfilled is that the interference rejection has to be performed without any information on pump and telemetry signals and thus should be adjustable. Further investigations of this chapter concern different proposals on hybrid algorithm development to achieve efficient, robust and simple data recovery in MPT applications. The above-mentioned issues are discussed in depth in the following sections.

5.1 A review on transform domain filtering issues

The pump signal analysis in Section 2.2 demonstrates that the pump signal is a kind of non-stationary narrowband interference relative to the mud pulse telemetry signal. Similar interference signals are encountered in different fields of applications such as communication systems, digital synthesis of musical sound and biomedical signal processing. There are many publications about the suppression of such narrowband interferences especially in direct-sequence spread spectrum communication systems [1, 30, 44, 6, 45, 64].

An effective and widely applied scheme to suppress narrowband interferences in a wide-band system is notch filtering. Traditionally such kind of filters is realized in time domain and found out to be infeasible concerning aspects such as tunability, efficiency, etc. [102]. Recent application of this approach is performed directly in frequency domain by means of Fourier transforms. Such transformations usually require additional preprocessing such as segmentation and windowing to avoid spectral leakage [102]. Frequency domain notch filtering does not exhibit deficiencies and is of several advantages concerning complicated processing issues [102]. Efficient interference suppression applying notch filters relies on the assumption of known interference. The concept of adaptive notching investigated in [103, 6] is a promising scheme. However, the notch filtering encounters difficulties in the presence of multiple-tone interferences if only one notch filter is used. On the other hand,

the desired signal might be distorted in the absence of the interference. Besides, the notch filtering usually does not work well if the interference is of non-stationary nature [6, 103].

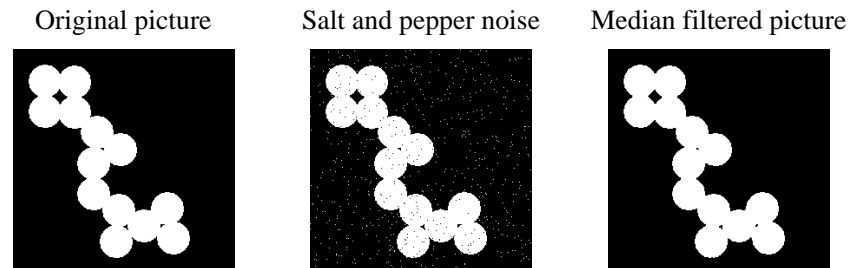


Fig. 5.1: Image restoration using median filter

The problem encountered in MPT is that, the non-stationary pump signal is strong, impulsive, of multiple tones in the frequency domain, while the telemetry signal is very weak and of wide bandwidth. Thus, the traditional notch filtering fails to work efficiently. In image processing, the median filter (MF) is widely used to suppress impulsive noises such as “salt and pepper” noise in a corrupted image in **Fig. 5.1**, while preserving the fine details of the image by smoothing relevant signals [35]. Similarly, recent communication systems based on direct-sequence spread spectrum profit from the median filters to reject non-stationary narrowband interferences. Utilizing median filters for interference suppression is motivated by the fact that in the transform domain narrowband interfering signals exhibit large and impulsive complements compared to the data signal [93]. On this account, the problem discussed in this thesis is similar to that exposed in image processing and thus the idea of median filtering will be investigated in this chapter [97].

5.2 Application of transform domain median filtering

Linear filter have been widely used in signal and image processing. However, linear filters are often inefficient in the presence of non-additive or signal dependent noise, in systems exposing non-linearities and non-Gaussian statistics [8]. The deficiencies can be overcome somehow by utilizing various types of non-linear filters. Median filter (MF), a non-linear filter proposed by Tukey (1977) [13] is deployed in several areas of digital signal processing. The major application field of median filtering is to enhance and de-noise the corrupted image information. The MF has the ability to remove narrowband and impulsive noise from corrupted pixels, whereas the image details are retained. Along with the superior performance of MF over linear smoothing approaches, MFs might result in additional signal distortions, especially if the applied filter length is large. Moreover, impulse like image information can be removed as well [35, 104]. In past decades, the MFs have been extended and improved in terms of capability and efficiency. Max/median, multistage median, weighted median and median filters with continuously adjustable filter length have been developed [104, 76]. Additionally, in physiological monitoring e.g. heart rate and blood pressure monitoring, the application of a hybrid MF is recommended by [88]

to filter out the measurement artifacts. The proposed method utilizes both temporal and spatial diversities (**Fig. 5.2**) to align the artifacts. According to [88] the spatial median filter requires at least three-receiver structure and is able to suppress artifacts if the measurements of one receiver is corrupted. However the proposed temporal-spatial hybrid scheme in [88] works with two-receiver structure, but is capable to remove special types of artifacts present in more than one receiver.

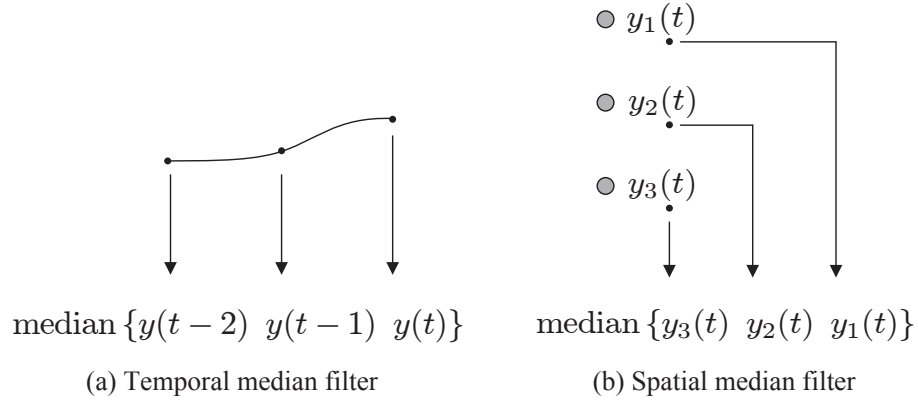


Fig. 5.2: Different realizations of median filtering

The median filter is a local processor, in which the input sequence is slotted by the filter length of N_f and at each position the output is the median value of the samples within the slot as

$$z_i = \text{median} \{y_j | j = i - k, \dots, i + k\} .$$

As mentioned, the non-linear median filtering is of twofold effects: first the signal with smoother transitions is retained, second the signals elements narrower than $k = \frac{N_f - 1}{2}$ are removed [102, 104].

Concerning the MPT problem description, the concept of median filter is realized in the frequency domain and simplifies suppression of the narrowband interferences. The suppression procedure as demonstrated in **Fig. 5.3** includes the following steps:

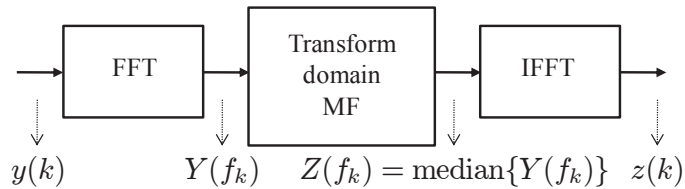


Fig. 5.3: Concept diagram of transform domain median filtering

- The received signal $y(k)$ is transformed to the frequency domain using Fast Fourier Transformation (FFT)

- Fourier magnitude transform of the received signal $Y(f_k)$ is processed by MF
- $M(f_k)$ is the MF output of an odd sized filtering window with the length N_f
- The output of median filter is transformed to the time domain using Inverse Fast Fourier Transformation (IFFT)

It should be noticed that overlap add preprocessing is a part of suppression procedure. As long as the signals to be processed exhibits a smooth frequency response, the above-mentioned method is an efficient interference removal scheme and does not induce additional distortions due to the undesired smoothing of the signal of interest. However, most of the signals, e.g. pseudo-noise (PN) random binary sequences, used in communication systems just as in MPT systems do not satisfy the smooth spectral condition. On this account, some modification of MF approach is required to deal with the signals with jittering or non-smooth spectrum. A conditional median filter (CMF) is proposed in [93, 102], where the signal components having values close to their median is not changed and only impulsive components of large magnitude are removed. The processing procedure is given by

$$Z(f_k) = \begin{cases} M(f_k) & \text{if } |Y(f_k) - M(f_k)| > C(f_k) \\ Y(f_k) & \text{otherwise} \end{cases}$$

where $Y(f_k)$ and $Z(f_k)$ are the filter input and output signals respectively, $M(f_k)$ is the median value and $C(f_k)$ is a variable threshold. Large impulses will be rejected if their duration in transform domain is narrower than $\frac{N_f-1}{2}$. The median filter length N_f specifies the maximum bandwidth of the impulsive interference encountered and can be removed. The minimum magnitude of the impulse can be controlled by the parameter $C(f_k)$. Some particular features of this scheme can be summarized as below [93, 102]:

- The frequency and bandwidth of the impulsive interference is not required
- No adaptation time after the transform is included and thus it is suited for removing non-stationary interferences
- Removing multiple interferences is performed automatically
- Real-time realizations of this technique are feasible

It is of great importance to specify $C(f_k)$ properly to avoid possible distortions resulted by the undesired signal smoothing. Since $C(f_k)$ has to be set individually at each frequency, it is challenging to define the threshold condition. In other words, the threshold has to be adjusted with respect to the signal strength. On this account, the normalized conditional median filter (NCMF) is proposed, where $C(f_k)$ is substituted by a constant threshold value C in the following equation:

$$Z(f_k) = \begin{cases} M(f_k) & \text{if } \frac{|Y(f_k) - M(f_k)|}{M(f_k)} > C \\ Y(f_k) & \text{otherwise} \end{cases}$$

The self-adaptive thresholding provided here is based on the examinations of probability distribution function (PDF) of the magnitude of the Fourier transform of the signal of

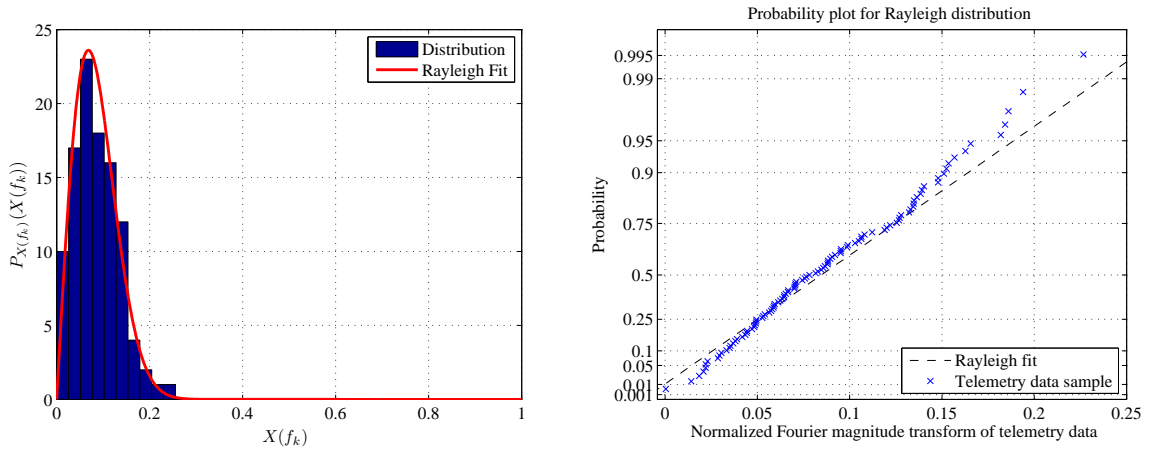


Fig. 5.4: Illustration of Fourier magnitude transform distribution in telemetry data

interest. A method of threshold establishment can be obtained if each sample of the signal spectrum is respectively compared and normalized with the expected value of the signal spectrum. In the context of NCMF, the expected value is replaced by the median value. In the MPT system a PN sequence is modulated to form the telemetry signal. As shown in Fig. 5.4 the PDF of Fourier magnitude spectrum of the telemetry signal is approximately Rayleigh. The mean value of Rayleigh distributed signals is roughly 1.5 times of the median value reflected in the NCMF equation [93]. The above-mentioned thresholding concept is drained by replacing the expected value with the median value and for the threshold value the 1.5 factor is considered.

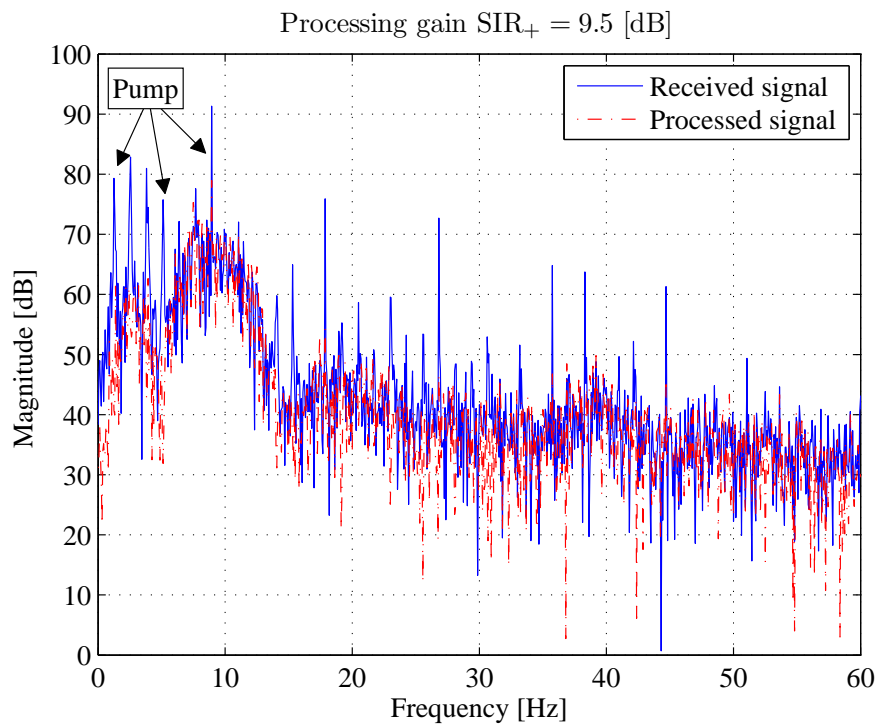


Fig. 5.5: Frequency-domain demonstration of NCMF ability in pump interference rejection

For testing the applicability of NCMF in removing pump interference a scenario is considered, where a sample data of BCPM modulated telemetry signal of 1000 bits, carrier frequency of $f_c = 10$ Hz and data rate of $R = 5$ bit/s is transmitted. The pump signal power is 10 dB higher than that of the telemetry signal. The parameter setup of median filter is $N_f = 25$ sample and FFT length of 25 s. The frequency-domain presentation of the received and processed signals in bandpass is displayed in **Fig. 5.5**. It is noticeable that the signal at the frequency corrupted by the pump is smoothed without any requirement on a-prior knowledge. A processing gain of $SIR_+ = 9.5$ dB is achieved utilizing NCMF scheme. Also the time-domain representation of the received and median-filtered signals in **Fig. 5.6** demonstrates the improvement of detection performance in terms of BER.

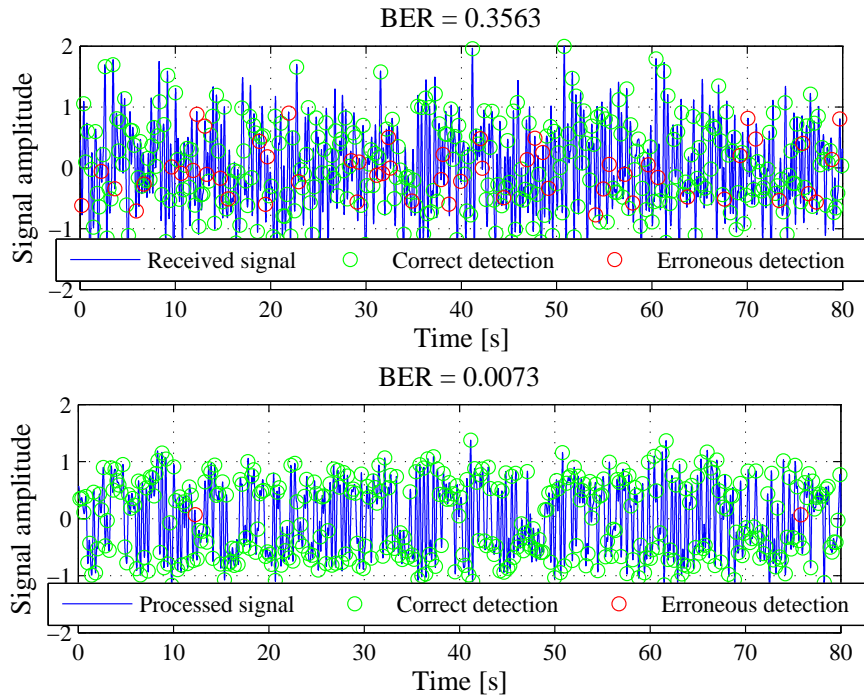


Fig. 5.6: Time-domain demonstration of NCMF ability in pump interference rejection

Some results on general residual error analysis of CMF and NCMF reported in [103] indicate superior performance of these techniques comparing to that of the notch filtering scheme. In the context of MPT, the interference rejection ability is examined in some respects. In the first step, the processing gain achievable by NCMF at different SIRs is determined. For the above-mentioned scenario the SIR at the output of median filter SIR_{out} is plotted vs. the one at its input SIR_{in} . The results in **Fig. 5.7** submit that as SIR_{in} decreases, the SIR_+ increases.

The second part of examinations, which concerns the impact of parameter setup on the performance results, is twofold: first the window size of overlap add pre-processing, second the smoothing length N_f . The evaluations with different setups of window size and filter length is performed on a data set obtained from a borehole. The evaluation results in terms of BER and calculated SNR vs. window size as well as filter length N_f are displayed in **Fig. 5.8** and **Fig. 5.9**.

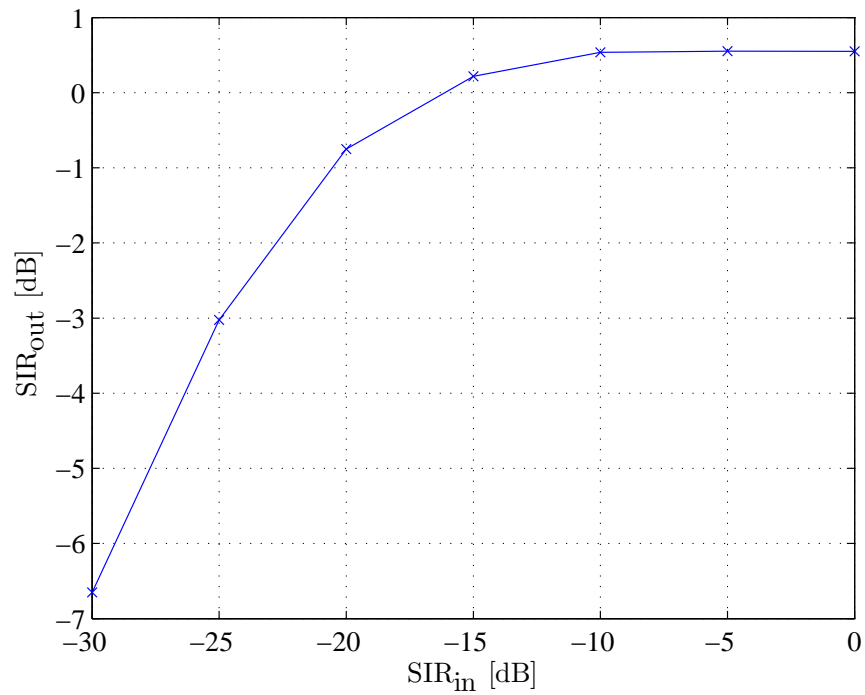


Fig. 5.7: Processing gain ($SIR_+ = SIR_{out} - SIR_{in}$) achieved by NCMF

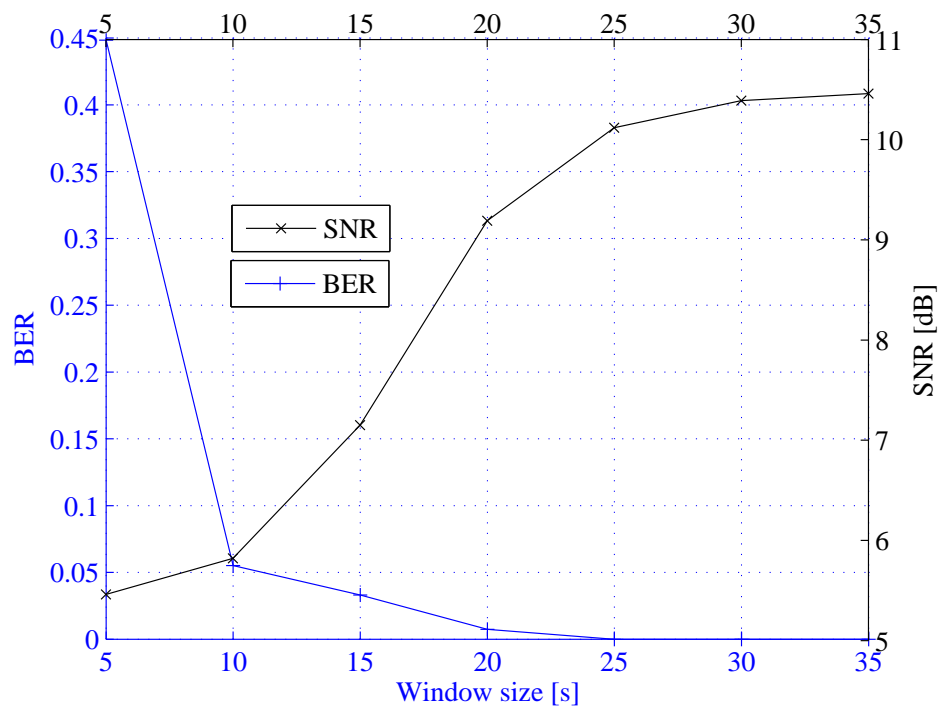


Fig. 5.8: BER/SNR performance vs. window size applied in overlap add pre-processing (better BER/SNR at larger window size)

It is noticeable that appropriate parameter settings are of great importance and allow the

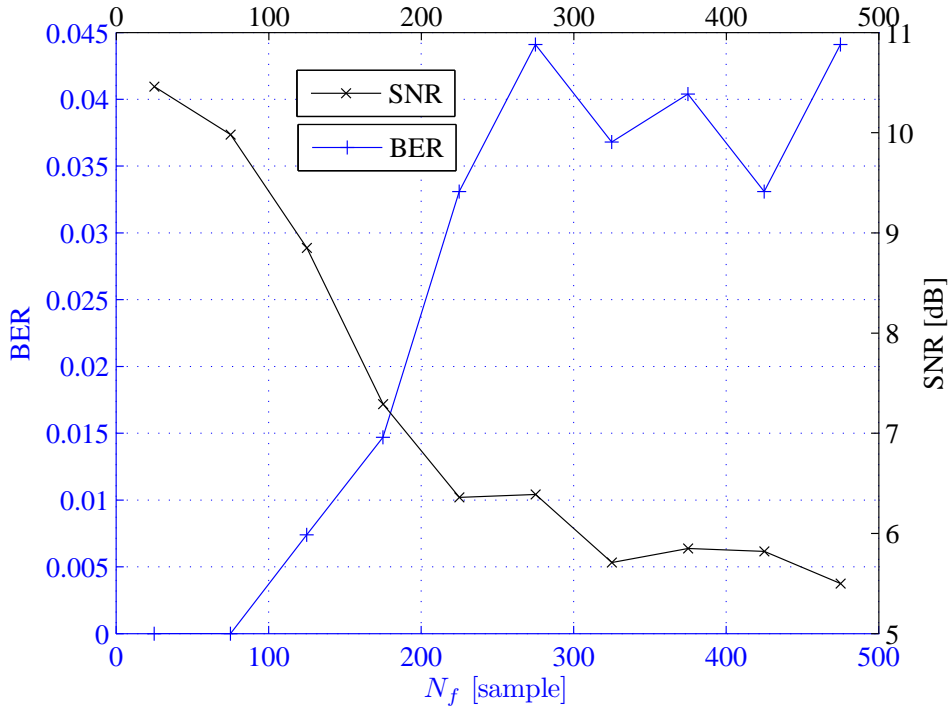


Fig. 5.9: BER/SNR performance vs. median filter length (better BER/SNR at smaller window size)

algorithm to deliver best performance. Better performance is provided by a larger window size or FFT length, which again induces a larger processing delay. As mentioned before the filter length complies the bandwidth of interference to be suppressed. In other words, the wider the interference bandwidth is, the larger the filter length will be. The inferior performance of NCMF with larger filter lengths in **Fig. 5.9** indicates the shortcoming of NCMF in cancelling wideband interferers.

5.2.1 Simulation and experimental results

In this section a more comprehensive performance study of NCMF is provided, where both simulative and field-test data from different boreholes are analyzed.

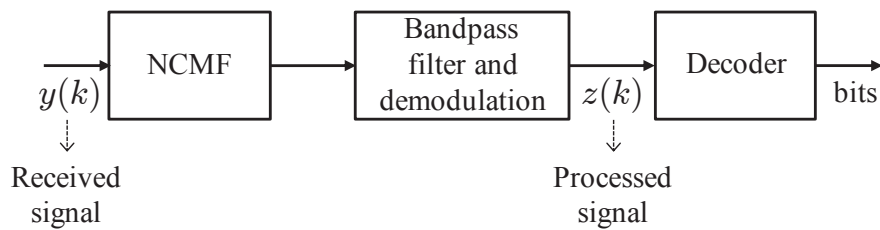


Fig. 5.10: Receiver arrangement considered in the evaluations of NCMF

To get an assessment of the efficiency of proposed scheme in MPT applications, the method using pump strobe sensors is also used in the investigations. Finally the evaluation results are compared and discussed. However the three-receiver structure facility in MPT system also offers deploying the spatial NCMF, but the performance of this scheme is rather poor. Because the spatial NCMF is unable to remove interfering signals, if two or all of the received signals are affected. In this regard, a Single-Input Single-Output (SISO) system structure given in **Fig. 5.10** is considered in the evaluations.

Similar to the previous chapters, an initial performance study is carried out in a simulation environment arranged according to the MPT system model presented in Chapter 1. Extracted CIRs from a test borehole (see **Appendix. B.1**) are used in the simulations. The simulation setup is summarized in **Table 5.1**.

Modulation type	BCPM
Carrier frequency	$f_c = 40$ [Hz]
Data rate	$R = 40$ [bps]
Sampling rate	$f_s = 1024$ [Hz]
SNR range	0 – 30 [dB]

Table 5.1: Simulation parameter setup in the evaluation of NCMF

For different media noise with the same SNR 100000 Monte-Carlo trials are performed in the simulations. The parameter setup for NCMF scheme is given in **Table 5.2** and applies to all evaluations in this section.

Sectioning and windowing method	Overlap add
Window type	Hamming
Window size	25 [s]
FFT size	25 [s]
Window shift percent	40%
Median filter length (N_f)	25 [sample] or 1 [Hz]

Table 5.2: Parameter setup of NCMF

In the simulative part of studies, an interference free scenario is considered, where the telemetry signal is affected explicitly by the mud channel and AWGN. The performance results are provided in **Fig. 5.11** as a function of BER vs. SNR and compared with the one, where no processing is performed. It is seen that the resulting BER by NCMF approaches the one without processing. Similar result has been reported in [93] as well, where the data signal has been subject to a Rayleigh fading. In other words, the NCMF scheme does not degrade the system performance in the presence of the mud channel.

In addition to the simulations, field-test data obtained from different rigs are analyzed to examine the performance of the proposed algorithm experimentally and to have a comparison with the performance of processing utilizing pump strobe sensors.

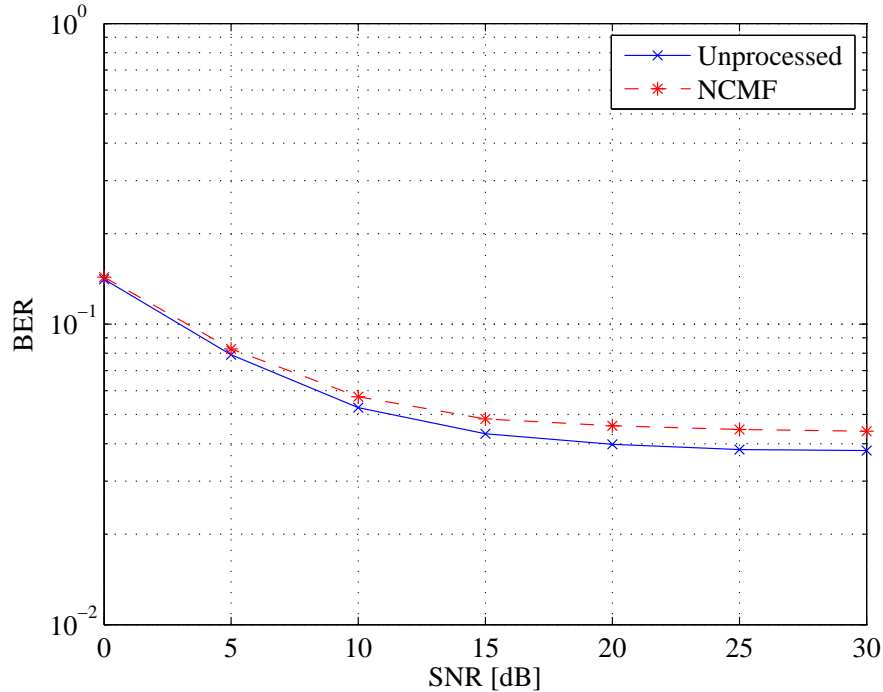


Fig. 5.11: BER vs. SNR results in absence of the pump interference

First, the efficiency of NCMF in removing the pump interference is compared to that using pump strobe sensors by means of spectrogram presentation of the received and processed field-test sample data. **Fig. 5.12** and **Fig. 5.13** confirm the narrowband interference suppression ability of NCMF promised by the theory. Furthermore, the spectrogram of processed data in **Fig. 5.13** and **Fig. 5.14** demonstrates an even better efficiency of the NCMF in comparison to the scheme using pump strobe sensors.

Similarly 60 field-test data sets are involved in the evaluations and the BER frequency/counts is used as the performance measure. The evaluation results illustrated in **Fig. 5.15** show the ability of NCMF processing approach in removing the pump interference. However the BER performance (lower than 10^{-3}) of the method based on pump strobe sensors is partly better than that of NCMF, but in total both schemes are of comparable efficiency, especially for the BER around 10^{-2} . This is due to the fact that, the NCMF is not able to avoid the interference components with $SIR \approx 0$. In other words, if the FFT magnitude value of the interference component is comparable with that of the telemetry data, it cannot be recognized as the interference and removed by the NCMF. This might result in erroneous data detection.

It must be noticed that a better performance utilizing NCMF can be achieved by overall parameter optimization with respect to all field-test data, e.g. precise knowledge on the maximum bandwidth of pump interference encountered in MPT systems. Because of no need on any kind of a-priori knowledge and cost-efficiency, NCMF attains great attraction in MPT applications. By deploying NCMF as a preprocessing function to increase the SIR, not only the synchronization task but also the reliability of channel estimation and signal detection can be greatly improved.

On this account, it is also of great importance to investigate the effect of NCMF on

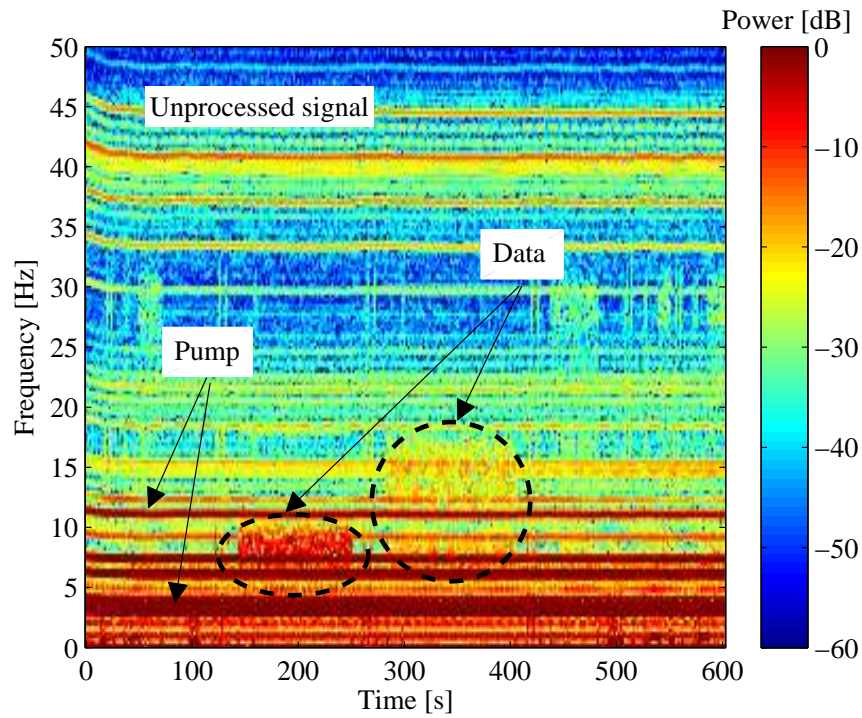


Fig. 5.12: Spectrogram of the unprocessed received field-test data (horizontal lines show harmonic pump signal and labeled areas bandpass data signal)

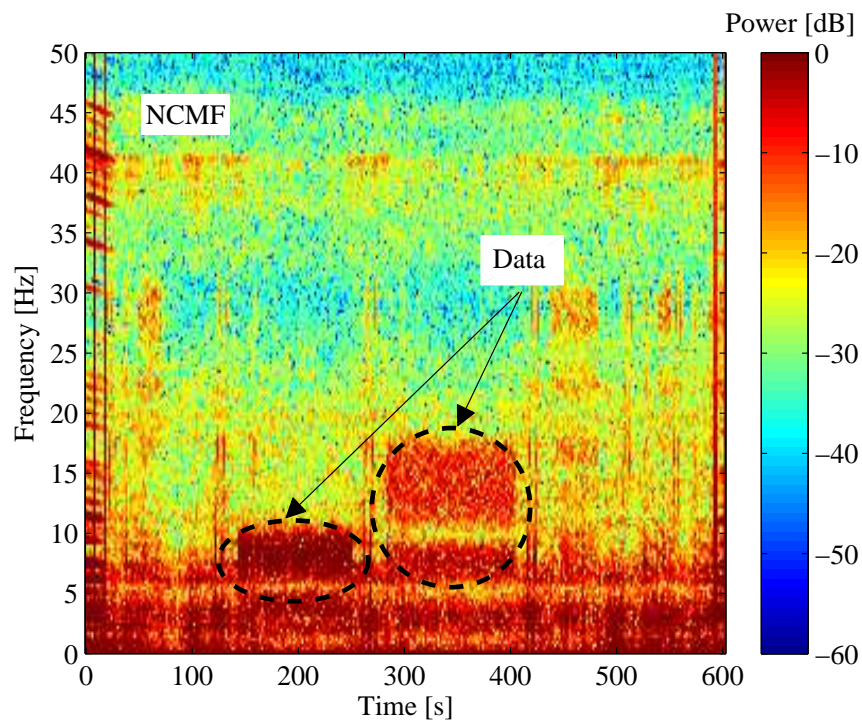


Fig. 5.13: Spectrogram of the processed field-test data using NCMF (labeled areas show bandpass data signal)

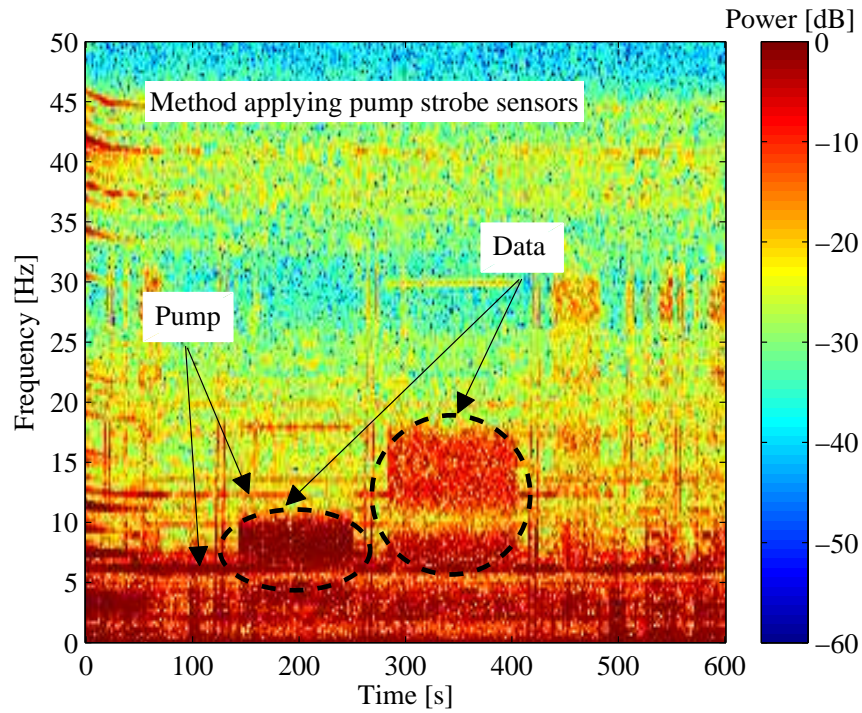


Fig. 5.14: Spectrogram of the field-test data processed using pump strobe sensors (horizontal lines show residual harmonic pump signal and labeled areas bandpass data signal)

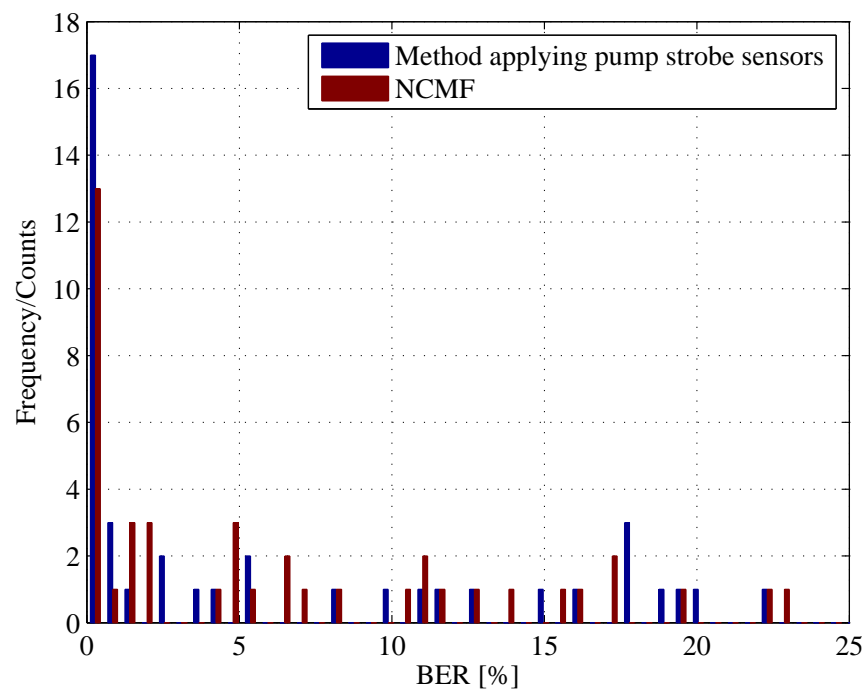


Fig. 5.15: Field-test date based performance analysis of NCMF

FC signals, which are used for the synchronization and CIR extraction. Accordingly, the impact of the NCMF on the signal shape and the autocorrelation property of FC is demonstrated in **Fig. 5.16**. Since the FFT magnitude of FC signal is of less oscillation, as expected the NCMF does not induce notable distortions to the FC signal, whereas the pump interference is removed. Especially the auto-correlation function, an important function of synchronization and channel estimation methods, is almost unaffected by NCMF. Since synchronization is not the scope of this work, it is not further explored.

Referring to the above-mentioned discussion, a reliable preprocessing scheme for removing the strong pump signal interference is provided by NCMF. Since the FC signal applied for the channel extraction does not experience any additional distortions, more precise CIR estimation can be delivered. The CIR extraction issue is discussed in depth in the following section.

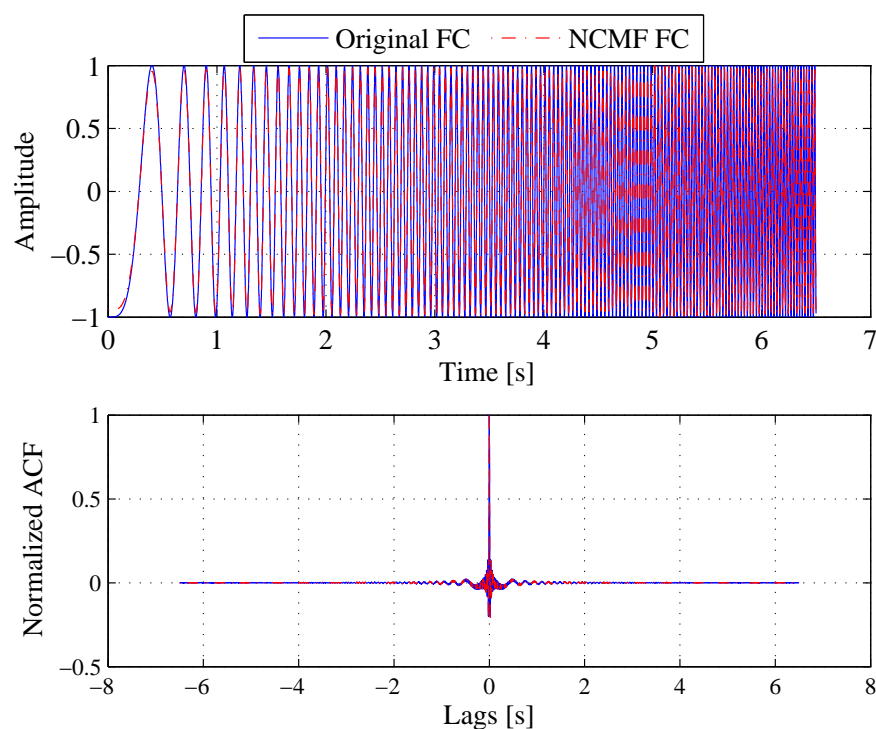


Fig. 5.16: The impact of NCMF on the shape and the autocorrelation characteristic of FC signal

5.3 Hybrid schemes

The issues of this section are motivated by the investigations of the previous chapters. The strong pump signal inherent in MPT systems is the major difficulty in accurate channel estimation and telemetry data reconstruction. By now, it is focused mainly on the signal recovery without distinct investigation of the distortions cause. The application of NCMF provides the facility to explore the interference and channel effects individually.

In other respects, signal reconstruction strategies can be developed much more efficiently and reasonably. This section investigates deployment of hybrid schemes, namely NCMF in combination with other schemes proposed in this thesis. In this regard, the following contributions are delivered in this section:

- Suggestion of schemes based on hybrid NCMF and clean algorithm to extract the mud channel impulse response and deliver some knowledge on characteristics of the transmission medium.
- Investigation of NCMF in combination with adaptive diversity combining schemes; where schemes based on a training sequence as well as semi-blind approaches are conducted.
- Real-world evaluation and comparison of the proposed schemes using field-test data obtained from different boreholes.

5.3.1 Mud CIR extract via combined NCMF and CLEAN algorithm

As stated, the MPT channel extraction in this work is performed to support the simulation experiments. So far, conventional channel estimation methods alone are not sufficient to fulfill accurate channel extraction and deliver reliable information on behavior of the transmission medium. Therefore, the deployment of additional signal processing is reasonable to increase the reliability of channel estimation schemes. In this regard, the combination of NCMF and clean algorithm seems to be a suitable construction. In general, the channel extraction can be performed by applying a time- or frequency-domain technique or a sliding correlator [105].

In this thesis, time-domain schemes are mainly used for the signal processing and thus the channel extraction is also based on a time-domain scheme. The CLEAN algorithm is a well-known time-domain scheme for the channel estimation, especially in ultra-wideband systems. Among the algorithms proposed for the channel estimation, the CLEAN algorithm due to its simplicity and high-resolution capability is seen as a promising approach [101]. The reason is that, the CLEAN algorithm directly compares the cross-correlation function (CCF) and auto-correlation function (ACF) of the received and transmitted signals to extract the CIR. As shown in Section 5.2.1 the ACF of the FC signal is unaffected after applying NCMF and thus is a reliable characteristic to derive the CIR.

The CLEAN algorithm is basically a deconvolution method, where the CIR is provided iteratively. The basic algorithm is proposed in [90] for the narrowband channel assumption and is further enhanced to be applicable in wideband channel characterization [91]. The major feature of the CLEAN deconvolution scheme is that the estimate of CIR $\hat{h}(\tau)$ is modeled as a discrete FIR filter. To extract the CIR, the availability of a signal known to the receiver, also known as the template is assumed. The ACF and CCF properties of the template affect the performance of this scheme. The synchronization chirps (FCs) imbedded in the MPT system serve as a template and can be deployed to extract the CIR.

The CLEAN algorithm is described in many publications [101, 19] and different realization of this approach are proposed. In the following, the procedure of CLEAN algorithm applied

to the MPT system is demonstrated. If $x_{\text{FC}}(k)$ is the template signal and $y_{\text{FC}}(k)$ the received signal, each iteration of the CLEAN algorithm to find the CIR involves the following steps [101]:

1. A temporary channel impulse vector is defined by $c_k(\tau)$ and initialized by zeros $c_0(\tau) = 0$.
2. The auto-correlation of the template and the cross-correlation of the received signal and the template is calculated as follows:

$$R_{x_{\text{FC}}x_{\text{FC}}}(\tau) = E [x_{\text{FC}}(k)x_{\text{FC}}(k + \tau)]$$

$$R_{y_{\text{FC}}x_{\text{FC}}}(\tau) = E [y_{\text{FC}}(k)x_{\text{FC}}(k + \tau)]$$

3. A temporary vector $d_k(\tau)$ is defined and initialized with the CCF as $d_0(\tau) = R_{y_{\text{FC}}x_{\text{FC}}}(\tau)$
4. The relative time delay $\hat{\tau}_k = \arg \max_{\tau} |R_{y_{\text{FC}}x_{\text{FC}}}(\tau)|$ and the normalized amplitude $\hat{\alpha}_k = R_{y_{\text{FC}}x_{\text{FC}}}(\hat{\tau}_k)$ are calculated.
5. The CIR is recovered by $c_k(\tau) = c_{k-1}(\tau) + \hat{\alpha}_k \delta(\tau - \hat{\tau}_k)$
6. The temporary CCF vector is updated by $d_k(\tau) = d_{k-1}(\tau) - \hat{\alpha}_k R_{x_{\text{FC}}x_{\text{FC}}}(\tau - \hat{\tau}_k)$.
7. If the correlation peak $\hat{\alpha}_k$ is below a set threshold value (e.g. -20 dB in this thesis) the algorithm stops and goes to step 8, otherwise it returns to step 4.
8. The CIR is $\hat{h}(\tau) = c_k(\tau)$.

As stated, the above steps are repeated till the signal energy descend below a predefined threshold. The threshold of the peak path strength specified in many publications is in the range of 15 - 25 dB. It must be noted that an optimal threshold is chosen by taking the energy capture ratio (ECR) and the relative error (RE) into account. In the following, the definition of ECR and RE is given [65]:

$$ECR = \frac{\|\hat{y}_{\text{FC}}(k)\|^2}{\|y_{\text{FC}}(k)\|^2}$$

$$RE = \frac{\|\hat{y}_{\text{FC}}(k) - y_{\text{FC}}(k)\|^2}{\|y_{\text{FC}}(k)\|^2} .$$

In the MPT system, to extract the CIR, measurements of the boreholes considered, where in certain intervals of around 3.5 minutes a FC transmitted. The basic channel extraction procedure is demonstrated in **Fig. 5.17**. As seen, the procedure includes three steps: first the pump distortions are removed utilizing NCMF, second a coarse synchronization is performed to find the received template, and finally the clean algorithm is applied to extract the mud channel, namely the channel from the drill bit to the surface. The

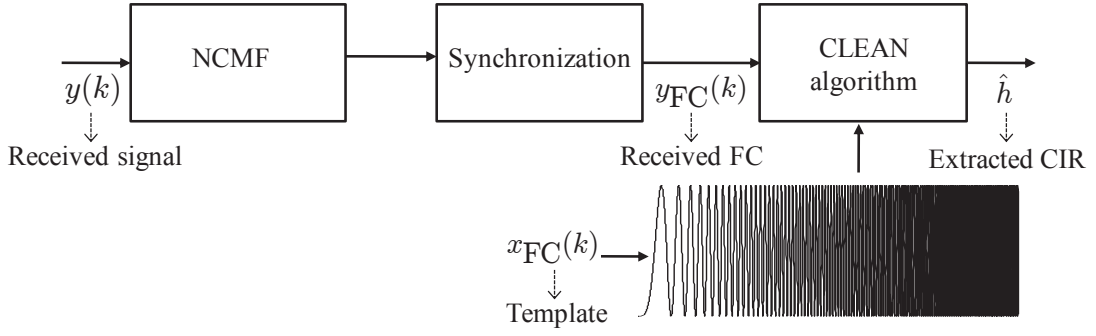


Fig. 5.17: Block diagram of the channel extraction concept

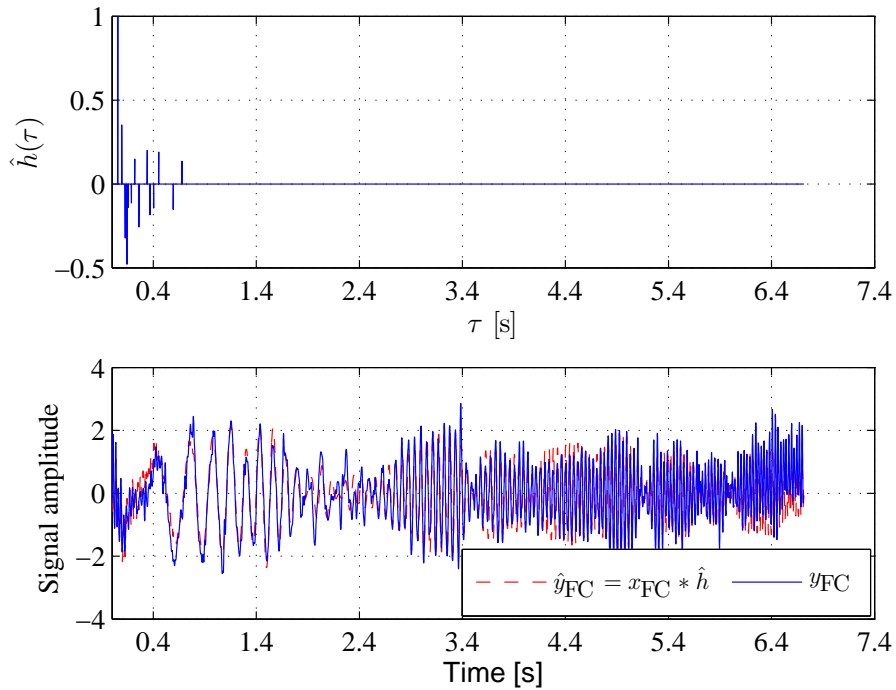


Fig. 5.18: Sample CIR extracted from field-test measurements

threshold amounts 20 dB and is determined using ECR and RE. A sample extracted CIR is shown in **Fig. 5.18**, with $ECR = 0.857$ and $RE = 0.175$.

Moreover, the extracted CIRs for all FCs of the measurements provides some information, e.g. how mud channel changes over time. An example of extracted CIRs is illustrated in **Fig. 5.19**. As seen, the variation of the sample channel over the time is marginal and thus the assumption of time-invariant channel is eligible.

In the final step of the examinations, the channel frequency response (CFR) of different measurements is explored. Based on our observations exemplary shown in **Fig. 5.20**, it can be concluded that the mud channel has a similar function of a low pass filter and attenuates higher frequency. Also, a frequency selective behavior of the channel is expected. As observed, the maximum delay τ_{max} or the meaningful duration of the channel might be up to 1 s. If this exceeds the symbol duration of transmitted data, due to the channel

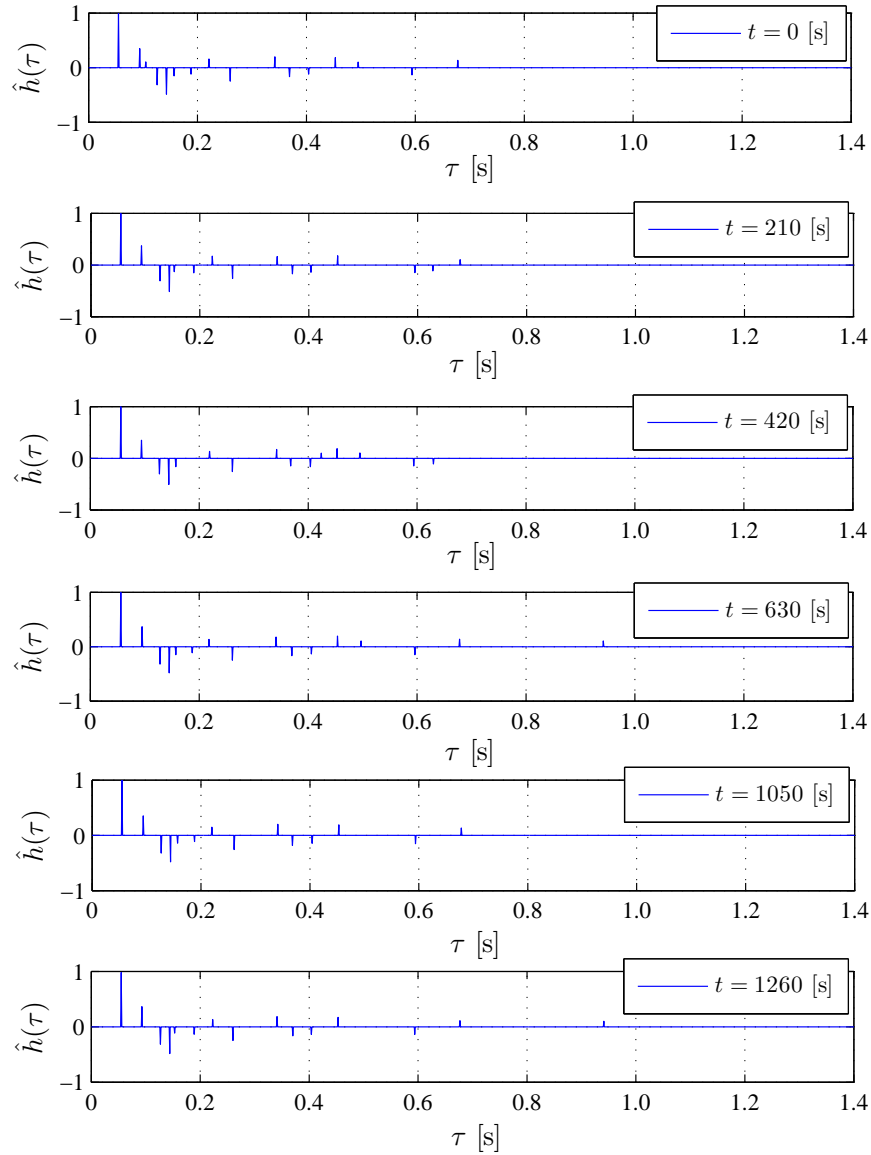


Fig. 5.19: Observation of channel behavior over the time

frequency selectivity ISI distortions are caused. Therefore, for high data rates distortions caused by the mud channel are of the same importance as those caused by pump interference. In this case, the channel equalization is necessary for error free detection of the telemetry data.

Moreover, an estimate of some important parameters to describe the mud channel characteristics e.g. the mean delay $\bar{\tau}$ and the root mean square (rms) delay spread τ_{rms} can be obtained ¹. An estimate of $\bar{\tau}$ and τ_{rms} for sample borehole measurements are given in **Table 5.3**.

$${}^1 \bar{\tau} = \frac{\sum_{k=1}^{k_{\tau_{max}}} \tau_k |\hat{h}(\tau_k)|^2}{\sum_{k=1}^{k_{\tau_{max}}} |\hat{h}(\tau_k)|^2}, \text{ and } \tau_{rms} = \frac{\sum_{k=1}^{k_{\tau_{max}}} (\tau_k - \bar{\tau})^2 |\hat{h}(\tau_k)|^2}{\sum_{k=1}^{k_{\tau_{max}}} |\hat{h}(\tau_k)|^2} \quad [15].$$

borehole	$\bar{\tau}$ [s]	τ_{rms} [s]
Test	0.0540	0.0699
Commercial	0.1584	0.1347

Table 5.3: Estimated $\bar{\tau}$ and τ_{rms} for sample boreholes

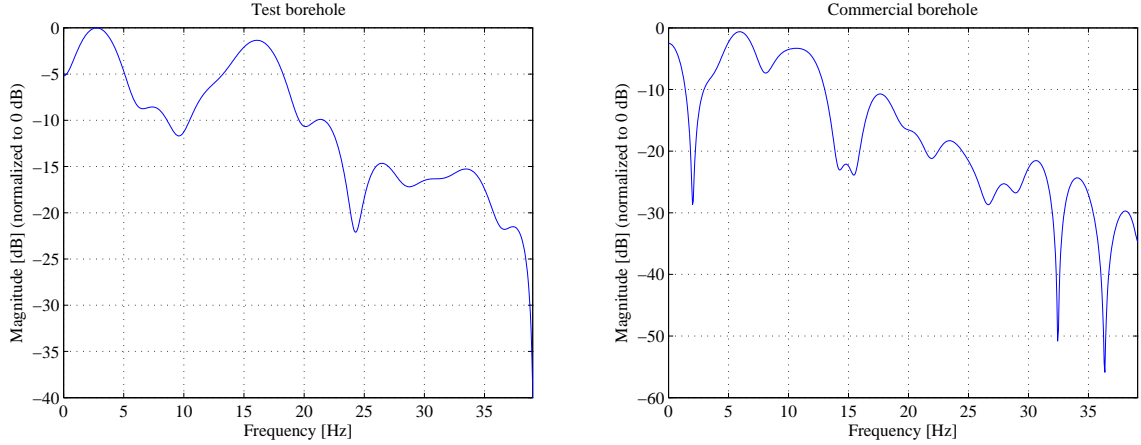


Fig. 5.20: Sample CFRs extracted from field-test measurements

Based on the investigations within the realms of the possibility, it can be stated, that the mud channel is approximately time-invariant and exhibits frequency selective property. It must be noticed that providing a channel model for mud transmission medium requires special field-test measurements and goes beyond the scope of this thesis.

5.3.2 Combined NCMF and adaptive diversity combining schemes

This section deals with hybrid schemes aiming efficient signal reconstruction. Signal distortions caused by the interference and the channel in MPT systems are compensated individually. In other words, a two-step sequential procedure is followed; first the signal distortions caused by the pump interference are suppressed utilizing NCMF, second the distortions caused by the mud channel and/or by any other source are equalized. By this means, however, the automatic tracking of interference avoidance section is ensured. But for the equalization section the necessity as well as the strategy of tracking has to be investigated. In fact, development of a robust and cost-efficient receiver is pursued according to the MPT requirements in practical applications.

Some fusion methods for hybrid signal reconstruction schemes using NCMF and adaptive diversity combining are suggested. These techniques rely on the multichannel CMA semi-blind and the TB joint multichannel algorithms of Chapter 3 and Chapter 4. In the following, these methods are described and the advantage and drawback of each scheme is discussed.

5.3.2.1 Hybrid NCMF and multichannel blind schemes

The combination of NCMF and multichannel semi-blind schemes has the potential of being a desired fusion method for MPT applications in terms of automatic tracking during the regular operation. Such receiver architecture provides the facility of compensation of both interference and channel effects without requiring any a-priori information. A block diagram of the receiver architecture based on hybrid NCMF and a multichannel semi-blind scheme is illustrated in **Fig. 5.21**. Because no VO and/or reference signal is required by the proposed hybrid scheme, it is of great attraction in real-time MPT applications.

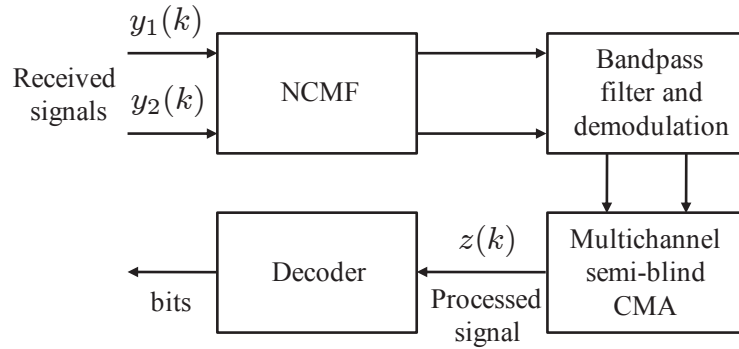


Fig. 5.21: Block diagram of hybrid NCMF and multichannel semi-blind scheme

As shown in Chapter 3, the multichannel (MC) blind and semi-blind signal recovery schemes are not efficient for both channel equalization and/or interference cancellation. After removing the interference, the multichannel scheme can be utilized to deal with the channel distortions. Provided the channels are independent from one another, blind multichannel equalization is almost feasible with robust and accurate estimation. The multichannel structure, also known as SIMO system, is provided whether by the space diversity e.g. two-receiver structure of the MPT system or/and by the time diversity e.g. oversampling. According to [58], global convergence of HOS-based techniques (e.g. CMA) is proved in MC systems. Also, SOS of the received signals is sufficient for blind equalization having MC structure [58]. As is generally known, two estimation policies can be utilized: estimate the channels and apply either a nonlinear equalizer (e.g. Viterbi algorithm) or linear FIR equalizer e.g. Zero-Forcing (ZF)/ Minimum Mean Square Error (MMSE) to recover the transmitted signal, or bypass the channel estimation step and estimate the equalizer, in other words, the signal directly [22]. Due to the high robustness and advantages for low complexity online demodulation, the direct equalizer estimation is the most preferred scheme.

In general, three kinds of MC equalizer estimations methods are available [58]; Linear prediction (LP) method, signal subspace (SS) method and mutually referenced equalizer (MRE) method. The latter is of good estimation accuracy, moderate computational, closed form solution, globally convergent, adaptive implementable and robust to SNR and ill-defined equalizer length. Therefore it is preferred at most in practice.

MC MRE scheme is investigated comprehensively in [21, 22] and compared with the MC CMA scheme. However, the performance results of MC MRE approach is comparable to

that of MC CMA, even partly better in terms of convergence rate, but is less reliable due to the strict assumption of independent channels. Since MC CMA is also supported by signal property restoration, it is seen as a more reliable approach in MPT applications.

To explore the signal correlation in the MPT channel, the correlation between the received signals can be observed. Large receiver separation leads to spatially uncorrelated channels. As mentioned before, the receiver spacing in MPT system is restricted and results in higher correlation. The correlation coefficients obtained from an example of field-test data in **Table 5.4** confirm this claim.

f_c [Hz], R [bps]	correlation coefficient
9, 3	0.7455
10, 5	0.8135
15, 5	0.7831
20, 20	0.5188
30, 10	0.6055
40, 40	0.3968

Table 5.4: Correlation coefficients in a representative field-test measurement

Therefore, the MC MRE scheme solely relying on the assumption of uncorrelated channels is less efficient. Moreover, usually the system is reduced to a SISO system and as expected, the MC CMA also suffers from the existence of local minima and poor convergence as shown in Chapter 3.

The main drawback of the proposed fusion method lies on the multichannel CMA semi-blind equalization section. As mentioned, instability, divergence possibility and parameter-reliant performance of semi-blind CMA increase the BER of telemetry system and make the algorithm inefficient in practice.

5.3.2.2 Hybrid NCMF and TB multichannel diversity combining adaptive schemes

A more robust and reliable hybrid estimation approach is offered by realizing the equalization section based on a training sequence scheme. In this regard, two consecutive architectures are conceivable, discussed within this section.

Pre-NCMF and multichannel adaptive diversity combining post-equalization

According to the first proposal for the MPT receiver structure, interference avoidance by deploying NCMF on each received signal is carried out first. Afterwards the channel effects are equalized by exploiting the two-receiver structure and training sequence facility in the MPT system. Note that automatic tracking is provided solely in the interference cancellation part. The equalization section is of adaptive structure and can be tracked either by a decision feedback approach or using periodically transmitted signals (e.g. synchronization chirps). The block diagram of such receiver architecture is illustrated in **Fig. 5.22**.

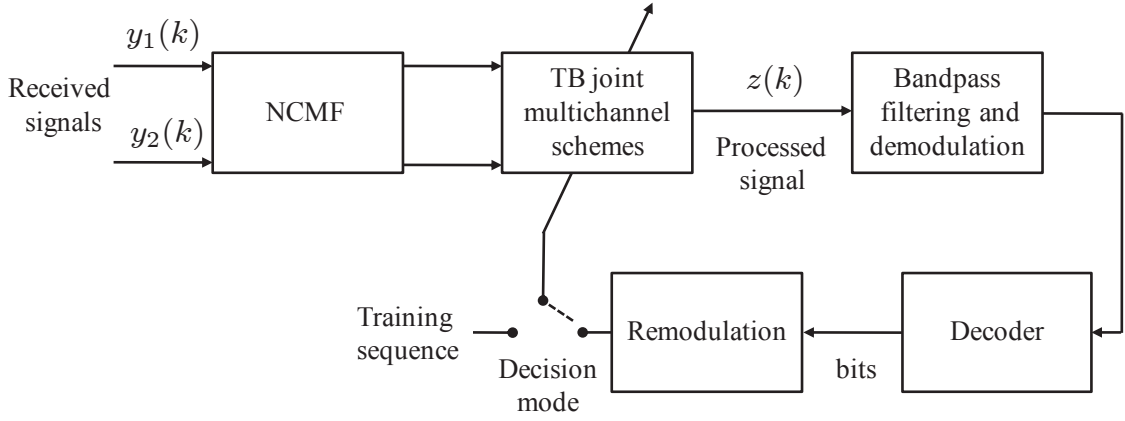


Fig. 5.22: Block diagram of hybrid pre-NCMF and multichannel post-equalization

The concept of diversity and multichannel processing is quite often used together. In a multichannel system, the situation, where multiple replicas of the same signals are observed through multiple independent channels, is described as diversity. Improved signal reconstruction quality (e.g. lower BER) and increased channel capacity or data rate are indicated as diversity gain [58].

As generally known, there are different processing strategies for multichannel systems as below [58]:

- Selective combining, where the equalization is based on the best channel. Despite simplicity, this approach encounters with the problem of best channel definition in the convolutive systems.
- Separate processing and post-combining, where the equalization is performed separately for each channel and then fed into an equal gain combiner or maximum ratio combiner. This procedure maximizes SNR of desired signal in the presence of AWGN.
- Joint processing, where the equalization is performed by joint processing of the received signals to reconstruct the desired signal. This approach provides the best performance gain.

In MRC, each branch is scaled prior to the combining. In direct equalizer estimation, branch gains are obtained in a different way than that in conventional MRC, where knowledge on the channel and the SNR is required. As shown in **Fig. 5.23**, in the proposed MRC scheme the processed branches are scaled by the corresponding branch gains and combined thereafter. The output of such separate processing and post combining based on MRC is given by [66]

$$z_{MRC}(k) = \sum_{d=1}^D \lambda_d z_d(k) ,$$

where λ_d represents the branch gain of the d -th branch and D is the number of diversity branches. There are some alternatives to provide an estimate of branch gains. In the first approach called here MRC (Type I), the branch gains are estimated during the training

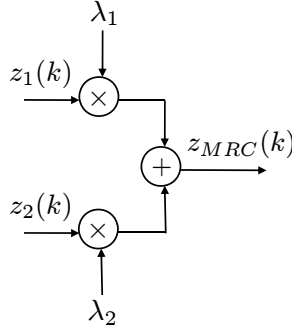


Fig. 5.23: Separate processing and post-combining based on MRC

phase by calculating the correlation coefficient of the processed signals and the training sequence at each branch as below:

$$\lambda_d = \frac{\rho_d^2}{\sum_{d=1}^D \rho_d^2} ,$$

where $d \in \{1, 2\}$ and

$$\rho_d = \frac{\sum_{k=1}^K (z_d(k) - \bar{z}_d)(x_2(k) - \bar{x}_2)}{\sqrt{\sum_{k=1}^K (z_d(k) - \bar{z}_d)^2} \sqrt{\sum_{k=1}^K (x_2(k) - \bar{x}_2)^2}}$$

stands for the correlation coefficient of the corresponding branch, whereas $z_d(k)$ and $x_2(k)$ are the equalized signal of the d -th branch and the training sequence respectively. \bar{z}_d and \bar{x}_2 are the mean values of K samples of the equalized and training signals. Another approach proposed in [66, 27] and here referred to as MRC (Type II), utilizes the normalized variance of the processed/equalized signal samples to obtain the branch gains given by

$$\lambda_d = \frac{\sum_{k=1}^{K-1} (z_d(k) - \bar{z}_d)^2}{K \max(z_d(k))} .$$

Usually the branch gains are normalized prior to the combining as follows:

$$\lambda_d = \frac{\lambda_d}{\lambda_{max}} ,$$

where λ_{max} is the largest branch gain. In the following section, a comparison of proposed MRC schemes are provided by analyzing a set of field-test data.

It should be noticed that due to the relative higher correlation observed in telemetry channels, both separate and joint processing schemes might deliver comparable performance [36].

The main achievement is that both receiver sections operate without any knowledge about the interference and thus tracking task regarding the interference avoidance is fulfilled.

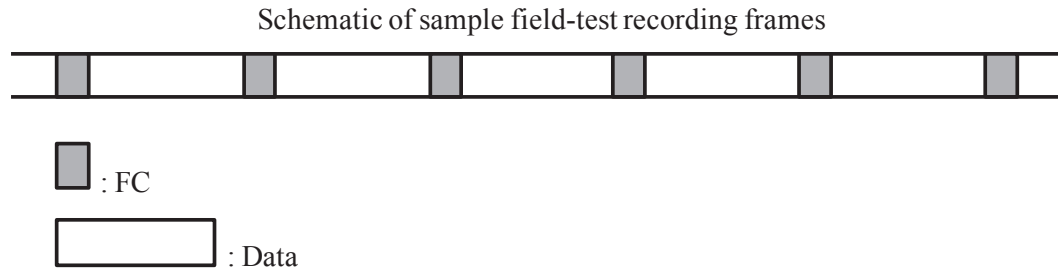


Fig. 5.24: The structure of filed-test data record to clarify the procedure of tracking examination

To explore if the proposed receiver arrangement requires tracking and how often this has to be carried out, the alternative reference signals, FCs, are utilized to adapt the equalization section. In the first part of evaluations, the equalizer adjustment is performed for all data of each field-test record, having the structure as in **Fig. 5.24**. In the second part of examinations, the equalizer is adjusted only once and is used for all data of the corresponding field-test record.

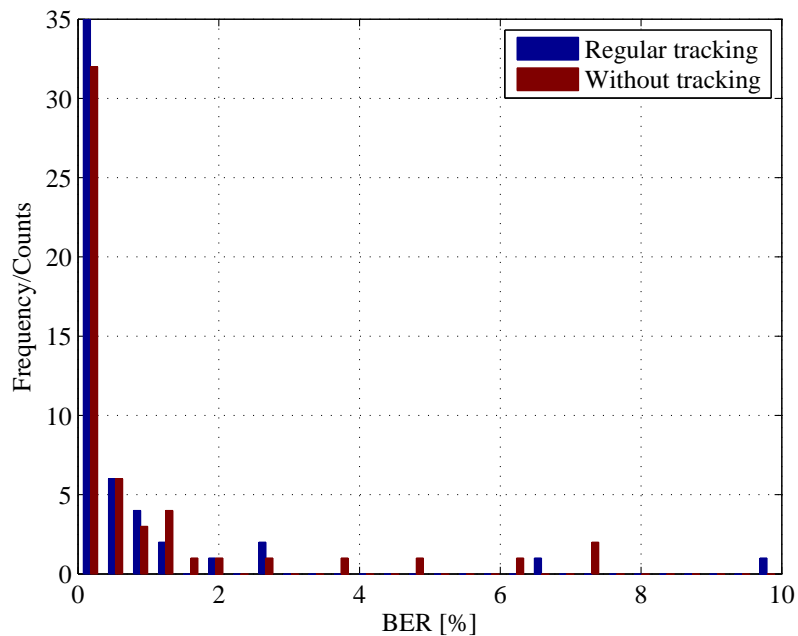


Fig. 5.25: Field-test data based performance evaluation to explore the tracking necessity in pre-NCMF and multichannel adaptive diversity combining receiver-system

The performance loss observed in the receiver system without regular parameter re-adaptation in comparison to that with regular tracking is marginal. Therefore the proposed fusion structure is beneficial in terms of tracking. In other words, a frequent tracking of equalizer section is not required and it would be sufficient to renew the estimation occasionally.

Multichannel optimal combining and post-NCMF The success of joint interference cancelation and equalization schemes is demonstrated in Chapter 4 and termed as optimal combining. The MPT receiver arrangement at the surface of the drilling rig results in diversity in interference channels and accordingly delivers superior performance over conventional diversity combining schemes such as MRC with co-channels interferences. The efficiency of multichannel optimal combining with co-channel interferences motivates another alternative concept for the MPT receiver design. Accordingly, both interference and channel effects are removed jointly by exploiting optimal combining, where the received signals are processed in an adaptive manner so that telemetry signal components correlated with the temporal reference are enhanced and uncorrelated components are eliminated. Afterwards complementary interference rejection is performed by NCMF to combat with residual components of the pump interference. The block diagram of such receiver architecture is illustrated in **Fig. 5.26**.

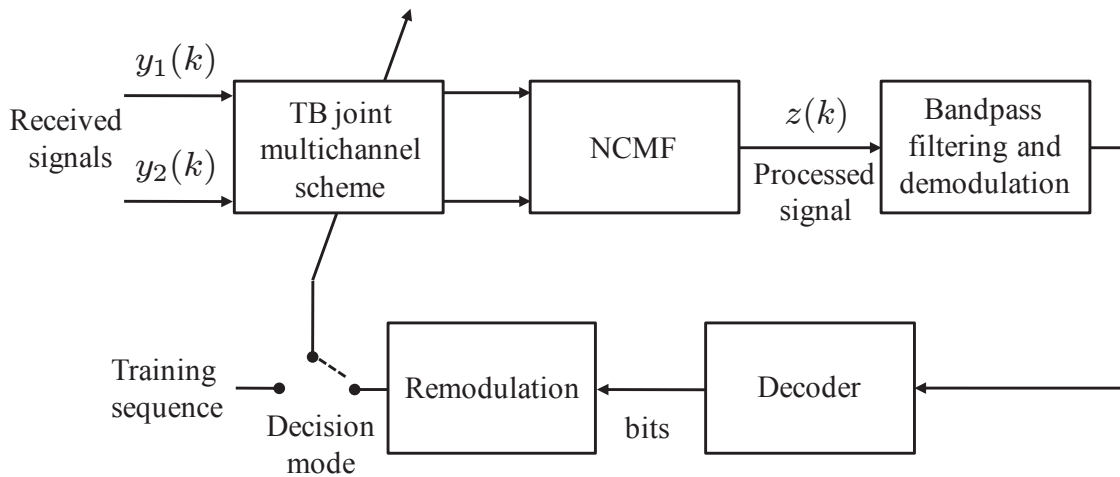


Fig. 5.26: Block diagram of hybrid multichannel adaptive diversity combining and post-NCMF

Similarly, since no knowledge about the interference is required by the optimal combining method, the tracking task can be accomplished during the regular operation. As stated in Chapter 4, both interference and channel distortions are treated jointly by the optimal combiner. The telemetry channels are approximately time-invariant and thus the equalization of these distortions requires no tracking. However, due to the unpredictable changes of pump signal, the interference characteristics are subject to some changes over the time. Therefore, a need for the tracking is expected.

For tracking examination, the optimal combiner adjustment is performed using FC signals in front of each data. Similarly, first the optimal combiner is adjusted before each data transmission in field-test records. In other words, the data detection is supported by regular tracking. In the second step of evaluations, the optimal combiner is estimated only once and is not updated for the rest of field-test data.

From the evaluation results in **Fig. 5.27**, it can be seen that, the detection performance with regular parameter re-adjustment is partly better than that without tracking. Consequently, the tracking is seen to be of much more importance in the proposed fusion

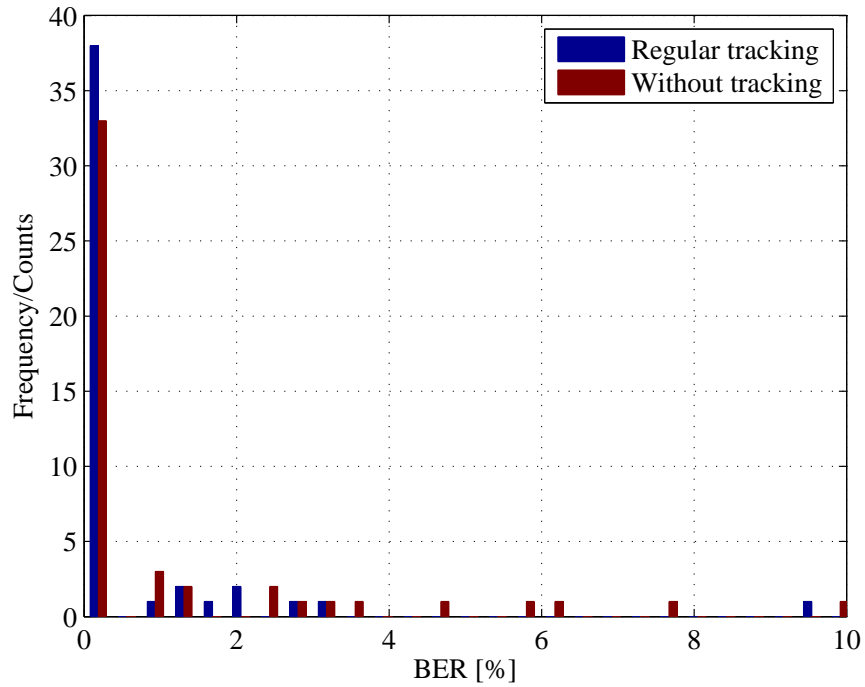


Fig. 5.27: Field-test data based performance evaluation to explore the tracking necessity in multichannel optimal combining and post-NCMF receiver-system

method. In other words, it would be beneficial in terms of BER performance to renew the estimation of optimal combiner in certain periods of time. Thereon, there are two possibilities to accomplish the tracking task:

- Initial adjustment of adaptive optimal combiner using a training sequence of data type and tracking by switching to the decision feedback mode during the regular operation.
- Initial estimation of adaptive optimal combiner utilizing an alternative training sequence such as synchronization FC signals and updating the estimation using periodically transmitted synchronization signals.

5.4 Overall performance evaluation

The performance evaluations of this section are mainly based on field-test data. Similarly, the BER frequency/counts is considered as the performance measure.

Firstly, to demonstrate that the fusion of NCMF and multichannel CMA semi-blind schemes is of less efficiency in terms of BER, 40 field-test data sets are processed to compare NCMF and hybrid NCMF and multichannel CMA semi-blind scheme. As seen in **Fig. 5.28** the performance improvement of proposed hybrid scheme is not considerable and confirms the statements in Subsection 5.3.2.1.

In the rest of evaluations, 60 field-test data sets are considered. The proposed methods in Subsection 5.3.2.2 are evaluated in some respects. First, all proposed schemes are com-

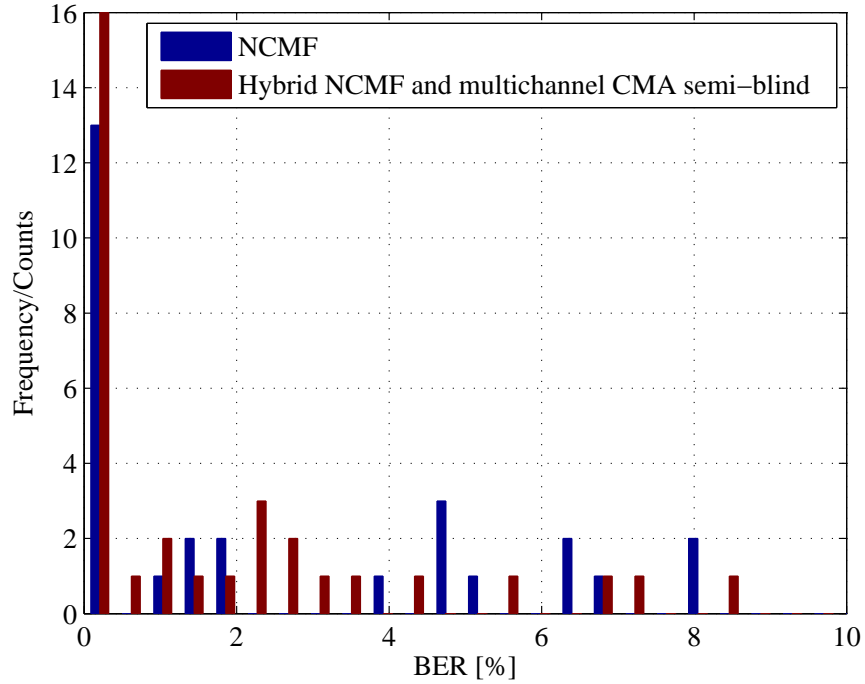


Fig. 5.28: Field-test data based performance evaluation of hybrid NCMF and multichannel CMA semi-blind receiver-arrangement

pared concerning their performance with the current estimation scheme. Finally the most efficient receiver structure is specified and discussed concerning complementary improvements.

By now the best performance of MPT system is delivered by combining the methods based on pump strobe sensors and two-receiver VO-based cascade scheme. As mentioned, in the first part of examinations, the receiver part with interference cancellation based on pump strobe sensors is replaced by the NCMF and compared with the original fusion structure. The performance results illustrated in **Fig. 5.29** demonstrate the comparable performance of both fusion schemes. Accordingly, the receiver part utilizing expensive pump strobe sensors can be successfully substituted by the economic NCMF.

Next step is to examine the algorithms based on hybrid pre-NCMF and multichannel adaptive diversity combining post-equalization. First, the fusion of NCMF and separate processing and post-combining schemes such as EGC and MRC proposed in Subsection 5.3.2.2 are evaluated and compared. The evaluation results in **Fig. 5.30** show that the fusion of NCMF followed by MRC (Type II) outperform other hybrid alternatives.

Second, the separate processing part of the proposed hybrid scheme is replaced by the joint processor. The performance of the most efficient hybrid scheme based on separate processing namely combining based on MRC (Type II) is compared with the one based on joint processing. As stated, the telemetry channels of MPT system are highly correlated and offer marginal diversity. Therefore, the performance of hybrid scheme based on MRC separate processing is partly better due to SNR maximization as seen in **Fig. 5.31**.

Finally, the multichannel optimal combining and post-NCMF scheme is evaluated and compared with all previous hybrid schemes. From the evaluation results in **Fig. 5.32**, it

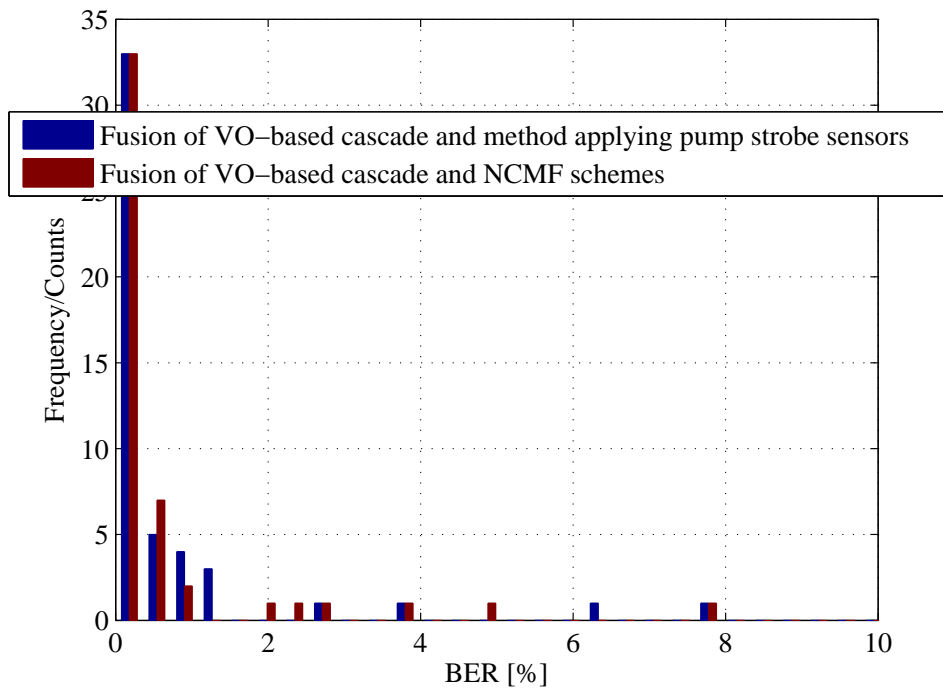


Fig. 5.29: Field-test data based performance comparison of the current VO-based cascade MPT receiver with pump strobe sensors and NCMF

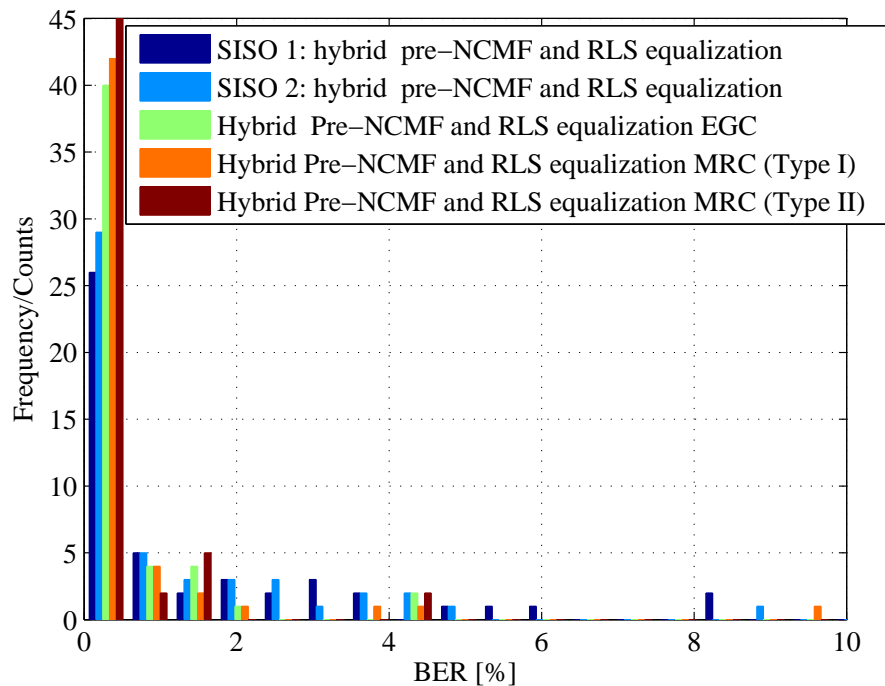


Fig. 5.30: Field-test data based performance comparison of hybrid pre-NCMF and separate processing schemes

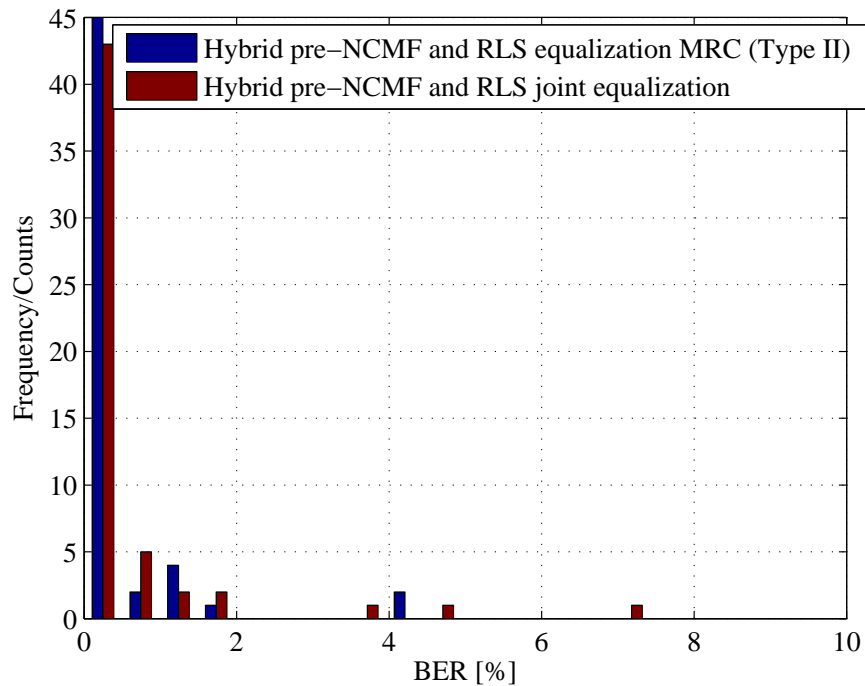


Fig. 5.31: Field-test data based performance comparison of hybrid pre-NCMF with both MRC (type II) separate and joint processing

is seen that the multichannel optimal combining and post-NCMF scheme is of superior performance compared to other hybrid schemes. However, the performance difference is not remarkable.

Consequently, among the proposed hybrid methods, the one with simple and efficient tracking facility is of practical interest in MPT applications. Recalling the discussion on the efficiency of the optimal combining with alternative reference signal in Subsection 5.3.2.2, the results of this scheme are also valid in all hybrid structures of this approach. Concerning the investigations on the tracking issue in this section, it seems that, despite the superior performance of multichannel optimal combining and post-NCMF scheme, the fusion of pre-NCMF and separate processing based on MRC (Type II) mostly complies with the requirements on tracking and thus is seen as a promising receiver structure in MPT practical applications. Furthermore, field-test data observations have been shown that the synchronization failed, provided no pump interference suppression in advance. This implies the importance of pre-NCMF for further processing and reliable detection of telemetry data.

Another observation is that, unlike the current MPT receiver structure all proposed receiver structures can be realized in baseband as illustrated in **Fig. 5.33** and provide a simple and straightforward tracking.

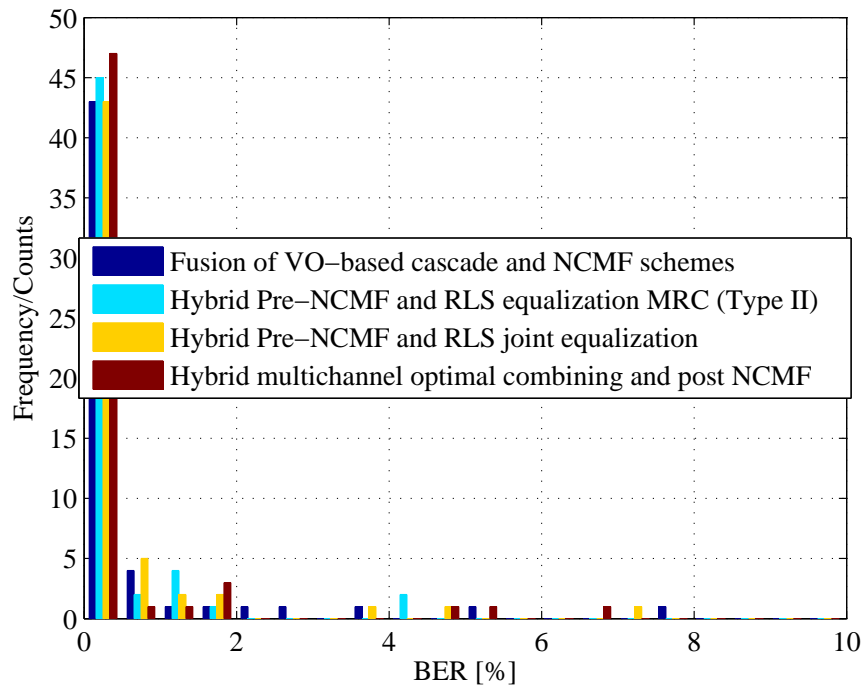


Fig. 5.32: Field-test data based performance analysis of the most relevant hybrid schemes

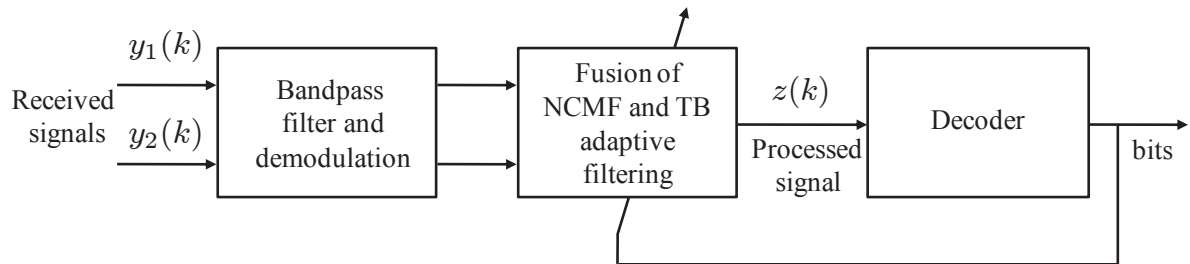


Fig. 5.33: Block diagram of the baseband realization of the proposed hybrid receiver-arrangements

5.5 Summary

In this chapter, the NCMF widely used to reject the nonstationary narrowband interference in direct sequence (DS) communication systems is applied for MPT applications and adjusted to meet the system requirements. The installation of expensive pump strobe sensors is not needed by applying NCMF with comparable efficiency. Therefore, NCMF interference suppression scheme is not only of economical interests but also provides the facility to extract accurate CIR of mud medium if combined with the CLEAN algorithm and to obtain useful information on the behavior of mud channels. This is also an encouragement to derive a model for mud telemetry channels by gathering large amounts of field-test measurements, though this goes beyond the scope of this work.

Next to this, increasing the system reliability in terms of synchronization is seen as a significant contribution of the NCMF scheme. The synchronization efficiency will further

progress utilizing the median filtering scheme in both time- and frequency-domains. The MF removal property of impulsive shaped signals can be used to determine the noise and any kind of wideband artifacts, which interfere in the impulsive ACF of FC signal. The procedure of the synchronization proposal as shown in **Fig. 5.34** includes three steps: first the NCMF is applied in frequency domain mainly to remove the pump interference, second the cross-correlation of the FC received signal and the template is obtained, and finally a time-domain MF is applied on the cross-correlation and the MF output is subtracted from the cross-correlation signal. In this manner the detection performance of synchronization chirps can be greatly increased.

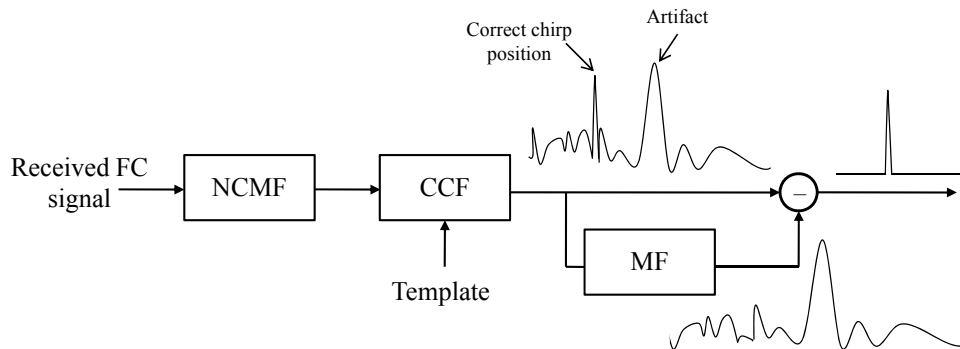


Fig. 5.34: Synchronization procedure based on time- and frequency domain median filtering

Furthermore, the design, realization and field-test data evaluation of hybrid receiver structures in the MPT system are presented and the main research goals formulated in Section 5.3 are achieved. In this context, two important performance criteria have been followed to allow a realistic deployment of the hybrid schemes in MPT systems. First, the design fusion scheme is efficient and robust. Second, reliable tracking is achievable.

It is shown that the fusion of NCMF and multichannel blind scheme is not feasible in practical MPT applications. An efficient receiver is introduced, where NCMF and TB adaptive schemes are combined. This hybrid structures increase not only the system performance and robustness but also facilitate simple and straightforward tracking. In addition, a real-world comparison of these hybrid schemes is conducted to verify the superior performance of them. Based on this investigation, the most efficient hybrid structure in terms of BER performance and reliable tracking is committed. A more comprehensive study on the need of tracking is recommendable and can be accomplished by recording long observations of field-test data.

Chapter 6

Conclusion and outlook

In this dissertation, the telemetry signal extraction problem in MPT is addressed and efficient solutions are provided for reliable data recovery. This is a big challenge considering the MPT system requirements and the multipath channel of the mud communication medium. It has been shown that the current technologies suffer from serious shortcomings such as installations expenses, complicated and inefficient tracking facilities. Throughout this dissertation, the basic structure and the MPT system configuration have been enhanced for practical MPT application. In this context, the receiver arrangement and estimation concepts are optimized under realistic system conditions to achieve best performance in terms of BER and reliable tracking. Therefore, the statistical characteristics of underlying MPT system signals have been investigated in Chapter 2 to develop relevant algorithms supporting particularly the tracking task. Based on these investigations, two semi-blind estimation schemes have been proposed in Chapter 3, which utilize telemetry and/or pump interference properties and mainly deal with interference suppression. It has been shown that these schemes are not efficient in practice due to the requirement on a-priori knowledge and individual parameter adjustment in each field-test measurement.

To cope with the demands of real MPT applications, the two-receiver structure and the reference signal facility for telemetry data available in the MPT system architecture are utilized. In this context, both cascade and joint schemes based on two-receiver structures have been developed in Chapter 4. It has been shown that the cascade structure is deficient in both structure and performance. The joint receiver structure, also called multichannel or optimal diversity combining scheme, delivers best performance in cancelling the interference without requiring any information on the interference signal. Furthermore, the specific multichannel structure of the joint scheme provides convenient and simple tracking following a decision feedback approach. Real-world field-test measurements have shown that the efficiency and robustness of the system can be greatly improved compared to current relevant technology. Furthermore, it has been shown that increasing the number of receivers thus by providing more diversities, leads to a considerable performance improvement at the cost of some computational effort.

To further increase the BER performance and to provide automatic tracking especially in removing the pump interference, the concept of hybrid receivers has been conducted in Chapter 5. The proposed hybrid receiver-structures aim to deal with the distortions caused by both the interference and the multipath channel. In this context, the NCMF has been proposed in Chapter 5, where the interference rejection is performed without any information on pump and/or telemetry signals and thus adjustable. In other words, the

automatic tracking in terms of interference rejection has been achieved. Real-world field-test measurements have shown that the application of NCMF is of several advantages; first the investigation on the characteristics of the mud telemetry channel has been enabled, second the robustness and performance of MPT system has been enhanced with different development of hybrid receivers. It has been demonstrated in Chapter 5 that the fusion of NCMF and TB adaptive multichannel signal processing not only improves the BER performance but also provides simple and reliable tracking of system parameters, and lastly significant improvement of the system reliability in terms of synchronization has been achieved by NCMF. The time- and frequency-domain median filtering proposal offers further possibility of the synchronization task. Moreover, not only the pump interference but also any other interference sources of narrowband characteristic can be remedied by using NCMF strategies.

This dissertation has contributed to the field of receiver design based on hybrid schemes under the aspect of robustness and efficiency in difficult MPT applications. The potential of proposed fusion structures has been confirmed by the real-world field-test data evaluations and acknowledged as the new technology of data recovery in MPT systems. Furthermore, it has been shown that the current communication protocol does not fully satisfy the requirement of reliable and robust data transmission in the MPT system. Thus, the transmission protocol is to be optimized referring to proposed receiver structures in this dissertation. Since there is no need for the valve-off period and the long time training sequence, the startup sequence is to be specified efficiently. Moreover, much more system robustness and reliability can be offered by periodically transmitting short time training sequences or proper synchronization chirps, at the cost of increased redundancy.

From a research viewpoint, a couple of open issues remain, which are the subject of future investigations in MPT systems. This includes a comprehensive study on possibility of increasing the number of receivers and their efficient placement, so that sufficient diversity is provided to improve the system performance. In addition, based on a large number of special field-test measurements, a channel model can be derived to describe the behavior of the mud transmission medium. Such kind of model provides simplicity and quickness in understanding effects encountered in the MPT system and efficient algorithm development based on simulative data and direct application on real data. Finally, the feasibility of the passive vibro-acoustical filters in the outlet of the pump decoupling the MPT system from the pump interference might be subject to future research.

Appendix A

MIMO-CMA derivation

$$\begin{aligned}
\frac{\partial J}{\partial \mathbf{w}_{11}} &= 2E \left[(|z_1(k)|^2 - |A(k)|^2) (2Y_1^T(k)Y_1^H(k)\mathbf{w}_{11}^* + 2Y_1^T(k)Y_2^H(k)\mathbf{w}_{21}^*) \right] \\
&+ 4 \sum_{\tau=\tau_1}^{\tau_2} R_{12}(\tau) E \left[\frac{\partial J}{\partial \mathbf{w}_{11}} (Y_1^T(k)\mathbf{w}_{11} + Y_2^T(k)\mathbf{w}_{21}) z_2^*(k - \tau) \right] \\
&= 4E \left[(|z_1(k)|^2 - |A(k)|^2) z_1(k)Y_1^*(k) \right] + 4 \sum_{\tau=\tau_1}^{\tau_2} R_{12}(\tau) E [z_2(k - \tau)Y_1^*(k)] .
\end{aligned}$$

$$\begin{aligned}
\frac{\partial J}{\partial \mathbf{w}_{21}} &= 2E \left[(|z_1(k)|^2 - |A(k)|^2) (2Y_2^T(k)Y_1^H(k)\mathbf{w}_{11}^* + 2Y_2^T(k)Y_2^H(k)\mathbf{w}_{21}^*) \right] \\
&+ 4 \sum_{\tau=\tau_1}^{\tau_2} R_{12}(\tau) E \left[\frac{\partial J}{\partial \mathbf{w}_{21}} (Y_1^T(k)\mathbf{w}_{11} + Y_2^T(k)\mathbf{w}_{21}) z_2^*(k - \tau) \right] \\
&= 4E \left[(|z_1(k)|^2 - |A(k)|^2) z_1(k)Y_2^*(k) \right] + 4 \sum_{\tau=\tau_1}^{\tau_2} R_{12}(\tau) E [z_2(k - \tau)Y_2^*(k)] .
\end{aligned}$$

$$\begin{aligned}
\frac{\partial J}{\partial \mathbf{w}_{12}} &= 2E \left[(|z_2(k)|^2 - 1) (2Y_1^T(k)Y_1^H(k)\mathbf{w}_{12}^* + 2Y_1^T(k)Y_2^H(k)\mathbf{w}_{22}^*) \right] \\
&+ 4 \sum_{\tau=\tau_1}^{\tau_2} R_{21}(\tau) E \left[\frac{\partial J}{\partial \mathbf{w}_{12}} (Y_1^T(k)\mathbf{w}_{12} + Y_2^T(k)\mathbf{w}_{22}) z_1^*(k - \tau) \right] \\
&= 4E \left[(|z_2(k)|^2 - 1) z_2(k)Y_1^*(k) \right] + 4 \sum_{\tau=\tau_1}^{\tau_2} R_{21}(\tau) E [z_1(k - \tau)Y_1^*(k)] .
\end{aligned}$$

$$\begin{aligned}
\frac{\partial J}{\partial \mathbf{w}_{22}} &= 2E \left[(|z_2(k)|^2 - 1) (2Y_2^T(k)Y_1^H(k)\mathbf{w}_{12}^* + 2Y_2^T(k)Y_2^H(k)\mathbf{w}_{22}^*) \right] \\
&+ 4 \sum_{\tau=\tau_1}^{\tau_2} R_{21}(\tau) E \left[\frac{\partial J}{\partial \mathbf{w}_{22}} (Y_1^T(k)\mathbf{w}_{12} + Y_2^T(k)\mathbf{w}_{22}) z_1^*(k - \tau) \right] \\
&= 4E \left[(|z_2(k)|^2 - 1) z_2(k)Y_2^*(k) \right] + 4 \sum_{\tau=\tau_1}^{\tau_2} R_{21}(\tau) E [z_1(k - \tau)Y_2^*(k)] .
\end{aligned}$$

Appendix B

Simulation channels

The simulative studies of this work are carried out with measured channel impulse responses (CIR) attained from both test and commercial rigs. In the following, extracted CIRs in different rigs and receiver structures are illustrated.

B.1 Simulation channel A

The simulation channels are provided from a test borehole with two-receiver structure. The CIR is obtained by the layered median filtering and clean algorithm scheme [101, 65]. The extract CIRs are illustrated in **Fig. B.1**.

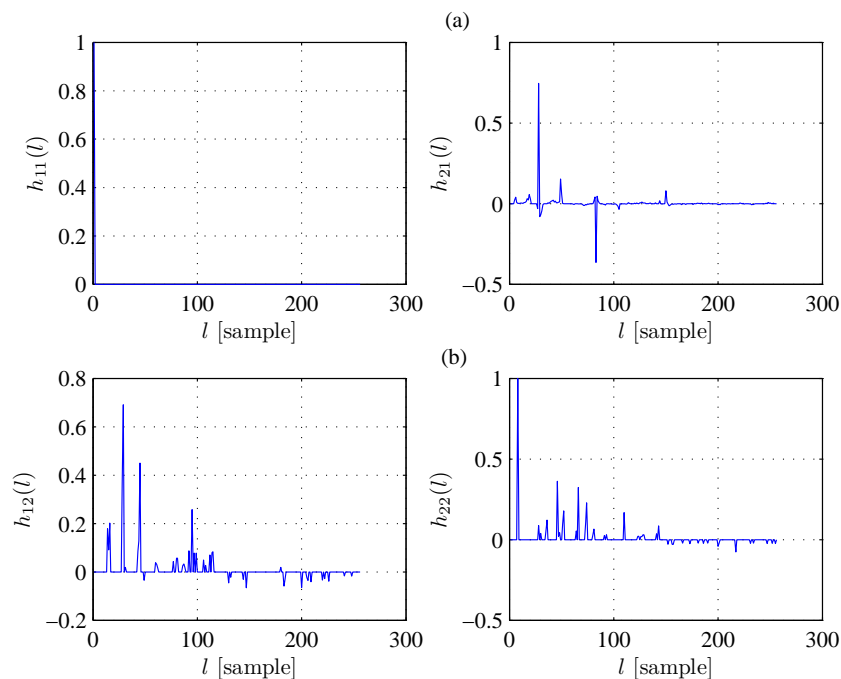


Fig. B.1: CIRs of a test rig with two-receiver structure: (a) Pump channels, and (b) Telemetry channels

B.2 Simulation channel B

The simulation channels are provided from a commercial borehole. The receiver structure and the estimation method is the same as in **B.1**. The obtained CIRs are shown in **Fig. B.2**.

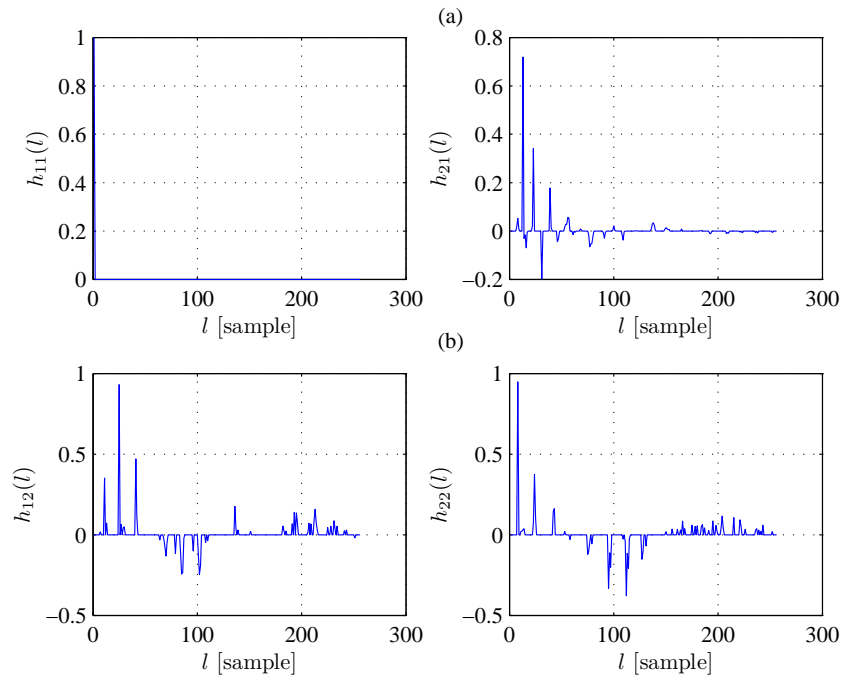


Fig. B.2: CIRs of a commercial rig with two-receiver structure: (a) Pump channels, and (b) Telemetry channels

B.3 Simulation channel C

The simulation channels are provided from a commercial borehole with three-receiver structure. The corresponding CIRs are illustrated in **Fig. B.3**.

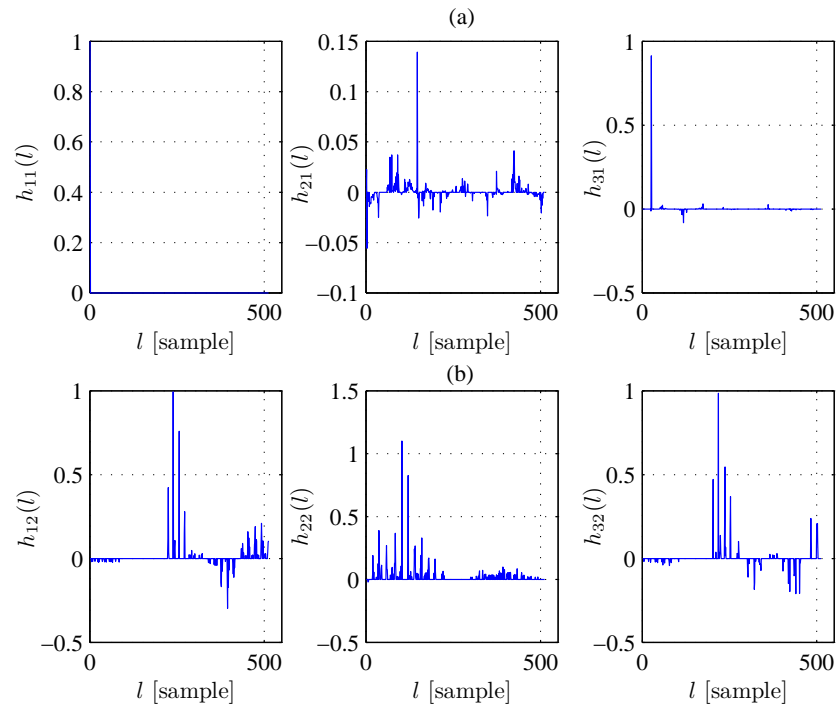


Fig. B.3: CIRs of a commercial rig with three-receiver structure: (a) Pump channels, and (b) Telemetry channels

List of Figures

1.1	Drilling rig	2
1.2	The figure to the left depicts the general concept of MPT system. The figure to the right shows idealized MPT system model used to analyze the performance of mud pulse telemetry	3
1.3	Spectrogram of a field-test data recorded at a test borehole (horizontal lines show harmonic pump signal and labeled areas bandpass data signal)	5
1.4	field-test data recorded at a commercial borehole (horizontal lines show harmonic pump signal and labeled areas bandpass data signal)	6
1.5	Overview of the dissertation.	10
2.1	Example of bandpass BPSK and BCPM modulated signal	14
2.2	Constant modulus/envelope property constellation	15
2.3	Example measurements of pump signal	16
2.4	Illustration of periodic $s(t)$ and stochastic $u(t)$ components of a sample pump signal $x(t)$	17
2.5	RMP signal generated by two pumps: a) Illustration of two pumps cumulation $x_1(t) + x_2(t)$, periodic part of the first pump $s_1(t)$ with the fundamental period of $T_1 = 0.5117$ s and stochastic part of the first pump $u_1(t)$ together with the second pump signal $x_2(t)$, b) Illustration of stochastic part of the first pump $u_1(t)$ together with the second pump signal $x_2(t)$, periodic part of the second pump $s_2(t)$ with the fundamental period of $T_2 = 0.7734$ s and stochastic parts of two pumps $u_1(t) + u_2(t)$	18
2.6	Cyclic spectrum of a sample pump signal with a fundamental frequency of $f_1 = 1.25$ Hz and cyclic frequency of $\alpha = 2.5$ Hz	19
2.7	Verification of RMP for a sample measurement of the pump signal	21
2.8	Signal coherence estimate for a sample measurement of the pump signal . .	22
2.9	Illustration of the modulation noise stationarity verified by the Chi-Square distribution of a sample $\hat{Z}(k)$	23
2.10	A sample pump signal measurement with variable flow rate	24
2.11	Estimation/tracking results of fundamental period for a sample pump signal measurement with variable flow rate	25

2.12	Estimation of the fundamental period for a sample measurement of the pump signal	26
2.13	Estimation of the fundamental periods for a sample measurement of the pump signal generated by two pumps	26
2.14	Estimation of the fundamental periods for a sample measurement of the pump signal from the convolutive mixture of telemetry and pump signals	27
3.1	General structure of the constant modulus adaptive algorithm	31
3.2	Error course in MSE and cost function of CMA	32
3.3	Error course as a function of J vs. adaptation time for different fadings	33
3.4	Overall performance evaluation of CMA algorithm (a) BER comparison between the chirp-based equalization and CMA , b) , c) and d) the effect of step size and filter length adjustment on the BER performance)	34
3.5	Error course as a function of J vs. adaptation time in the presence of AWGN for different SNRs	35
3.6	Error course as a function of J vs. adaptation time in the presence of pump signal for different SIRs	35
3.7	Conceptual scheme: a) CM array filtering, b) Extended MIMO decorrelation filtering	36
3.8	linear 2×2 MIMO-system model of the extended MIMO decorrelation scheme	37
3.9	Performance comparison of the CM array filtering and MIMO-CM methods in the present of the pump signal for high SIR case (both methods capture the telemetry signal)	39
3.10	Performance comparison of the CM array filtering and MIMO-CM methods in the present of the pump signal for low SIR case (CM-based array filtering captures the pump signal)	40
3.11	Convergence time of MIMO-CM methods in the present of the pump signal for high and low SIRs (the Convergence is faster at high SIR)	41
3.12	Poor performance of the MIMO-CM approach for high data rate/wideband transmission	41
3.13	TD-AS Concept	42
3.14	Averaging procedure	42
3.15	Effect of averaging length on the detection performance in an example of field-test data	42
3.16	Effect of averaging length on the simulative detection performance as a function of BER vs. SIR	43
3.17	Spectrum of the received sensor signal $y(k)$, the estimated periodic pump signal $\hat{s}(k)$ and the processed signal $z(k)$ in baseband	44
3.18	Baseband presentation of the received signal $y(k)$, the estimated periodic pump signal $\hat{s}(k)$ and the processed signal $z(k)$ compared to the original telemetry signal $x_2(k)$	45

3.19	SIR analysis of field-tests data sets	45
3.20	Estmation results of fundamental period during valve off and regular operation	46
3.21	Simulative performance analysis of the proposed semi-blind processing schemes in terms of BER vs. SNR at SIR = -15 dB	47
3.22	Field-test data based performance analysis of the proposed semi-blind processing schemes	48
3.23	Field-test data based performance comparison between the multichannel semi-BSS and the single channel semi-BSE followed by CMA	48
3.24	Concept block diagram of combining single channel semi-BSE based on the TD-AS and CMA	49
4.1	Conceptual diagram of conventional interference cancellation in a communication system	51
4.2	Block diagram of the cascade interference canceller/equalizer	52
4.3	Conceptual diagram of joint estimation for the cascade receiver structure	53
4.4	VO-based and TB impulse response estimation of interference canceller for low and high data rate cases	56
4.5	Examining the functionality of the equalizer section for low and high data rate cases	56
4.6	Spectrogram of the unprocessed received signals	57
4.7	Spectrogram of the processed signal using cascade interference canceller/equalizer	57
4.8	Block diagram of the joint interference canceller/equalizer	58
4.9	Spectrogram of the processed signal applying optimum combining joint interference canceller/equalizer	60
4.10	Convergence evaluation of the joint multichannel scheme for different SIRs regimes	61
4.11	Convergence evaluation of the joint multichannel scheme for different setup of filter lengths	61
4.12	Spectrogram of the unprocessed received signal distorted by a wideband two-pump interference	62
4.13	Spectrogram presenting the ability of optimum combining joint interference canceller/equalizer in rejecting wideband two-pump interference	62
4.14	Stability study of cascade and joint receiver structure on low data rate field-test measurements	63
4.15	Stability study of cascade and joint receiver structure on high data rate field-test measurements	64
4.16	Simulative performance analysis in terms of BER vs. SNR using CIRs obtained from a test borehole	65

4.17	Simulative performance analysis in terms of BER vs. SNR using CIRs obtained from a commercial borehole	65
4.18	Field-test data based performance analysis of the reference signal-based schemes	66
4.19	BER vs. SNR for different spatial diversity in the presence of AWGN and pump interference with $SIR = -15$ [dB]	67
4.20	BER vs. SIR for different spatial diversity in the presence of pump interference and a noise free channel	67
4.21	Field-test data based performance evaluation of joint multichannel scheme with alternative reference signals	68
5.1	Image restoration using median filter	71
5.2	Different realizations of median filtering	72
5.3	Concept diagram of transform domain median filtering	72
5.4	Illustration of Fourier magnitude transform distribution in telemetry data .	74
5.5	Frequency-domain demonstration of NCMF ability in pump interference rejection	74
5.6	Time-domain demonstration of NCMF ability in pump interference rejection	75
5.7	Processing gain ($SIR_+ = SIR_{out} - SIR_{in}$) achieved by NCMF	76
5.8	BER/SNR performance vs. window size applied in overlap add preprocessing (better BER/SNR at larger window size)	76
5.9	BER/SNR performance vs. median filter length (better BER/SNR at smaller window size)	77
5.10	Receiver arrangement considered in the evaluations of NCMF	77
5.11	BER vs. SNR results in absence of the pump interference	79
5.12	Spectrogram of the unprocessed received field-test data (horizontal lines show harmonic pump signal and labeled areas bandpass data signal)	80
5.13	Spectrogram of the processed field-test data using NCMF (labeled areas show bandpass data signal)	80
5.14	Spectrogram of the field-test data processed using pump strobe sensors (horizontal lines show residual harmonic pump signal and labeled areas bandpass data signal)	81
5.15	Field-test data based performance analysis of NCMF	81
5.16	The impact of NCMF on the shape and the autocorrelation characteristic of FC signal	82
5.17	Block diagram of the channel extraction concept	85
5.18	Sample CIR extracted from field-test measurements	85
5.19	Observation of channel behavior over the time	86
5.20	Sample CFRs extracted from field-test measurements	87

5.21	Block diagram of hybrid NCMF and multichannel semi-blind scheme . . .	88
5.22	Block diagram of hybrid pre-NCMF and multichannel post-equalization . .	90
5.23	Separate processing and post-combining based on MRC	91
5.24	The structure of filed-test data record to clarify the procedure of tracking examination	92
5.25	Field-test data based performance evaluation to explore the tracking necessity in pre-NCMF and multichannel adaptive diversity combining receiver-system	92
5.26	Block diagram of hybrid multichannel adaptive diversity combining and post-NCMF	93
5.27	Field-test data based performance evaluation to explore the tracking necessity in multichannel optimal combining and post-NCMF receiver-system	94
5.28	Field-test data based performance evaluation of hybrid NCMF and multichannel CMA semi-blind receiver-arrangement	95
5.29	Field-test data based performance comparison of the current VO-based cascade MPT receiver with pump strobe sensors and NCMF	96
5.30	Field-test data based performance comparison of hybrid pre-NCMF and separate processing schemes	96
5.31	Field-test data based performance comparison of hybrid pre-NCMF with both MRC (type II) separate and joint processing	97
5.32	Field-test data based performance analysis of the most relevant hybrid schemes	98
5.33	Block diagram of the baseband realization of the proposed hybrid receiver-arrangements	98
5.34	Synchronization procedure based on time- and frequency domain median filtering	99
B.1	CIRs of a test rig with two-receiver structure: (a) Pump channels, and (b) Telemetry channels	104
B.2	CIRs of a commercial rig with two-receiver structure: (a) Pump channels, and (b) Telemetry channels	105
B.3	CIRs of a commercial rig with three-receiver structure: (a) Pump channels, and (b) Telemetry channels	106

List of Tables

3.1	Simulation parameter setup for the proposed semi-blind processing schemes	46
3.2	Field-test data setup involved in the evaluation of semi-blind schemes . . .	47
4.1	Performance gain due to spatial diversity in field-test data based evaluation	68
5.1	Simulation parameter setup in the evaluation of NCMF	78
5.2	Parameter setup of NCMF	78
5.3	Estimated $\bar{\tau}$ and τ_{rms} for sample boreholes	87
5.4	Correlation coefficients in a representative field-test measurement	89

Bibliography

- [1] A. A. Alshehri. *Blind estimation of multi-path and multi-user spread spectrum channels and jammer excision via the evolutionary spectral theory*. Ph.D. Thesis , University of Pittsburg, School of Engineering, 2004.
- [2] A. Hyvarinen, and E. Oja. A neuron that learns to separate one signal from a mixture of independent sources. *IEEE International Conference on Neural Networks*, 1:62 – 67, 1996.
- [3] A. Hyvarinen, and E. Oja. A fast fixed-point algorithm for independent component analysis. *Neural Computation*, 9:1483 – 1492, 1997.
- [4] A.-J. van der Veen. Analytical method for blind binary signal separation. *IEEE Transactions on Signal Processing*, 45:1078 – 1082, 1997.
- [5] A. K. Nandi. *Blind estimation using higher-order statistics*. Kluwer Academic Publishers, 1999.
- [6] A. Ranheim. Narrowband interference rejection in direct-sequence spread-spectrum system using time-frequency decomposition. *IEE Proceedings on Communications*, 142(6):393 – 400, 1995.
- [7] A. T. Bourgoyne, K. K. Millheim, M. E. Chenevert, F. S. Young. *Applied Drilling Engineering (SPE Textbook Series)*. Society of Petroleum, First Printing, 1986.
- [8] A. V. Gautam, D. M. Dakhane, and V. R. Tripathi. Image denoising using non Linear filters. *International Journal of Information Technology and Knowledge Management*, 2:573 – 577, 2010.
- [9] B. Bohm, J.A. Schoonees, and R.M. Braun. Data to frequency mappings in various MSK schemes. *Electronics Communication Engineering Journal*, 6:13 –20, 1994.
- [10] B. Mulgrew, and C. F. N. Cowan. *Adaptive filters and equalizers*. Kluwer Academic Publishers, 1988.
- [11] B. Sklar. *Digital communications: Fundamentals and applications*. Prentice Hall, 2001.
- [12] B.-U. Köhler. *Konzepte der statistischen Signalverarbeitung*. Springer, Berlin Heidelberg, 2005.
- [13] B. Weiss. Fast median and bilateral filtering. *ACM Transactions on Graphics*, 25:519 – 526, 2006.

- [14] C. B. Papadias, and D. T. M. Slock. On the Convergence of Normalized Constant Modulus Algorithms for Blind Equalization. *Proc. DSP International Conference on Digital Signal Processing*, pages 245 – 250, 1993.
- [15] C. Kupferschmidt. *Modellierung zyklisch stationärer Kanäle für die funkgestützte Rotortelemetrie, Band 2.17 der Reihe Hannoversche Beiträge zur Nachrichtentechnik*. Shaker Verlag, Aachen, 2007.
- [16] C. S. Clay, and H. Medwin. *Acoustical oceanography: Principles and applications*. John Wiley & Sons, 1977.
- [17] C. T. Le. *Untersuchung blinder Verfahren zur Trennung von verzerrten akustischen Signalen*. Master thesis, Institute of Communications Technology, Gottfried Wilhelm Leibniz University of Hannover, 2009.
- [18] C. T. Le, S. Moghaddamnia, C. Kupferschmidt, and T. Kaiser. Performance evaluation of blind source separation algorithms based on source signal statistics in convolutive mixtures. *Third International Conference on Communications and Electronics (ICCE)*, pages 268 – 272, 2010.
- [19] C. Zhou, N. Guo, and R. Caiming Qiu. Time-reversed ultra-wideband (UWB) multiple input multiple output (MIMO) based on measured spatial channels. *IEEE Transactions on Vehicular Technology*, 58(6):2884 – 2898, 2009.
- [20] C.B. Papadias, and A.J. Paulraj. A constant modulus algorithm for multiuser signal separation in presence of delay spread using antenna arrays. *IEEE Signal Processing Letters*, 4:178 – 181, 1997.
- [21] D. Gesbert, P. Duhamel. Unimodal blind adaptive channel equalization: an RLS implementation of the mutually referenced equalizers. *IEEE Signal Processing Workshop on Signal Processing Advances in Wireless Communications*, pages 29 –32, 1997.
- [22] D. Gesbert, P. Duhamel, and S. Mayrargue. On-line blind multichannel equalization based on mutually referenced filters. *IEEE Transactions on Signal Processing*, 45:2307 –2317, 1997.
- [23] D. Godard. Self-recovering equalization and carrier tracking in two-dimensional data communication systems. *IEEE Transactions on Communications*, 28:1867 – 1875, 1980.
- [24] D. H. Nguyen. *Investigation of dual sensor algorithms for mud pump noise cancellation in mud pulse telemetry*. Master thesis, Institute of Communications Technology, Gottfried Wilhelm Leibniz University of Hannover, 2006.
- [25] D. Hahn, V. Peters, C. Rouatbi, and H. Eggers. Oscillating shear valve for mud pulse telemetry and associated methods of use. *US patent 6975244B2*, 2005.
- [26] D. R. Brillinger. *Time series: data analysis and theory*. Society for Industrial and Applied Mathematics, 2001.

- [27] D. Xue-jie, G. Ye-cai, and G. Fu-dong. A novel joint combining time-spatial diversity blind Equalization algorithm. *Proceedings of the International Workshop on Information Security and Application*, pages 97 – 100, 2009.
- [28] E. Weinstein, M. Feder, and A. V. Oppenheim. Multi-channel signal separation by decorrelation. *IEEE Transactions on Speech and Audio Processing*, 1:405 – 413, 1993.
- [29] G. C. Carter, C. H. Knapp, and A. H. Nuttall. Estimation of the magnitude-squared coherence function via overlapped fast Fourier transform processing. *IEEE Transactions on Audio and Electroacoustics*, 21:337 – 344, 1973.
- [30] G. Gelli, L.Paura, and A.M.Tulino. Cyclostationarity-based filtering for narrowband interference suppression in direct-sequence spread-spectrum systems. *IEEE Journal on Selected Areas in Communications*, 16:1747 – 1755, 1998.
- [31] G. Keller, and B. Warrack. *Statistics for Management and Economics (4th ed.)*. Belmont, CA: Duxbury, 1997.
- [32] G. Li, L. Ning, G. Yan, and Z. Jiongpan. Convergence behavior of the constant modulus algorithm controlled by special stepsize. *6th International Conference on Signal Processing*, 1:390 – 392, 2002.
- [33] G. Ungerboeck. Fractional Tap-Spacing Equalizer and Consequences for Clock Recovery in Data Modems. *IEEE Transactions on Communications*, 24:856 – 864, 1976.
- [34] H. Chanson, S. Jarny, and Coussot. Dam break wave of thixotropic fluid. *Journal Hydraulic Engineering*, 132:280–293, 2006.
- [35] I. Pitas, and A. N. Venetsanopoulos. *Nonlinear digital filters: principles and applications*. Kluwer Academic Publishers, 1990.
- [36] I. Rebai. *Untersuchung adaptiver Diversitätsverfahren zur optimalen Entzerrung in Mehrempfängersystemen*. Studienarbeit, Institute of Communications Technology, Gottfried Wilhelm Leibniz University of Hannover, 2011.
- [37] I. Wassermann. Pulse shape of binary PSK for NGTP. *Baker Hughes INTEQ Report*, 2006.
- [38] J. A. Chambers, and Y. Luo. A new cross-correlation and constant modulus type algorithm for PAM-PSK signals. *IEEE International Conference on Acoustics, Speech, and Signal Processing*, 5:133 – 136, 2003.
- [39] J. C. Kiefer. *Introduction to statistical inference*. Springer, New york, 1987.
- [40] J. Catipovic, M. Johnson, and D. Adams. Noise cancelling performance of an adaptive receiver for underwater communications. *Proceedings of the 1994 Symposium on Autonomous Underwater Vehicle Technology*, pages 171 – 178, 1994.
- [41] J. F. Adlard. *Frequency shift filtering for cyclostationary signals*. Ph.D. Thesis, University of York, 2000.

- [42] J. Fuhl, and E. Bonek. Temporal reference algorithms versus spatial reference algorithms for smart antennas. *Wireless Personal Communications*, 9:271 – 293, 1999.
- [43] J. G. Proakis. *Digital communications, (3rd ed.)*. McGraw Hill, New York, 1995.
- [44] J. Gevargiz, P. K. Das, and L. B. Milstein. Adaptive narrow-band interference rejection in a DS spread-spectrum intercept receiver using transform domain signal processing techniques. *IEEE Transactions on Communications*, 37:1359 – 1366.
- [45] J. Linatti. DS signal data detection using matched filter with median filter and with transversal filter in CW jamming. *Wireless Personal Communications: An International Journal archive*, 6, 1998.
- [46] J. Litva, and T. K.-Y. Lo. *Digital beamforming in wireless communications*. Artech House, Boston, London, 1996.
- [47] J. Macpherson. A primer on MWD telemetry. *Baker Hughes INTEQ Report*, 2004.
- [48] J. S. Thompson, P. M. Grant, and B. Mulgrew. Smart antenna arrays for CDMA systems. *IEEE Personal Communications*, 3:16 – 25, 1996.
- [49] J. Tao, Y. R. Zheng, X. Chengshan, T. C. Yang, and W.-B. Yang. Time-domain receiver design for MIMO underwater acoustic communications. *OCEANS*, pages 1 – 6, 2008.
- [50] J. Thomas, Y. Deville, and S. Hosseini. Time-domain fast fixed-point algorithms for convolutive ICA. *IEEE Signal Processing Letters*, 13:228 – 231, 2006.
- [51] J. Treichler. Adaptive algorithms that restore signal properties. *Acoustics, Speech, and Signal Processing, IEEE International Conference on ICASSP '84.*, 9:203 – 206, 1984.
- [52] J. Treichler, and B. Agee. A new approach to multipath correction of constant modulus signals. *IEEE Transactions on Acoustics, Speech and Signal Processing*, 31:459 – 472, 1983.
- [53] J. Treichler, and M. Larimore. New processing techniques based on the constant modulus adaptive algorithm. *IEEE Signal Processing Society*, 33:420 – 431, 1985.
- [54] J. Treichler, and M. Larimore. The tone capture properties of CMA-based interference suppressors. *IEEE Transactions on Acoustics, Speech and Signal Processing*, 33:946 – 958, 1985.
- [55] J. Winters. Optimum combining in digital mobile radio with cochannel interference. *IEEE Journal on Selected Areas in Communications*, 2:528 – 539, 1984.
- [56] J. Xu. A multiuser constant modulus algorithm for an antenna array. *International Conference on Wireless Communications, Networking and Mobile Computing*, 1:131 – 134, 2005.
- [57] J. Zhang, K.M. Wong, Z.Q. Luo, and P.C. Ching. Blind adaptive FRESH filtering for signal extraction. *IEEE Transactions on Signal Processing*, 47:1397 – 1402, 1999.

- [58] K. Abed-Meraim. Recent developments on multi-channel blind system identification (BSI). *ENST PARIS, Signal and Image Processing Dept.*
- [59] K. D. Kammeyer. *Nachrichtenübertragung*. Teubner, Stuttgart, 1996.
- [60] K. Huang, J. Wang, G. Chen, and Y. Wang. Smart antenna and spatial diversity-combining. *IEEE 55th Vehicular Technology Conference*, 1:340 – 344, 2002.
- [61] L. B. Felix, A. M. F. L. M. de Sa, E. M. A. M. Mendes, and M. F. D. Moraes. Statistical aspects concerning signal coherence applied to randomly modulated periodic signals. *IEEE Signal Processing Letters*, 13:104 – 107, 2006.
- [62] L. Parra, and C. Spence. Convolutional blind separation of non-stationary sources. *IEEE Signal Processing Society*, 8:320 – 327, 2000.
- [63] L. R. Rabiner, and B. Gold. *Theory and application of digital signal processing*. Englewood Cliffs, NJ: Prentice-Hall, 1975.
- [64] L. Milstein, and P. Das. An Analysis of a Real-Time Transform Domain Filtering Digital Communication System—Part I: Narrow-Band Interference Rejection. *IEEE Transactions on Communications*, 28(6):816 – 824, 1980.
- [65] M. A. Calderon. *Time-reversed MIMO for ultra-wideband communications: experiments and performance*. Master thesis, Faculty of the Graduate School Tennessee Technological University, 2009.
- [66] M. Baro, and J. Ilow. Cyclostationary-based diversity combining for blind channel equalization using multiple receive antennas. *Canadian Conference on Electrical and Computer Engineering*, 4:2375 – 2378, 2004.
- [67] M. Barrett, and R. Arnott. Adaptive antennas for mobile communications. *Electronics Communication Engineering Journal*, 6:203 – 214, 1994.
- [68] M. Enescu. *Adaptive methods for blind Equalization and signal separation in MIMO systems*. Dissertation for the degree of Doctor of Science, Helsinki University of Technology, 2002.
- [69] M. Geilen. *Mathematics for signal processing, the constant modulus algorithm*. Signal processing for communication, Eindhoven University of Technology, 2007.
- [70] M. H. Hayes. *Statistical digital signal processing and modeling*. John Wiley & Sons, 1996.
- [71] M. J. Hinich. A statistical theory of signal coherence. *IEEE Journal of Oceanic Engineering*, 25:256 – 261, 2000.
- [72] M. J. Hinich. Detecting randomly modulated pulses in noise. *Signal Processing*, 83:1349 – 1352, 2003.
- [73] M. J. Hinich, and P. Wild. Testing time-series stationary against an alternative whose mean is periodic. *Macroeconomic Dynamics, Cambridge University Press*, 5:380 – 412, 2001.

- [74] M. J. Hinich, and P. Wild. Detecting finite bandwidth periodic signals in stationary noise using the signal coherence spectrum. *Signal Processing, The Netherlands Bibliometrics*, 85:1557 – 1562, 2005.
- [75] M. Larimore, and J. Treichler. Convergence behavior of the constant modulus algorithm. *IEEE International Conference on Acoustics, Speech, and Signal Processing*, 8:13 – 16, 1983.
- [76] M. M. Hashem, A.-M. A. Wahdan, A. Salem, and T. Mostafa. Extending the application of conditional signal adaptive median filter to impulsive noise. *International Conference on Computer Engineering and Systems*, pages 355 – 360, 2006.
- [77] M. M. Lavrentev, V. G. Romanov, and S. P. Shishatskii. *Ill-posed Problems of Mathematical Physics and Analysis (Translations of Mathematical Monographs)*. American Mathematical Society, 1986.
- [78] M. Reich. The fascinating world of drilling technology. *Brochure Baker Hughes INTEQ*, 2, 2004.
- [79] M. S. Pedersen, J. Larsen, U. Kjems, and L. C. Parra. *A survey of convolutive blind source separation methods*. Springer handbook of speech processing and speech communication, Springer Berlin Heidelberg, 2007.
- [80] M. Stojanovic. Underwater acoustic communication. *Wiley Encyclopedia of Electrical and Electronics Engineering*, 1999.
- [81] M. Stojanovic, J.A. Catipovic, and J.G. Proakis. Reduced-complexity simultaneous beamforming and equalization for underwater acoustic communications.
- [82] M. Stojanovic, Z. Zvonar, J.A. Catipovic, and J.G. Proakis. Spatial processing of broadband underwater acoustic communication signals in the presence of co-channel interference. *OCEANS Proceedings*, 1:286 – 291, 1994.
- [83] N. Delfosse, and P. Loubaton. Adaptive separation of independent sources: a deflation approach. *IEEE International Conference on Acoustics, Speech, and Signal Processing*, 4:41 – 44, 1994.
- [84] N. Petrochilos, M. Rezk, A. H.-Madsen, V. Lubecke, and O. B.-Lubecke. Blind separation of human heartbeats and breathing by the use of a doppler radar remote sensing. *IEEE International Conference on Acoustics, Speech and Signal Processing*, 1:333 – 336, 2007.
- [85] P. B. Patnaik. The Non-Central χ^2 - and F -Distribution and their Applications. *Biometrika*, 36:202 – 232, 1949.
- [86] P. Billingsley. *Probability and measure, (3rd ed.)*. John Wiley, New York, 1979.
- [87] P. Mosen. MMSE equalization of interference on fading diversity channels. *IEEE Transactions on Communications*, 32:5 – 12, 1984.
- [88] P. Yang, G. A. Dumont, and J. M. Ansermino. Sensor fusion using a hybrid median filter for artifact removal in intraoperative heart rate monitoring. *Journal of Clinical Monitoring and Computing*, 23:75 – 83, 2009.

- [89] R. A. Fisher. Tests of significance in harmonic analysis. *Proceedings of the Royal Society London, Series A*, 125:54 – 59, 1929.
- [90] R. G. Vaughan, and N. L. Scott. Super-resolution of pulsed multipath channels for delay spread characterization. *IEEE Trans. Commun.*, 47(3):343 – 347, 1999.
- [91] R. J.-M. Cramer, R. A. Scholtz, and M. Z. Win. Evaluation of an ultra-wide-band propagation channel, a new multi-template clean algorithm for UWB channel impulse measurements. *IEEE Trans. Antennas Propagat.*, 1B(5):561 – 570, 2005.
- [92] R. P. Gooch, and B. Daellenbach. Prevention of interference capture in a blind (CMA-based) adaptive receive filter. *Twenty-Third Asilomar Conference on Signals, Systems and Computers*, 2:898 – 902, 1989.
- [93] R. S. Nelson, and T. Kasparis. Digital processing for non-stationary narrow-band interference suppression in fading channels. *Proceedings of the IEEE Southeastcon 'Creative Technology Transfer - A Global Affair'*, pages 408 – 412, 1994.
- [94] R. W. Barker, G.-A. Klutke, M. J. Hinich, C. N. Ramirez, and R. J. Thornhill. Development and application of a statistically based feature extraction algorithm for monitoring tool wear in Circuit Board Assembly. *Circuits, Systems, and Signal Processing*, 13:411 – 434, 1994.
- [95] R. W. Tennent, and W. J. Fitzgerald. Passband complex fractionally-spaced equalization of MSK signals over the mud pulse telemetry channel. *First IEEE Signal Processing Workshop on Signal Processing Advances in Wireless Communications*, pages 5 – 8, 1997.
- [96] S. Choi, and A. Beloucharni. Second order nonstationary source separation. *Journal of VLSI Signal Processing*, 32:93 – 104, 2002.
- [97] S. Moghaddamnia. Mud Pulse Telemetry. *Project Report, Baker Hughes*, 2010.
- [98] S. Moghaddamnia, and W. Emmerich. Evaluation of constant modulus algorithm for the compensation of multi-path distortions and co-channel interferences. *Maximizing Return on Technology Investment, Baker Hughes 2008 Technology Forum*, 2008.
- [99] S. Moghaddamnia, C. T. Le, F. Zheng, and T. Kaiser. A new channel estimation scheme based on second order statistics for mud pulse telemetry applications. *Third International Conference on Communications and Electronics (ICCE)*, 2010.
- [100] S. S. Moghaddam and M. S. Moghaddam. A comprehensive survey on antenna array signal processing*. *Trends in Applied Sciences Research*, 6:507–536, 2011.
- [101] T. C.-K. Liu, D. I. Kim, and R. G. Vaughan. A high-resolution, multi-template deconvolution algorithm for time-domain UWB channel characterization. *Canadian Journal of Electrical and Computer Engineering*, 32(4):207 – 213, 2007.
- [102] T. Kasparis. Frequency independent sinusoidal suppression using median filters. *International Conference on Acoustics, Speech, and Signal Processing*, 3:1969 – 1972, 1991.

- [103] T. Kasparis. Suppression of nonstationary sinusoidal interference using transform domain median filtering. *Electronics Letters*, 29:176 – 178, 1993.
- [104] T. Kasparis, N. S. Tzannes, and Q. Chen. Detail-preserving adaptive conditional median filters. *Journal of electronic Imaging*, 1:358 – 364, 1992.
- [105] T. S. Rappaport. *Wireless communication: principles and practice*. 2nd ed., Upper Saddle River, N.J.: Prentice-Hall, 2002.
- [106] U. A. Lindgren and H. Broman. Source separation using a criterion based on second-order statistics. *IEEE Transactions on Signal Processing*, 46:1837 – 1850, 1998.
- [107] W. A. Gardner. *Cyclostationary in communications and signal processing*. IEEE Press, New York, 1994.
- [108] W. Gardner, and L. Franks. Characterization of cyclostationary random signal processes. *IEEE Transactions on Information Theory*, 21:4 – 14, 1975.
- [109] W. L. Aranguren, and R. E. Langseth. Evaluation of a method of interference control in analog FM systems. *IEEE Transactions on Communications*, 27:762 – 767, 1979.
- [110] W. Liu, and S. Weiss. *Wideband beamforming: concepts and techniques*. John Wiley & Sons, 2010.
- [111] W. S. Burdic. *Underwater acoustic system analysis*. Longman Higher Education, 1984.
- [112] Z. Fang. *Analysis and implementation of FRESH filters for co-channel interference suppression in DMSK based telemetric transmission systems*. Master thesis, Institute of Communications Technology, Gottfried Wilhelm Leibniz University of Hannover, 2005.

Lebenslauf

Persönliche Daten:

Name Sanam Moghaddamnia
Geburtsdatum, -ort 25.07.1979, Tabriz-Iran

Wissenschaftlicher / Beruflicher Werdegang:

1997 Abitur am Gymnasium Bagherololumschule in Tabriz-Iran
1997 - 2003 Bachelorstudium (B.Sc.) Elektrotechnik an der technischen
Fakultät der Universität Tabriz-Iran
Englischkurs, TOEFL
Deutschkurs im Goethe-Institut Mittelstufe 3, Zertifikat
2003 - 2006 Masterstudium (M.Sc.) an der Leibniz Universität Hannover
Studienrichtung Nachrichtentechnik, Studienschwerpunkt
Kommunikationssysteme
seit 2006 Wissenschaftliche Mitarbeiterin an der Leibniz Universität
Hannover, Institut für Kommunikationstechnik